(NASA-CR-161368) BELLOWS FLOW-INDUCED VIBRATIONS Final Report (Southwest Research Inst.) 125 p HC A07/MF A01 CSCL 20D

N81-32420

Unclas
G3/34 37456

BELLOWS FLOW-INDUCED VIBRATIONS

by

J.E. Johnson

D.M. Deffenbaugh

W. J. Astleford

C. R. Gerlach

FINAL REPORT

Contract No. NAS8-31994

Control No. AP13-31994

SwRI Project No. 02-4548

SOUTHWEST RESEARCH INSTITUTE

SAN ANTONIO HOUSTON

SOUTHWEST RESEARCH INSTITUTE
Post Office Drawer 28510, 6220 Culebra Road
San Antonio, Texas 78284

BELLOWS FLOW-INDUCED VIBRATIONS

by
J.E. Johnson
D.M. Deffenbaugh
W. J. Astleford
C. R. Gerlach

FINAL REPORT
Contract No. NAS8-31994
Control No. AP13-31994
SwRI Project No. 02-4548

Prepared for

National Aeronautics and Space Administration
George C. Marshall Space Flight Center
Marshall Space Flight Center, Alabama 35812

October 15, 1979

Approved:

H. Norman Abramson, Vice President
Engineering Sciences

ABSTRACT

Results of theoretical and experimental investigations of bellows typical of those found in Space Shuttle external tanks are presented. New correlation parameters are identified which generalize the alternating stress calculations presented in an earlier SwRI study titled "Bellows Flow-Induced Vibrations and Pressure Loss." Alternating stress amplitudes and mean stress levels form the basis of a fatigue analysis incorporating seven-ordinate charts for 347 S.S., Alloy 21-6-9, and Inco 718. A crack propagation model is also presented. Computer programs for computing bellows fatigue life and Two Phase flow and material hardness topics are contained in the report.

ACKNOWLEDGEMENTS

Dr. C. Richard Gerlach, who is now the Chief Executive Officer of Gerlach Products, Inc. (San Antonio, Texas), served as a consultant to Southwest Research Institute. He contributed significantly to the early studies of bellows and likewise to the current study.

The authors of this report wish to express their sincere gratitude to Mrs. Adeline Raeke who cheerfully typed the text and to Mr. V. J. He andez for his skillful work on the figures.

We express a special word of thanks to Mr. Clinton Wood, Staff Technician, for his unique talents and ideas which were utilized in the design and fabrication of components required for the experimental apparatus. Mr. Wood also conducted many of the experimental tests and aided materially in the data reduction.

TABLE OF CONTENTS

TABLE OF CONTENTS (CONTD)

LIST OF FIGURES

I. INTRODUCTION

I.1 Overview

This report describes all work performed by Southwest Research Institute under Contract NAS8-31994, "Research Study of Flow Induced Vibrations." This study was performed for George C. Marshall Space Flight Center of the National Aeronautics and Space Administration, and it was administered by the Structures and Propulsion Laboratory, with Mr. R. H. Veitch serving as Technical Manager.

The general objective of this study was to evaluate bellows related theoretical assumptions either by analytical and/or experimental investigations. Emphasis was placed on obtaining a better understanding of the fluid-elastic excitation mechanism and upon developing a refined fatigue prediction methodology. The foundation of the current study is found in earlier research work performed by the Institute which is reported in a document titled "Bellows Flow-Induced Vibrations and Pressure Loss," by C. R. Gerlach, et al.(1)

Summary of Results

A number of significant findings have been made throughout this report; these are summarized below.

(a) Definition of C_F^* Parameter - A stress correlation parameter has been defined which generalizes the existing bellows data contained in Reference 1. Previous data were characterized by a number of parameters such as the specific spring rate, fluid state, geometric factors and a vortex force coefficient. All of these factors are accounted for in the C_F^* correlation and its usage.

(b) Damping Model - As an alternate method of predicting stress amplitudes, an empirical damping model was developed.

(c) Fatigue Prediction - A stress analysis has been coupled with the flow-induced vibration analysis in order to determine, with reasonable accuracy, the bellows fatigue life under varying environmental factors.

(d) Computer Program - A computer program has been developed to allow quick computation of the bellows mode frequencies, lock-in ranges, stress indicator, and stress level.

(e) Acoustic Resonance - The acoustic resonances as identified by analysis have been verified by limited experimental investigation.

(f) Special Problems - During the course of the contract, several urgent and special bellows related problems were addressed at NASA's request. The solution of these problems are included in this report.

I.2 Organization of Study

The bellows study has been broken into two separate methods of approach as indicated in the block diagram shown in Figure 1. The end objective of both methods is to predict the fatigue life of U-shaped bellows made of an arbitrary material, and in both cases, the alternating stress component is generated by flow induced vibrations. Method I incorporates the stress indicator concept, while Method II incorporates actual stress predictions which may be incorporated with 7-ordinate fatigue curves to predict bellows life. Method I suffers from the lack of a fatigue data base which must be generated by failing numerous bellows while influenced by flow induced vibrations. Method II suffers from underdevelopment of a realistic stress-deflection model where the convolute deflections can be predicted given an arbitrary geometry and flow conditions. Method I has been streamlined and somewhat generalized with the development of an envelope parameter designated as C_F* which is then used to determine the stress indicator. Method II efforts were directed toward the development of a flow induced stress model.

I.3 General Discussion of Study

The main propulsion system of the Space Shuttle is configured with three engines, a complex array of liquid and gas flow lines, and two large external tanks (ET). An elementary schematic of the main propulsion system is shown in Figure 2. Bellows are contained throughout the flow network; however, the bellows of primary interest are contained in the feed lines (LO_2 and LH_2) and in the small recirculation lines.

Earlier studies have shown that unshrouded shuttle application bellows (see Figure 3 for bellows nomenclature) will vibrate violently when the contained fluid is moving at a specific critical velocity. The oscillation is shown to occur at a reduced velocity $(U/f\sigma)$ of approximately 4.5. Vortex shedding from the individual convolutes was found to be the flow induced vibration mechanism.

METHODS OF APPROACH

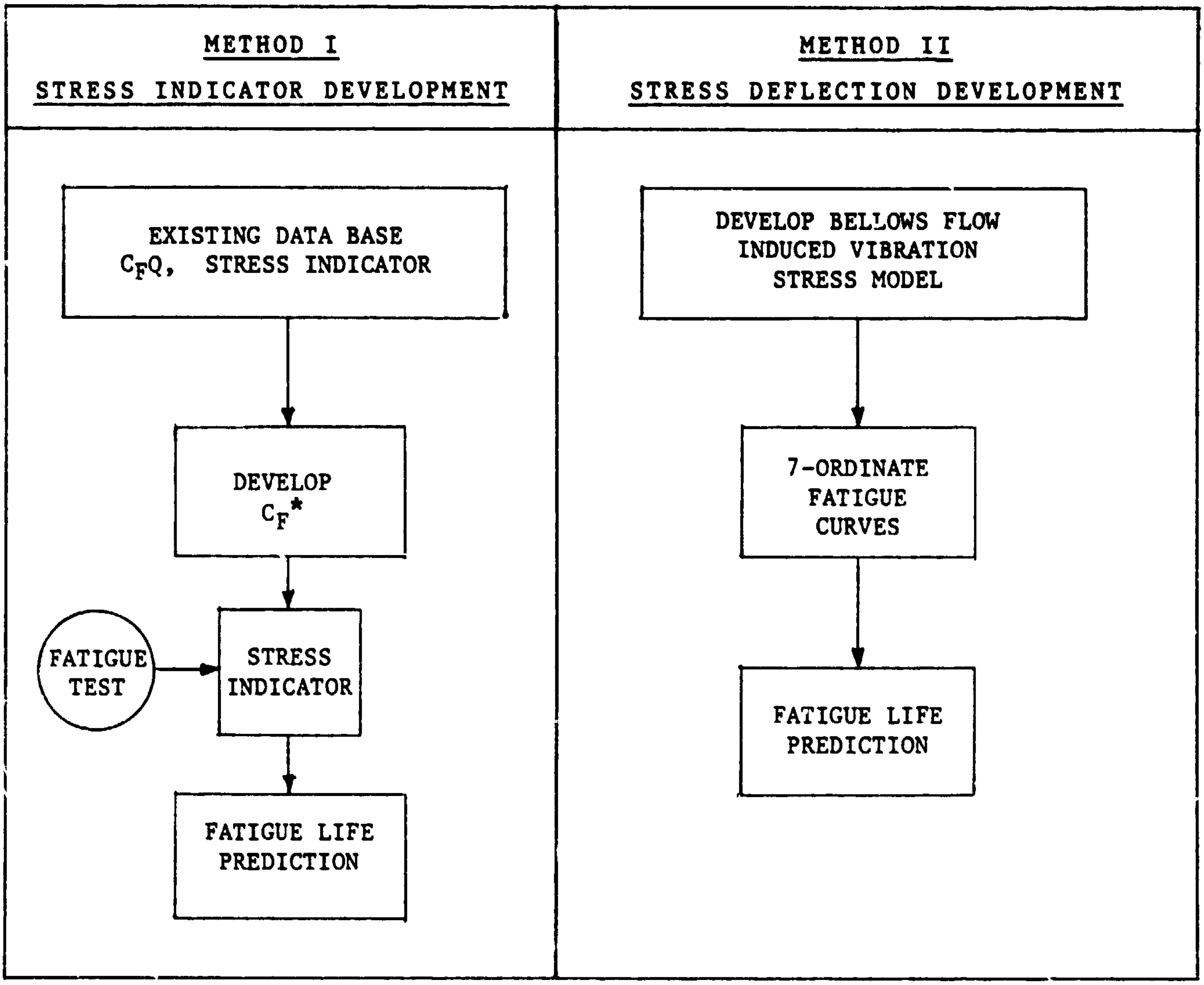

FIGURE 1. METHODS OF APPROACH INCORPORATED IN BELLOWS STUDY

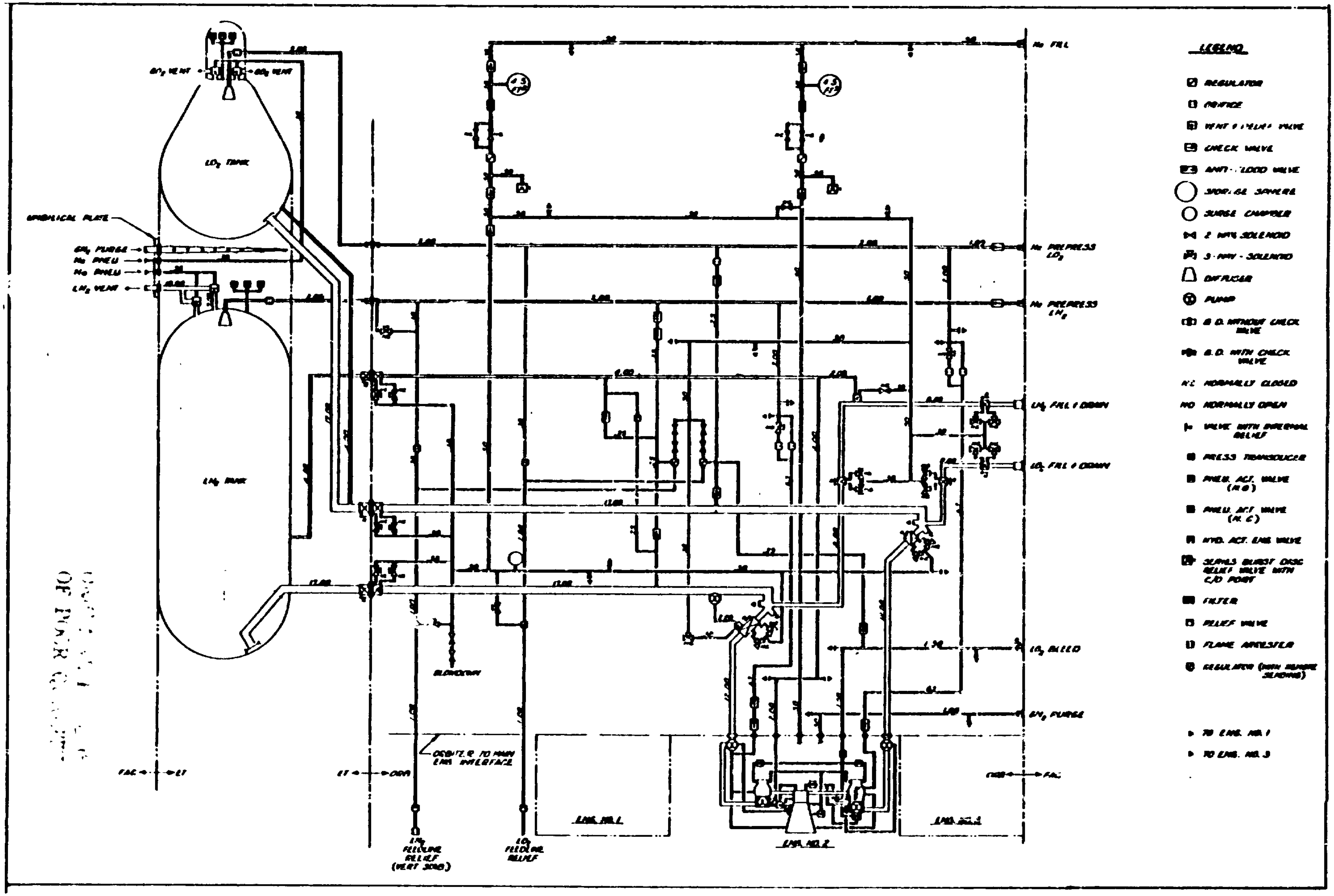

FIGURE 2. MAIN PROPULSION SYSTEM SCHEMATIC

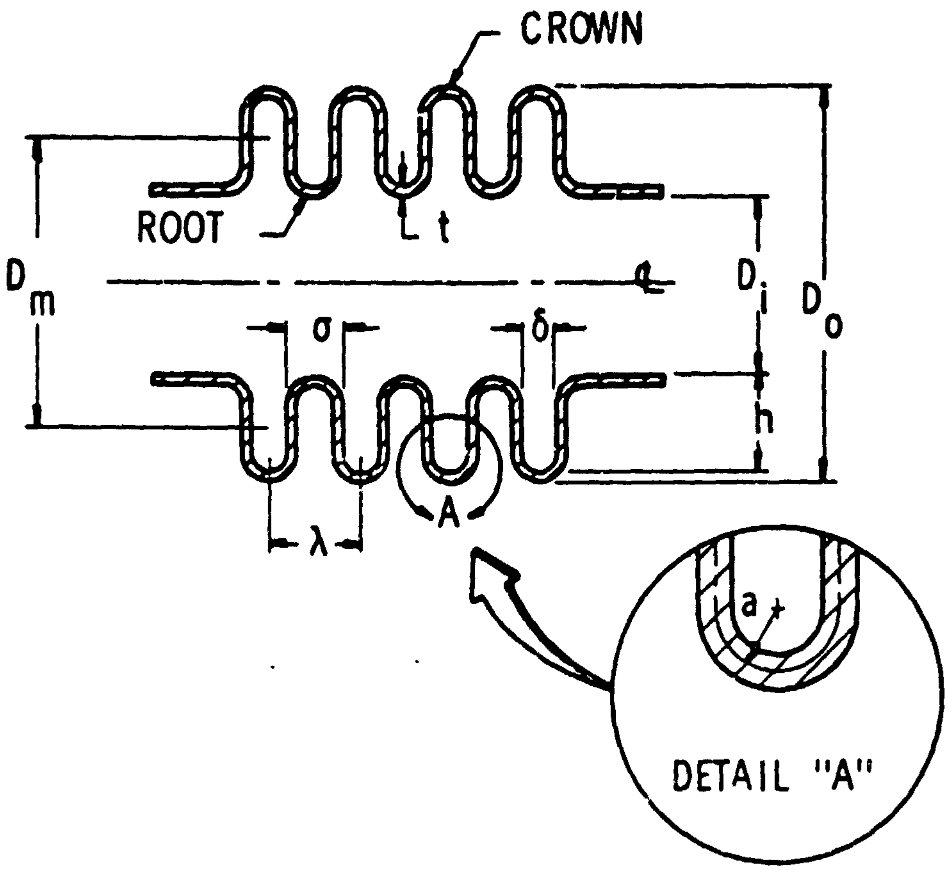

N_c = NUMBER OF CONVOLUTIONS COUNTED FROM THE OUTSIDE

N_p = NUMBER OF PLYS

D_m = MEAN BELLOWS DIAMETER

t = WALL THICKNESS (THICKNESS PER PLY IF MULTI-PLY)

λ = CONVOLUTE PITCH

σ = CONVOLUTE WIDTH

a = MEAN FORMING RADIUS

h = MEAN DISC HEICHT

FIGURE 3. BELLOWS NOMENCLATURE

Experimental data, obtained from the earlier studies, were parametrically correlated in terms of (1) the Strouhal number (convolute width is the characteristic dimension), (2) the bellows modal frequencies which included added fluid mass terms, and (3) a stress indicator which is proportional to the maximum dynamic stress.

It has been shown that the stress indicator is a function of a vortex force coefficient, C_F, and a forced response dynamic amplification factor, Q. These experimentally derived factors are shown in Figures 4 and 5 and Table I.

Finally, the observed fatigue life was related to the stress indicator as shown in Figure 6. The fatigue data were obtained for 321 S.S. only; although the general presentation could be expanded to include other materials if appropriate material factors could be included. Bellows for Space Shuttle applications are constructed of Inco 718 and steel alloy 21-6-9 materials.

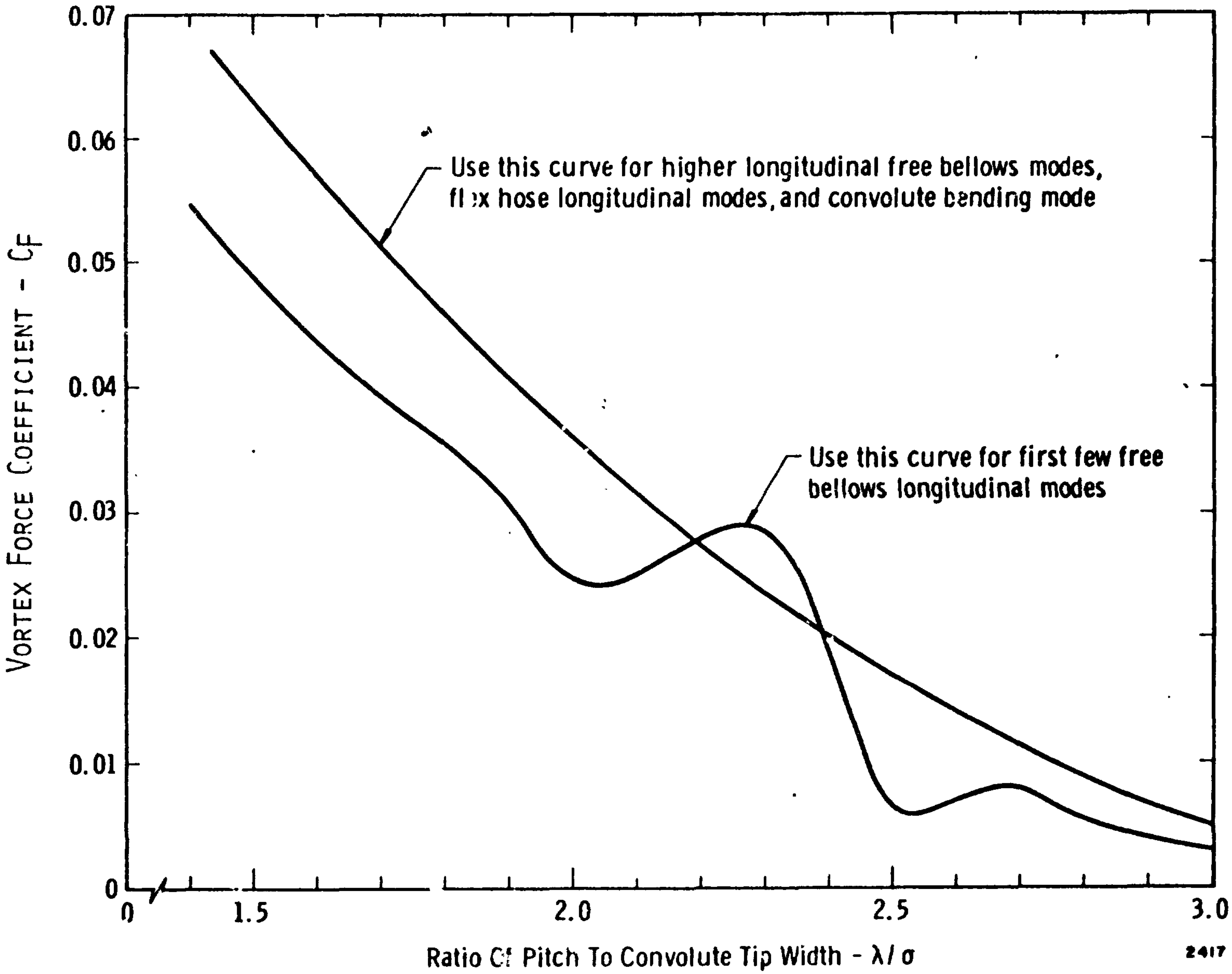

FIGURE 4. SUMMARY OF BELLOWS VORTEX FORCE COEFFICIENT EXPERIMENTAL DATA

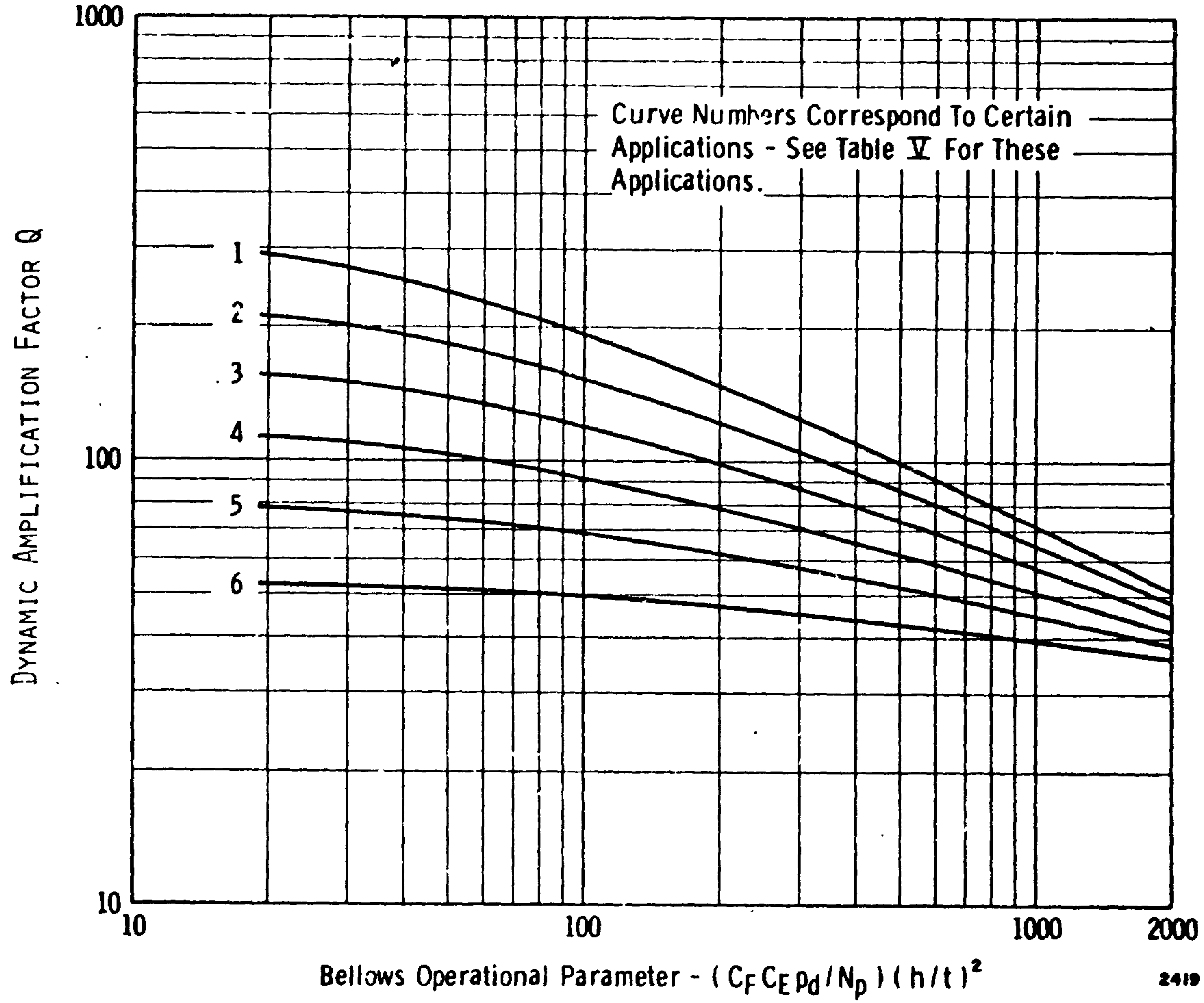

FIGURE 5. DYNAMIC AMPLIFICATION FACTORS FOR VARIOUS BELLOWS APPLICATIONS

TABLE I.

APPLICATIONS INFORMATION FOR USE WITH Q VALUE DATA IN FIGURE 5

Specific Spring Rate (see Note 1)	Number Plies	Internal Media (see Note 2)	Curve No.
all ranges	1	low pressure gases	1
over 2000 lb/in^2	1	high pressure gases, light liquids	1
over 2000	1	water, dense liquids	2
under 2000	1	high pressure gases, light liquids	2
under 2000	1	water, dense liquids	3
over 3000	2	all	3
2000 - 3000	2	all pressure gases	4
under 2000	2	all pressure gases	5
2000 - 3000	2	all liquids	5
under 2000	2	all liquids	6
over 3000	3	all	4
2000 - 3000	3	all	5
under 2000	3	all pressure gases	5
under 2000	3	all liquids	6

Use of Table - To use table, first calculate bellows specific spring rate, then look up application curve r ıber corresponding to this specific spring rate, numbeı of plies, and internal media.

Note 1: The specific spring rate is here defined as

$$S.S.R. = \frac{K_A N_c}{D_m N_p}$$

or is the spring rate per convolute, per ply, per unit of diameter.

Note 2: Low pressure gases will be defined here as being those gases below 150 psia. Light liquids will be defined as having a density, relative to water, of less than 0.2.

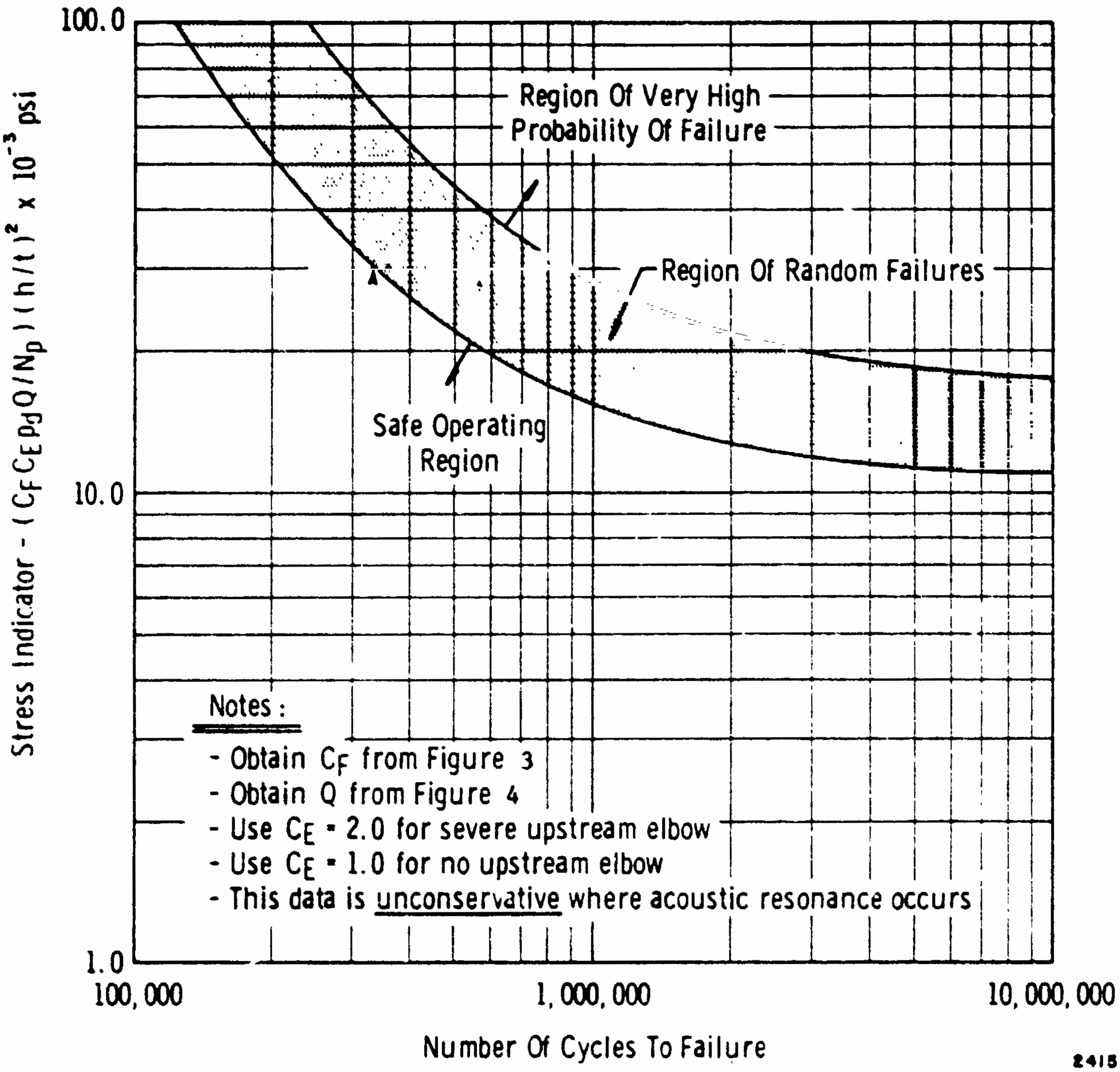

FIGURE 6. PRELIMINARY BELLOWS FATIGUE LIFE DATA

I.4 Review of Relevant Literature

The following list of reviewed sources of bellows information is included to help direct the interested reader build a background knowledge which is needed for detailed evaluation of bellow related topics.

(1) Kleppe, S. R., "High Pressure Expansion Joint Studies" ASME Petroleum Mechanical Engineering Conference, New Orleans, Sept. 25-28, 1955, Paper No. 55-PET-10.

A semi-torus expansion joint was extensively strain-gaged and hydrostatically tested. Test results compared favorably with R. A. Clark's theory as presented in "On the Theory of Thin Elastic Toroidal Shells," Journal of Mathematics and Physics, Vol. 29, 1950, pp. 146-178.

(2) Turner, C. E., and Ford, H., "Stress and Deflection Studies of Pipeline Expansion Bellows," Proceedings of the Institute of Mechanical Engineering, pp 596-552, Vol. 171, No. 15, 1957.

This paper presents a theoretical solution together with an experimental study of axial compression of certain bellows mainly of the corrugated-pipe type, used in the pressureless state. The total strain energy is written in terms of the circumferential stress and the axial loading moment. A Rayleigh - Ritz method is used to solve for a minimum strain energy condition. Ultimately the surface stresses are analytically determined. The paper contains a short literature review covering the period from 1916 to 1953.

(3) Feely, F. J., Jr., and Goryl, W. M., "Stress Studies On Piping Expansion Bellows," Journal of Applied Mechanics, Paper No. 44-APM-22.

In this paper a formula has been derived to show the total stress induced in the material as a result of the combined effects of pressure and movement. The validity of the approximations used in the formula have been verified by laboratory strain measurements. The paper deals primarily with flat disc type bellows.

(4) Samans, Walter, "Endurance Testing of Expansion Joints," ASME Paper No. 54-A-103.

This paper presents the results of testing 19 bellows of various types to their endurance limit. The types include (1) welded roots, (2) hydraulically formed, and (3) welded disk. The bellows material consisted of stainless steel types 304, 321, and 347. A typical stress-distribution diagram for a 12-inch diameter hydraulically formed bellows is presented (case of axial extension and compression, and internal pressure). Strain measurements were taken with SR-4 strain gages. The maximum stress range for both radial and circumferential stresses occurs near the root of the corrugation.

(5) Haringy, J. A., "Instability of Bellows Subjected to Internal Pressure," Philips Res. Report 7, 189-196, 1952.

Bellows may become unstable when loaded by internal pressure. The critical value of this pressure is governed by the rigidity of the bellows with respect to bending. Critical pressures have been analytically determined for rectangularly shaped corrugations and these critical pressures may be considered to agree with those obtained experimentally for U-shaped bellows when considering the approximations introduced and the variation of wall thickness.

(6) Laupa, A., and Weil, N. A., "Analysis of U-Shaped Expansion Joints," Journal of Applied Mechanics, Transactions of the ASME, pp 115-123, March 1962.

An elastic analysis of U-shaped expansion joints under axial loads and internal or external pressure is presented. The analysis employs the energy method for the toroidal sections, and the theory of symmetrical bending of circular plates augmented by thick walled cylinder analysis for the annular plate connecting the two toroidal sections.

(7) Sack, L., "Avoiding Fluid-Line Failure in Bellows and Convoluted Tubing," Machine Design, May 27, 1971.

Flexline response frequencies are modeled as a lumped parameter system where the characteristic frequency is determined by knowledge of the convolute effective mass and the effective fluid compressibility. Bellows longitudinal natural frequencies are modeled as a spring-mass analog where a dimensionless frequency parameter is utilized for evaluating all the longitudinal modal frequencies. An attempt has been made to define the maximum alternating stress.

(8) Baylac, G., et al., "Calculation of Acoustical Resonances in Irregular Cavities with Application to Noise-Induced Stress in Expansion Joints," ASME Paper No. 75-DET-64.

An analytical and experimental study of the acoustic behavior of seven and nine corrugation expansion joints (bellows) used in a nuclear reactor is presented. Resonant frequencies obtained from a computer program using a matrix method are given. Experimental test results on seven corrugation expansion joints are in good agreement with the computations. It is concluded that the calculation of acoustic frequencies of expansion joints with internal sleeves can be utilized to avoid the coincidence of these frequencies with those of a mechanical or flow-induced noise nature and thus reduce the loads on expansion joint corrugations.

(9) T. M. McCrary, "Evaluation of Inconel 718 Bellows Material," SD73-SA-0014, Rockwell International Space Division, Mar. 1973.

Life cycle testing was performed on 10" diameter bellows with nominal 3/8-inch high convolutions (.008-inch thick, Inconel 718). Testing was similar to that conducted for Boeing Company by Strazar. Metallurgical and fatigue properties were evaluated. This report does present a source of fatigue data as a function of bending stress (bellows), and percent of tensile ultimate strength (specimens only).

(10) "Effect of Surface Irregularities on Bellows Fatigue Life," R7250 Rocketdyne, NASA Contract NAS8-19541.

The report presents the results of a brief test program aimed at generating data on bending life of notched CRES sheet specimens. Emphasis of the study is directed toward the quantitative evaluation of bellows' defects, particularly those resulting from accidental damage. An empirically derived procedure for evaluating bellows' surface irregularities and determining service life is presented.

II. GENERALIZED CORRELATION PARAMETER: C_F^*

II.1 Introduction

Through the efforts of Gerlach, et al.[1] and Sack[8] is has been well established that a series of lumped spring-mass elements can represent a free bellows and the modal frequencies can be computed with a high degree of accuracy. The work of Gerlach went on to show that the flow excitation mechanism is a vortex shedding phenomena that occurs in the entrance region of a convoluted bellows. When the vortex shedding frequency is near a bellows longitudinal structural frequency, the vortex shedding frequency will "lock-on" and the structure will vibrate at an amplitude dependent upon the amount of fluid and structural damping present.

Ultimately, the most fundamental question is how to determine the amplitude of convolute displacement and hence the resultant maximum alternating stress amplitude. Two stress prediction models will be addressed in this section.

II.2 C_F^* Correlation Parameter

Reference 1 contains the derivation and application of a stress indicator concept. It must be emphasized that the original form of the stress indicator was merely a bench mark showing relative stress intensities as a function of fluid and geometric parameters. Its purpose was to guide a designer when obtaining fatigue predictions. The stress indicator concept is a valid method for predicting fatigue life so long as a substantial data base is developed; unfortunately, a large data base does not exist.

Before describing the C_F^* ("C sub F Star") model, the original stress indicator model is reviewed. It has been shown that the maximum convolute stress due to flow induced vibration is

$$\sigma_{alt} = K \frac{C_F Q}{N_p} (h/t)^2 \; 1/2 \; \rho_f \; V_{crit}^2 \tag{II.1}$$

The K term contains factors of proportionality relating to geometric constraints and this factor was extracted from Equation (II.1) to produce a single simple expression for stress which contains only readily known bellows dimensional data, parameters, and flow variables. Therefore, the indicator is given as

$$S.I. = \frac{C_F Q}{N_p} (h/t)^2 \ 1/2 \ \rho_f \ V_{crit}^2 \qquad (II.2)$$

Table II compares the calculated stress indicator and measured stress on the crown of the second convolute (see Appendix B for a description of the experimental techniques). Several items are worth noting in this table. The K factor ranges from 0.585 to 3.61 for the limited test conducted and there is a downward trend in the K factor as the mode number increases. This shows that the stress indicator may or may not be a conservative estimator of stress levels, and the K factor is not constant as assumed in Reference 1.

TABLE II. MEASURED CONVOLUTE RADIAL STRESS AND CALCULATED STRESS INDICATOR COMPARISON

Bellows* Ident.	Mode No.	Measured Radial Stress KSI (peak)	Stress Indicator KSI	Measured / Calculated
4	1	2.93	2.21	1.325
4	2	8.02	8.24	.97
4	3	8.94	11.48	.775
6	1	.765	.93	.82
6	2	3.67	3.70	.99
6	3	4.59	7.83	.585
15	1	2.82	.78	3.615
15	2	7.84	3.18	2.46
15	3	8.51	6.76	1.225
E	1	4.57	2.28	2.00
E	2	8.41	7.91	1.05

*Dimensional Data is contained in Appendix C.

The stress indicator contains two terms, C_F and Q, that are dependent upon factors of damping, internal pressure, convolute geometry, and the flow media. Values for C_F are obtained from Figure 4 while values for Q are obtained from Figure 5 and Table I. The data contained in these sources have been correlated in the form of one universal stress function curve as discussed below.

All data contained in Reference 1 has been evaluated in terms of a correlation parameter defined as

$$C_F^* = C_f Q(N/N_C)$$

Figures 7 through 9 show plots of the force coefficient parameter for representative samplings of the total data base. The effect of changes in λ on the force coefficient parameter C_F^* is illustrated in Figure 7. Here, a single bellows was tested at various pitch values, λ, and the peak response of the first longitudinal mode (N=1) was noted. It is noted that spring rate is affected somewhat by changes in λ.

The reduced data shown in Figure 8 clearly illustrates the effect of vortex reinforcement and vortex retardation on the flow induced response of the bellows.

A <u>vortex reinforcement</u> occurs when the vortex shedding from an upstream convolute arrives at the adjacent downstream convolute at the right moment to aid in the formation of the vortex forming at that adjacent convolute. <u>Vortex retardation</u> has the opposite effect. The vortex shed from an upstream convolute arrives at the adjacent downstream convolute at the right moment to detract from the formation at that location. As we will soon discuss, it is our present concept that <u>vortex reinforcement</u> is most prevalent and effective in the higher longitudinal modes. (Figure 6 from the final report "Bellows Flow-Induced Vibrations and Pressure Loss" clearly shows a visualization of vortex reinforcement for a higher longitudinal mode.) In the first two or three modes of a bellows, vortex reinforcement and vortex cancellation both come into play, as illustrated by Figure 8. However, for the intermediate modes, the vortex retardation phenomena is prevalent.

Figure 8 presents a plot of C_F^* versus the mode number N for four test bellows that have constant values of the parameter (h/t) but have h values ranging from 0.2 to 0.5. Since spring rate is proportional to (h/t), this family had similar modal frequencies, so that the effect of convolute height h should be revealed. Also, however, each of the four bellows was tested for three or four values of λ achieved by stretching. Note that there is a spread of the combined C_F^* values for these four bellows for each mode number of N value. This spread is caused by a

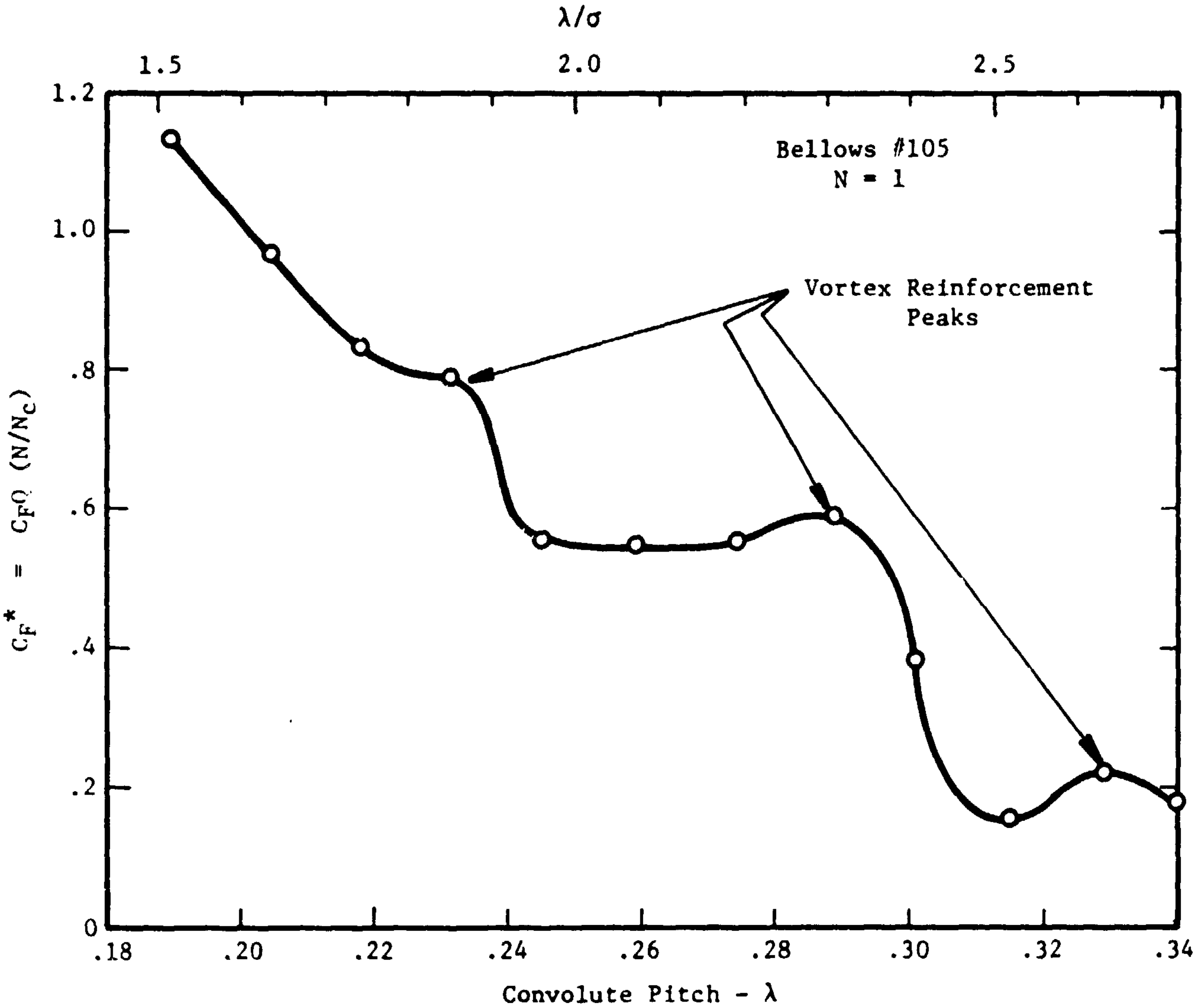

FIGURE 7. VORTEX FORCE COEFFICIENT C_F^* VS. PITCH FOR THE FIRST MODE OF BELLOWS 105

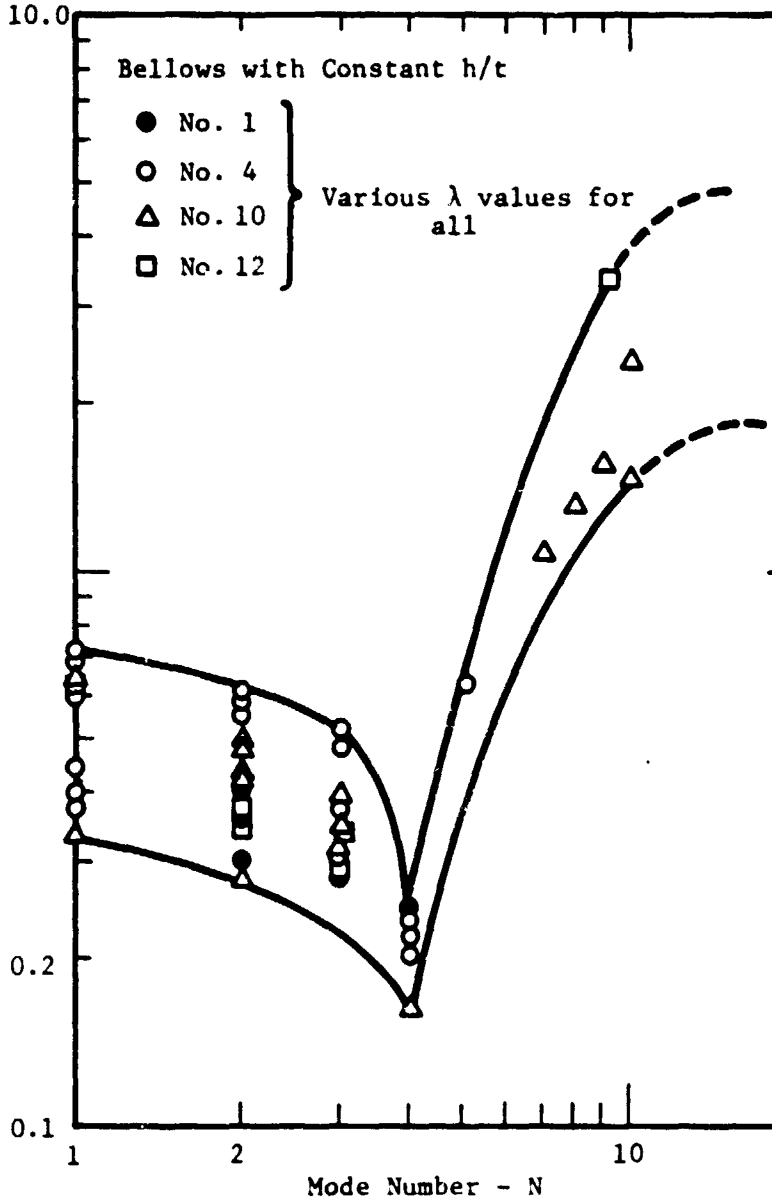

FIGURE 8. VORTEX FORCE COEFFICIENT $\dot{C}_F^*$ AS A FUNCTION OF MODE NUMBER FOR BELLOWS WITH CONSTANT (h/t)

combination of two factors. First, it represents the influence of the effect of changing λ as illustrated previously in Figure 7, and, secondly, it reflects the normal variation expected in flow-induced vibration experiments of bellows where slight changes in alignment, clamping of the ducting, etc. cause changes in the peak response point.

From Figure 8, we have concluded the following:

(a) Other than for the No. 1 specimen, which had $h = 0.2$ or a very short convolute, the effect of h was not apparent between the bellows. Specimen No. 1 had lower C_F^* values than the other bellows, probably because short convolutes do not couple so well as taller convolutes. After all, the limiting case is $h = 0$ which represents a straight pipe which has no response of the type under consideration.

(b) The vertical spread of C_F^* for each mode is primarily caused by vortex reinforcement or vortex cancellation.

(c) The pronounced minimum of C_F^* is a result of an optimum vortex cancellation effect for this mode number range.

(d) The rapid rise of C_F^* for the higher longitudinal modes is a result of a predominance of vortex reinforcement for these modes.

(e) Many of the higher modes simply never appear because other modes close to them predominate and prevent their occurrence.

Figure 9 presents C_F^* as a function of mode number N for three bellows having similar convolute geometry but different numbers of convolutes. The bellows No. 19 illustrates yet another phenomena. Note that the C_F^* values for this bellows are quite low for the first two longitudinal modes. Aslo note the strong presence of the first cocking mode plotted for $N = 1.5$. For this bellows the cocking mode was stronger than normal so it suppressed the first and second longitudinal modes causing their C_F^* values to be abnormally low.

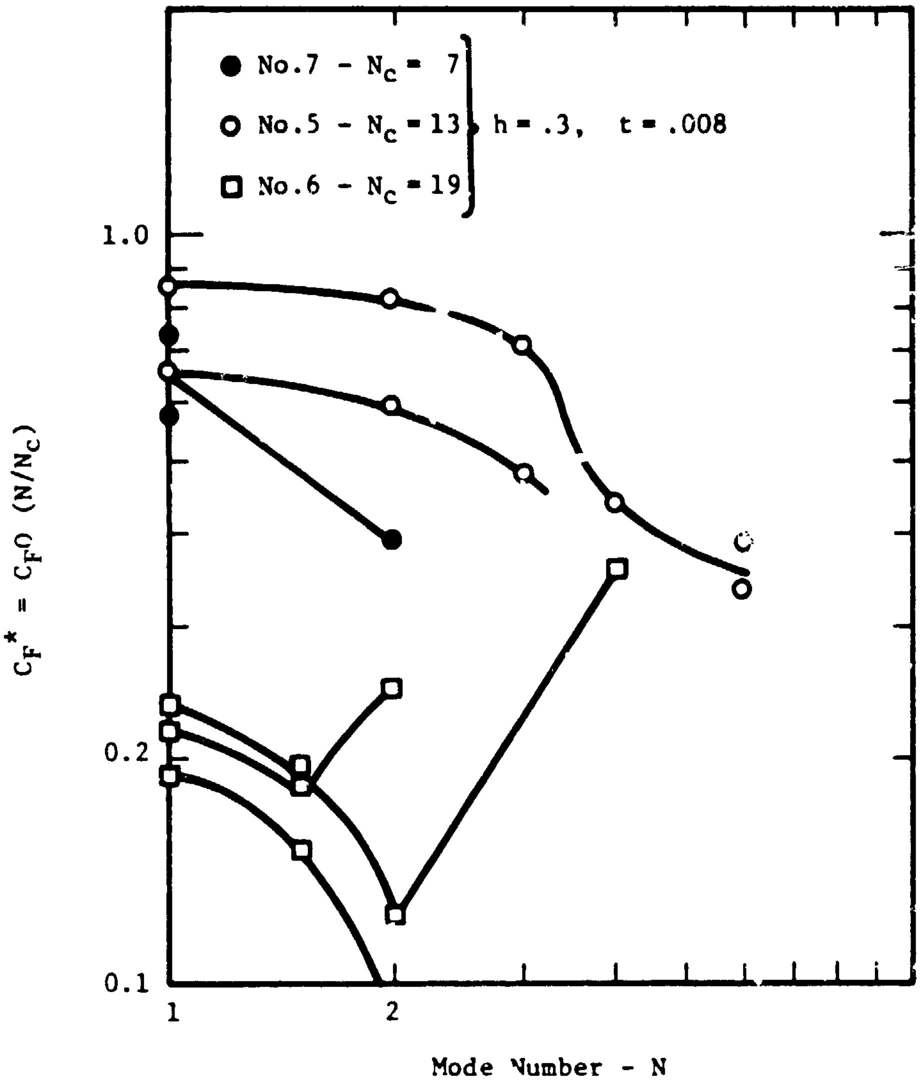

FIGURE 9. VORTEX FORCE COEFFICIENT $C_F{}^*$ AS A FUNCTION OF MODE NUMBER FOR BELLOWS WITH DIFFERENT N_c

The primary intent of the C_F^* relation is to mathematically collapse all of the experimentally generated Q surfaces into one relationship that applies to all ranges of the bellows operational parameters; hence, the stress indicator is computed

$$S.I. = \frac{C_F^* N_c}{N N_p} (h/t)^2 (1/2 \rho V_{crit}^2) \qquad (II.3)$$

The parameter C_F^* is obtained from Figure 10 which is a somewhat conservative curve that envelops all previously generated experimental bellows data. This curve contains all inherent information relating to C_F and Q.

II.3 Summary of Design Analysis Procedure

The procedure for analyzing a given bellows design to assure freedom from flow-induced vibration failure consists of several distinct steps which are listed below.

Step 1. Calculate the natural frequencies for all modes of the bellows.

Step 2. Determine the lock-in or critical velocity range for each possible mode of vibration.

Step 3. Calculate the Stress-Indicator for each mode at the critical velocity.

Step 4. Determine the potential for failure of the bellows using the Stress-Indicator versus Cycles-to-Failure curve.

Pages 23 and 24 present a detailed step-by-step procedure that may be used for hand calculations. A more sophisticated calculation procedure is contained in a computer program (see Appendix A).

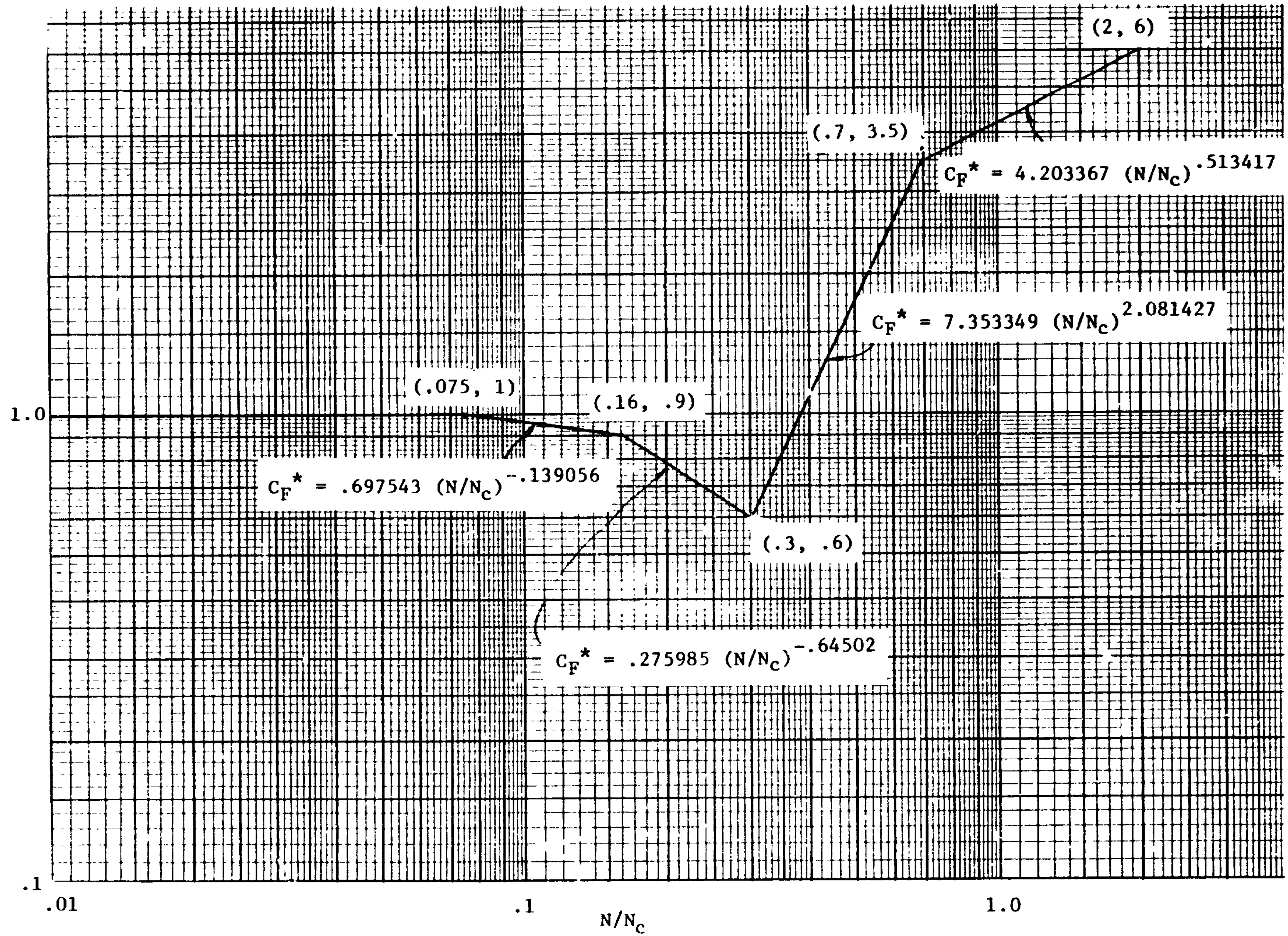

FIGURE 10. ENVELOPE CURVE FOR C_F^* CORRELATION

TABLE III.

SUMMARY OF FREQUENCY AND STRESS LEVEL CALCULATIONS

STEP A — Consider the bellows structure representable by a lumped mass-spring mechanical model.

STEP B — Calculate the elemental spring rate value K from the expression

$$K = 2\ N_c\ K_A$$

where K_A is the overall spring rate determined from a force-deflection test or from the following expression:

$$K_A = D_m\ E\ \frac{N_p}{N_c}\ (t/h)^3$$

STEP C — Calculate the elemental metal mass M_m

$$M_m = \pi \rho_m t\ N_p\ D_m\ [\pi a + (h-2a)]$$

STEP D — Calculate the fluid added mass M_f, for the first few longitudinal modes and for the higher longitudinal modes as

$$M_f = \pi/2\ \rho_f\ D_m h\ (2a-tN_p) \quad \Big\}\ \text{First few N values}$$

and

$$M_f = \frac{\pi\ D_m\ \rho_f\ h^3}{3\delta} \quad \Big\}\ \text{Higher N values}$$

STEP E — Calculate the reference frequency f_o from the expression

$$f_o = 1/2\pi \sqrt{k/m}$$

where $m = m_m + m_f$

TABLE III (CONTD)

SUMMARY OF FREQUENCY AND STRESS LEVEL CALCULATIONS

STEP F

Calculate the dimensionless frequencies and then multiply the dimensionless frequencies by the reference frequencies to obtain the true mode frequencies

$$B_i = \sqrt{2\left[1 + \cos\left(\frac{\pi(2N_c - i)}{2N_c}\right)\right]} \quad \Bigg\} \text{ Dimensionless frequency for the i-th mode}$$

$$i = 1,2,3, \ldots 2N_c-1$$

$$f_i = B_i \, f_o \quad \Bigg\} \text{ True frequency for the i-th mode}$$

Alternately, the dimensionless frequency factors may be obtained from Table I, Appendix A.

STEP G

Calculate the first convolute bending mode from the expression

$$f_b = 1/2\pi \sqrt{8k/m}$$

where $m = m_m + m_f$

and $m_f = \pi \, D_m \, \rho_f \, h^3/3\delta$

STEP H

Calculate stress indicator from the following expression:

$$S.I. = C_F^* \left(\frac{N_c}{N \, N_p}\right) \quad (h/t)^2 \; (1/2 \; \rho \; V_{crit}^2)$$

The parameter C_F^* is obtained from the curve presented in Figure 10.

STEP I

Calculate bellows expected life from the data presented in Figure 6, which is a plot of stress indicator versus cycles to failure. If the fatigue life is greater than 10^5 cycles, then the data are conservative for materials classified as Inco 718 and alloy 21-6-9.

If the calculated number of cycles is less than 10^5, then the expected life of alloy 21-6-9 will be less than that indicated for SS-321 or its equivalent SS-347.

III. STRESS LEVELS

III.1 Introduction

While section II presented a method for calculating vibration frequencies and stress-like quantities that may be used with the appropriate analysis to predict fatigue life, this section will explore various properties of actual stress levels experienced during the flow induced vibration process. As of this writing, an exact method has not been developed to calculate actual stresses; however, several important aspects of the problem are presented along with a reasonable stress calculation procedure.

III.2 Stress Envelope

Test data, shown in Table IV, has been reduced in terms of non-dimensional stress and velocity ratios for each longitudinal mode of vibration. The velocity ratio is formed by dividing the critical velocity of a particular mode by the first mode velocity and the stress ratio is formed in a similar fashion. The correlation in Figure 11 shows that similar families of curves are developed. The data may be further collapsed by referencing the curves to a particular damping ratio. For the present case, an average damping ratio of .00635 served as the reference damping value. Figure 12 shows the results of the damping normalization. From the limited data presented, the second and third mode stress may be calculated by the following empirical equation,

$$\sigma_{alt_N} = \sigma_{alt_1}\left(\frac{.00635}{\zeta}\right) F_N \qquad \text{(III.1)}$$

where $F_2 = 2.75$

$F_3 = 3.05$

Equation III.1 was developed from data obtained from a series of 3", 321 S.S. bellows with a constant convolute height. The material thickness, number of plys and number of convolutes were allowed to vary and the measured spring rates were significantly different. The alternating stress component referred to is the convolute radial stress. Radial stresses were calculated from biaxial strain data (radial and circumferential) as described below.

TABLE IV. THREE-INCH BELLOWS STRESS RESULTS

Specimen No.	Mode No.	V_F, fps	σ_{alt}, ksi	Velocity Ratio V_N/V_1	Stress Ratio $\frac{\sigma_{alt} @ N}{\sigma_{alt} @ N=1}$	Average Damping Ratio, ζ	ζ/ζ_{ref}
4	1	5.40	2.93	1.0	1.0	.007	1.102
	2	10.80	8.02	2.0	2.74		
	3	15.89	8.94	2.9[illegible]	3.05		
6	1	4.18	0.765	1.0	1.0	.0027	.425
	2	8.35	3.67	1.99	4.79		
	3	12.53	4.59	2.99	6.0		
15	1	7.26	2.82	1.0	1.0	.0064	1.0
	2	14.52	7.84	2.0	2.78		
	3	21.79	8.5[illegible]	3.0	3.02		

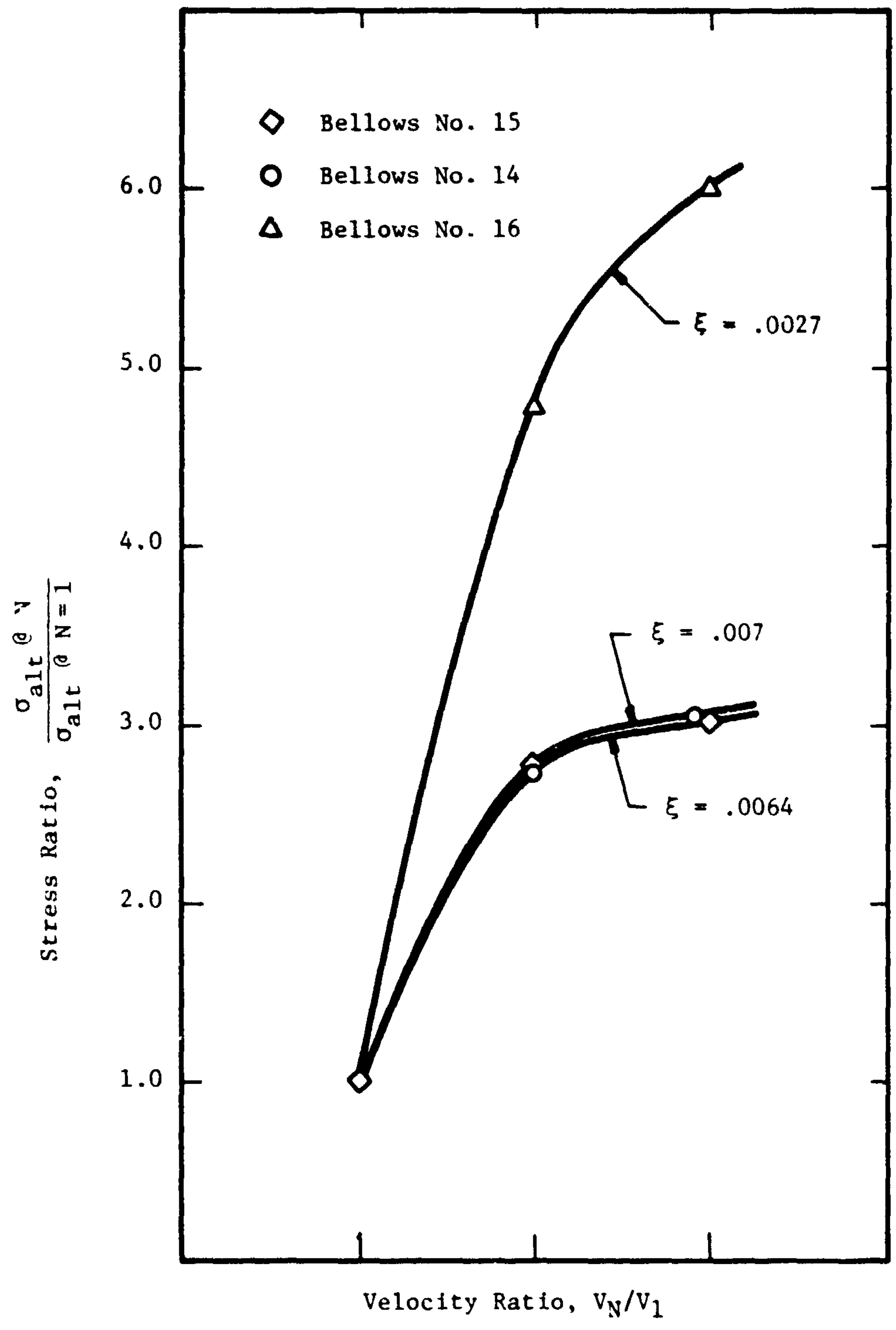

FIGURE 11. VELOCITY RATIO VS. STRESS RATIO

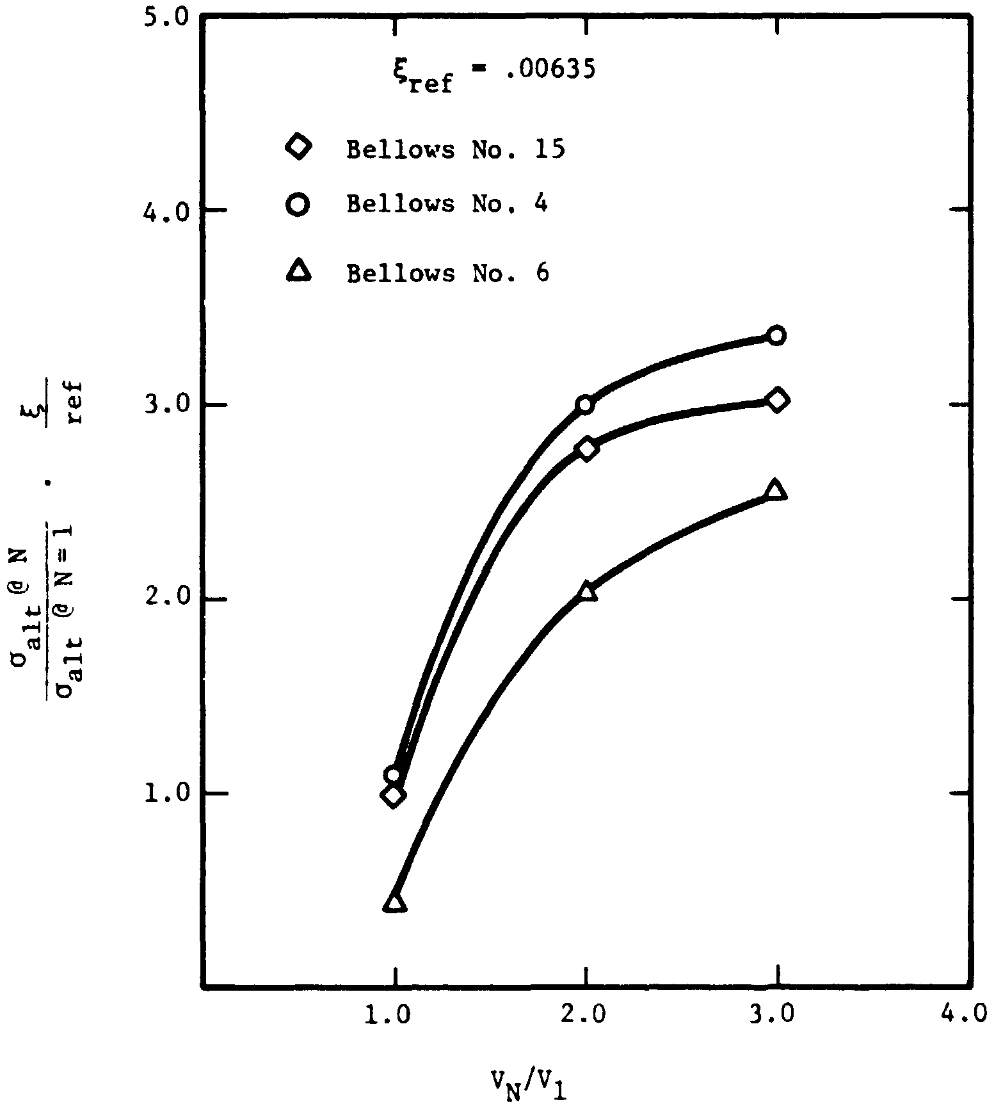

FIGURE 12. NORMALIZED STRESS RATIO

Each bellows was strain gaged (see Figure 3, Appendix B) on the second and middle convolute in the radial and circumferential directions which are the assumed principal directions. Principal stresses are calculated from the measured principle strains,

$$\sigma_R = \frac{E}{1 - \mu^2} (\varepsilon_R + \mu \varepsilon_c) \qquad \text{(III.2)}$$

$$\sigma_c = \frac{E}{1 - \mu^2} (\varepsilon_c + \mu \varepsilon_R) \qquad \text{(III.3)}$$

where

σ_R = radial stress, psi
σ_c = circumferential stress, psi
E = modulus of elasticity, psi
μ = Poisson ratio
ε_R = radial strain, microinches
ε_c = circumferential strain, microinches

III.3 Two-Ply Bellows

Multi-ply bellows flow-induced strain characteristics are significantly different than those of single-ply bellows. Figure 13 shows the flow-induced strain for a 3" single-ply bellows and a 3" two-ply bellows. In each case, the first mode has been flow excited. Note that the alternating strain level for the single-ply bellows is independent of internal pressure, while the strain magnitude and lock-in range for the two-ply bellows is strongly dependent upon internal pressure. For the particular bellows exhibited, it was found that the alternating strain component varies inversely and as a linear function of pressure (see Figure 14).

The most plausible explanation of this phenomena is that Coulomb friction damping is experienced between the plys of the bellows. The Coulomb friction force is directly proportional to the normal force acting in a manner to compress the plys together. To bear out this fact, a two-ply bellows was impulsed into vibration and then allowed to decay. The decay traces are shown in Figure 15 where it is obvious that the damping is a function of the internal pressure which is th mechanism generating the normal force on the convolute sidewalls.

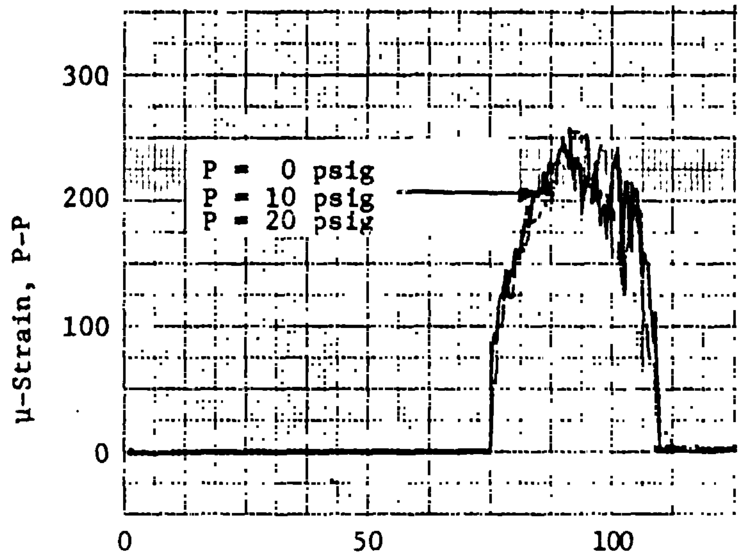

(a) 3" Bellows No. 6 - 1 Ply

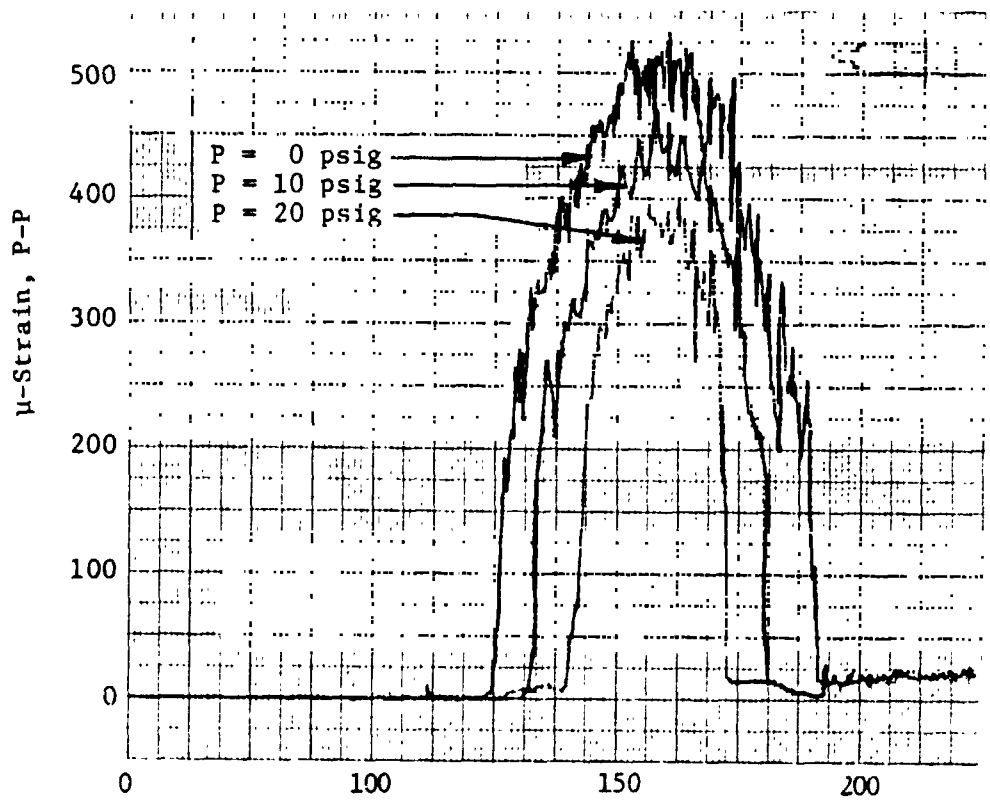

(b) 3" Bellows No. 15 - 2 Ply

FIGURE 13. FLOW INDUCED STRAIN FOR SINGLE AND DOUBLE PLY BELLOWS AS A FUNCTION OF PRESSURE

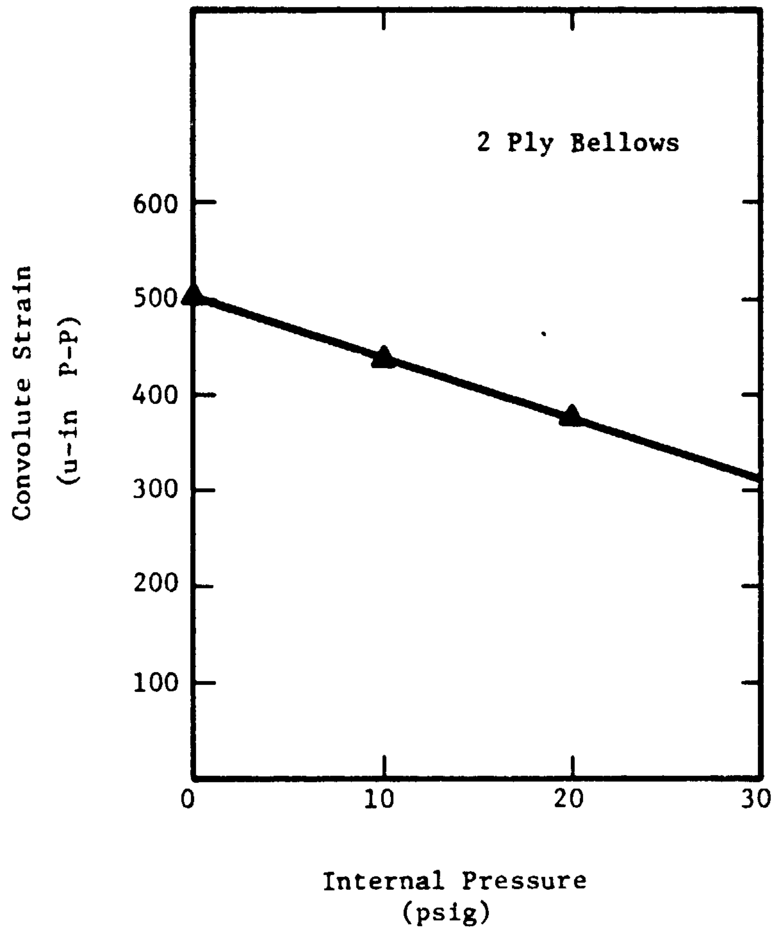

FIGURE 14. CONVOLUTE STRAIN (ALTERNATING COMPONENT)
AS A FUNCTION OF INTERNAL PRESSURE

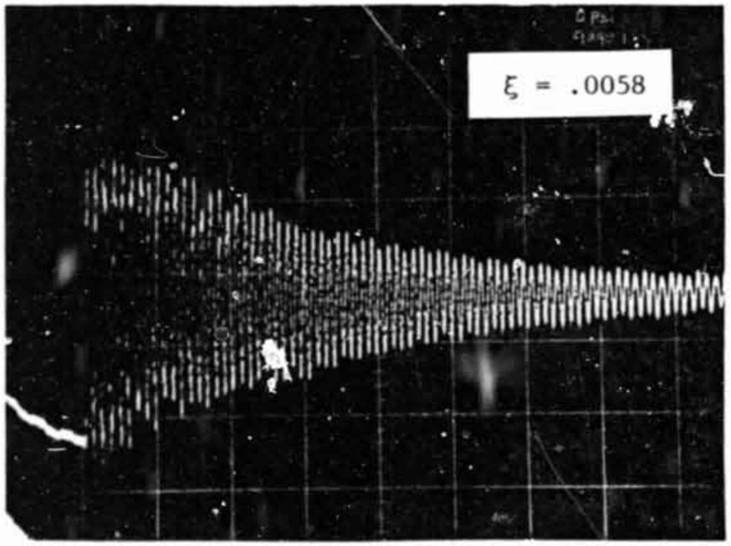

(a) Internal Pressure = 0 psig

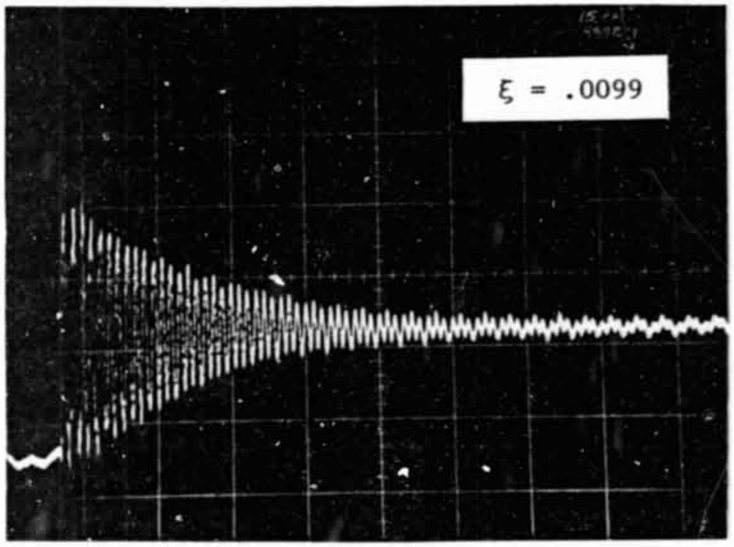

(b) Internal Pressure = 10 psig

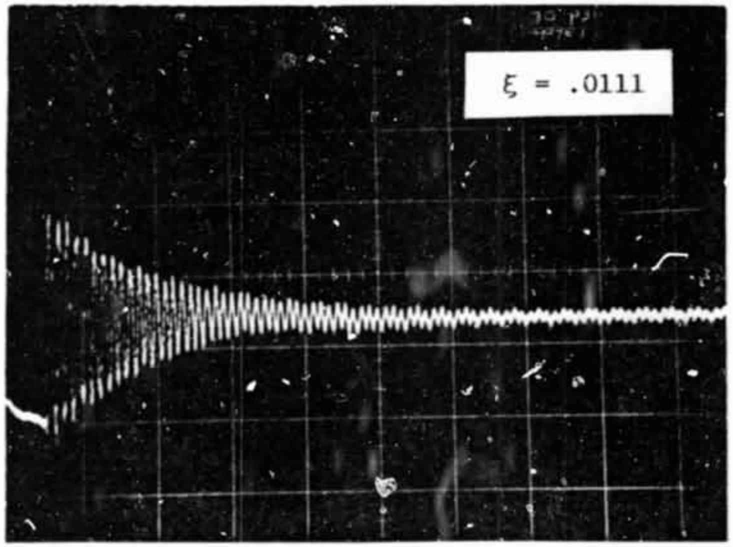

(c) Internal Pressure = 30 psig

FIGURE 15. DAMPING RATIO AS A FUNCTION OF INTERNAL PRESSURE FOR A TWO PLY BELLOWS

The results of these pressure tests suggest that multi-ply bellows vibrate with a lesser magnitude when they are internally pressurized; thus, when single-ply stress calculations are performed on a multi-ply bellows exhibiting the same damping ratio at zero gage internal pressure, the calculated alternating stress component will be conservative (higher stress) for the internal pressurization case. These tests suggest that it may be practical to include damping material between plys as an alternative to including flow liners.

III.4 Convolute Mean Stress

Typically, alternating stresses which are generated by flow induced vibrations are superimposed upon a mean stress which results from internal static pressure and/or bellows axial extension or compression preload forces By observing a typical seven-ordinate fatigue chart (for example, see Figure 23), it is noted that fatigue life is decreased with increasing mean stress magnitude. For example, a bellows that is operated at high static pressures would fail sooner than one operated at lower pressure even if the alternating stress component were equal for both cases. The derivation and use of the seven ordinate curves will be discussed in Section IV; however, the important issue is that the seven ordinate charts allow for mean stress contribution which is not present in cycle-to-failure (S-N) curves.

III.4.1 Internal Pressure Stress

Figure 16 presents the strain data obtained on Bellows No. SwRI-E during an internal pressurization test (ends of the bellows were clamped). The maximum principal stress was calculated for Convolute No. 2 and No. 7 and these stress values compared to the following equation taken from Reference 4.

$$\sigma_p = P/2\ (h/t)^2 \qquad \text{(III.4)}$$

Table V summarizes the results which are evaluated at a pressure of 30 psig. Note, σ_p is a compressive stress on the convolute crown. The table compares the compressive stress, σ_p, to the measured radial stress, σ_{max}.

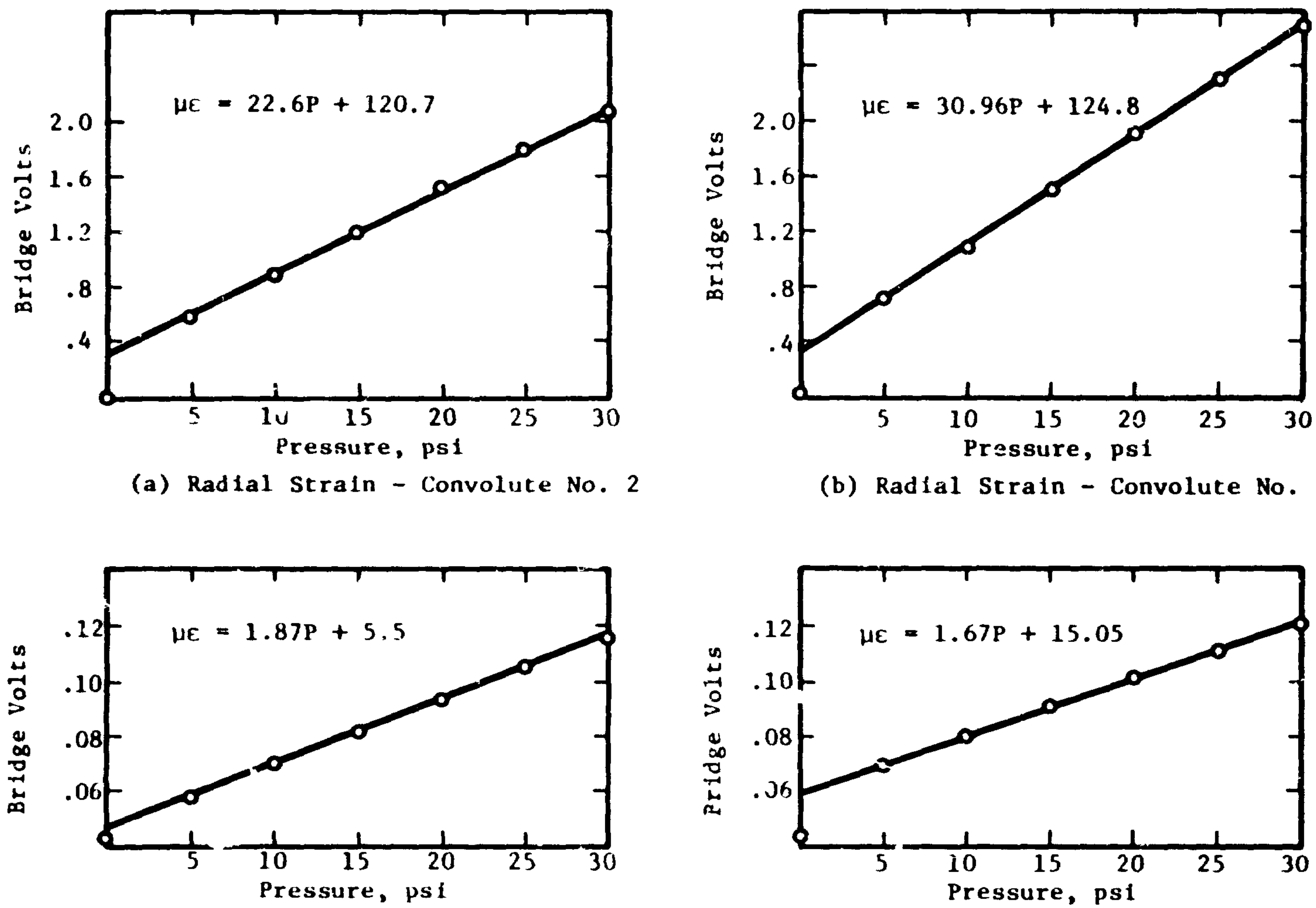

(a) Radial Strain - Convolute No. 2

(b) Radial Strain - Convolute No. 7

(c) Circumferential Strain - Convolute No. 2

(d) Circumferential Strain - Convolute No. 7

FIGURE 16. STRAIN DATA FOR INTERNAL PRESSURE LOADS - 6" BELLOWS NO. E.

TABLE V. INTERNAL PRESSURE STRESS AT 30 PSI

Convolute No.	σ_{max} (KSI)	σ_p (KSI)	% Error
2	-24.9	-21.1	-18
7	-33.0	-21.1	-56

It is noted that Equation (III.4) under-predicts the radial stress (maximum principal) by as much as 56%. It is also noted that the radial stress in the center region of the bellows is higher. Most likely this higher center stress is caused by a "ballooning" effect in the mid-span of the bellows. The conservative approach when considering multi-ply bellows is to assume that the plys are not in complete contact; thus, the effective thickness is less than $N_p \cdot t$. Due to the limited data obtained with respect to ply-coupling effects, it is recommended that the calculated single ply stress be used when multiple plys are incorporated in a design.

III.4.2 Compression Preload Stress

The same 6" bellows that was used for pressure tests was subjected to compression loading test. This is accomplished by placing calibrated weights on the open end edge of a free bellows which is placed in an upright position on a hard surface. This procedure is used to obtain the bellows spring constant K_A; however, in this test the strain gage readings are also recorded. Figure 17 shows the strain data obtained versus compression loads. By noting that

$$\frac{d\ \mu\varepsilon}{d\ell} = (K_A)\left(\frac{d\ \mu\varepsilon}{d\ F_c}\right) \tag{III.5}$$

where $\frac{d\ \mu\varepsilon}{d\ell}$ = change in microstrain per unit change in live length ($\mu\varepsilon$/in)

K_A = bellows spring constant (lb/in) (slope of deflection-load curve)

$\frac{d\ \mu\varepsilon}{d\ F_c}$ = change in microstrain per unit change of load ($\mu\varepsilon$/lb) (slope of strain-load curve),

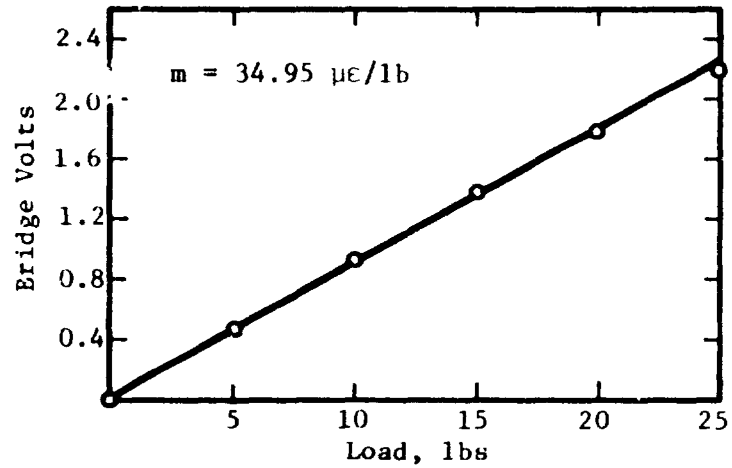

(a) Radial Strain - Convolute No. 2

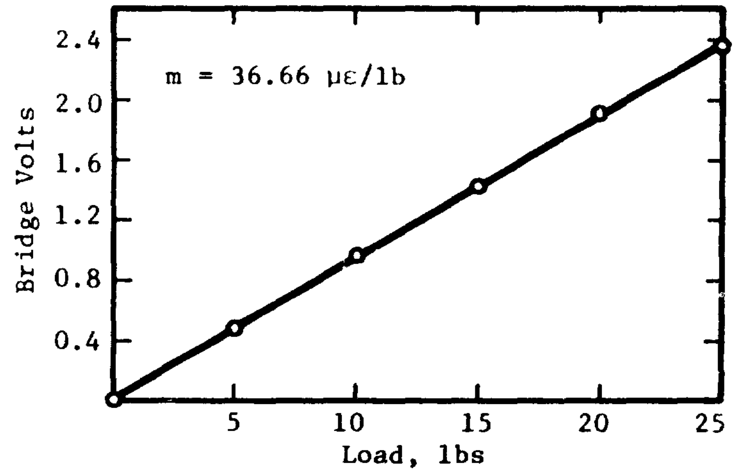

(b)Radial Strain - Convolute No. 7

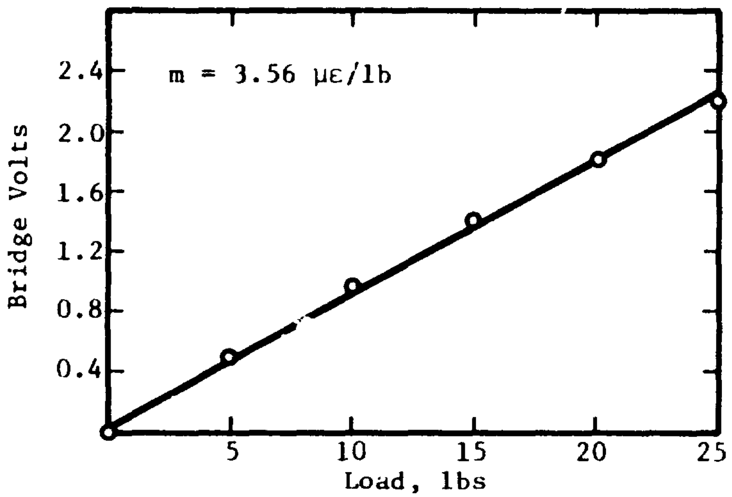

(c) Circumferential Strain - Convolute No. 2

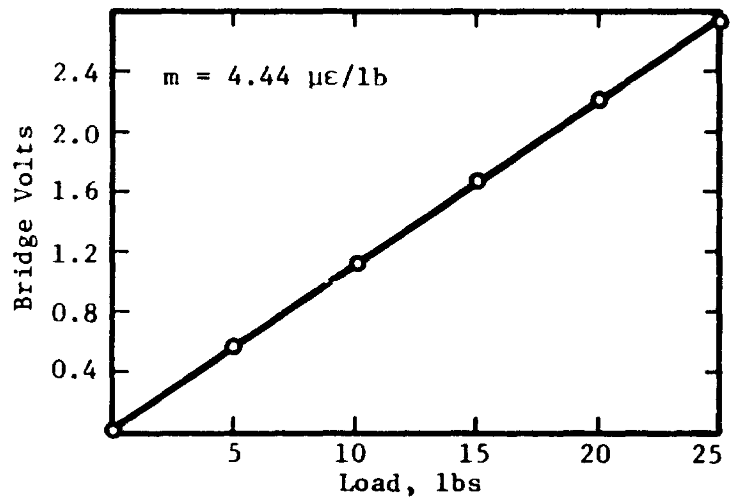

(d) Circumferential Strain - Convolute No. 7

FIGURE 17. STRAIN DATA FOR AXIAL COMPRESSION LOAD - 6" BELLOWS NO. E

it is possible to determine the convolute strain-load characteristic. The deflection-load curve is pres‹ ‹ɜd below (Figure 18) ꞉rom which the bc'lows spring rate, K_A, can be determ ɜd.

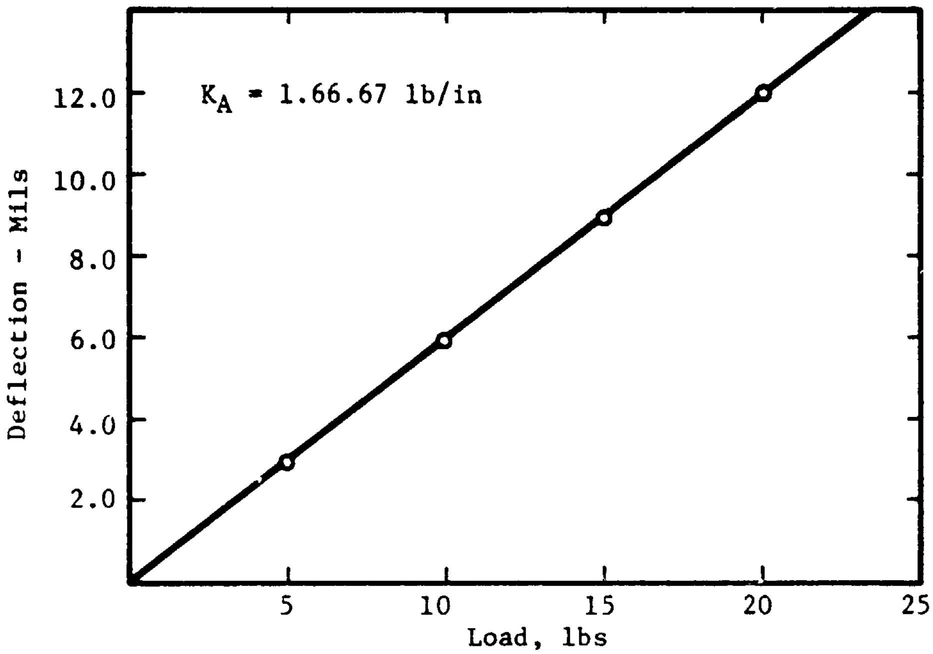

FIGURE 18. LOAD-DEFLECTION CURVE - BELLOWS NO. E

Axial compression stresses as obtained experimentally have been compared to the following equation:

$$\sigma_c = \frac{E\, t\, \Delta}{h^2\, N_c} \tag{III.6}$$

where

σ_c = stress due to compression or extension load ($\sigma_c > 0$ for compression load, $\sigma_c < 0$ for extension load), psi

Δ = deflection of live length, inch.

Table VI has been prepared to compare experimental results with Equation (III.6) for a preload of 20 lbs.

TABLE VI. PRELOAD STRESS AT 20 POUNDS

Convolute No.	σ_{max} (KSI)	σ_c (KSI)	% Error
2	22.96	22.09	-3.9
7	24.21	22.09	-9.6

It is observed that Equation (III.6) gives reasonable accuracy and it provides a means for relating relative convolute motion to convolute radial stress level. Equation (III.6) can be used in a dynamic situation; however, it must be emphasized that the deflection value used is relative to adjacent convolutes.

Equation (III.6) is easily modified to incorporate preload rather than deflection if the bellows spring constant is known.

$$\Delta = F_c/K_A$$

thus,

$$\sigma_c = \frac{Et\ F_c}{h^2\, N_c\, K_A} \tag{III.7}$$

III.4.3 <u>Compression Preload With Internal Pressure</u>

A schematic illustrating the nature of the radial fiber strains in the region of the bellows root and crown is shown in Figure 19. The strains are the result of bending moments generated in root and crown. For analytical considerations, the bellows is envisioned to be restrained by the external piping for the case of internal pressurization. It is immediately obvious from Figure 19 that while it may be possible to reduce the crown radius stress state by simultaneous compression loading and internal pressurization, the root stresses are intensified by the combination loading. Therefore, the root stress may be estimated as follows:

$$\sigma_{cp} = \sigma_p + \sigma_c \tag{III.8}$$

where σ_{cp} = combined stress due to pressure and compression load. By substitution of Equation (III.7) and (III.4) into (III.8),

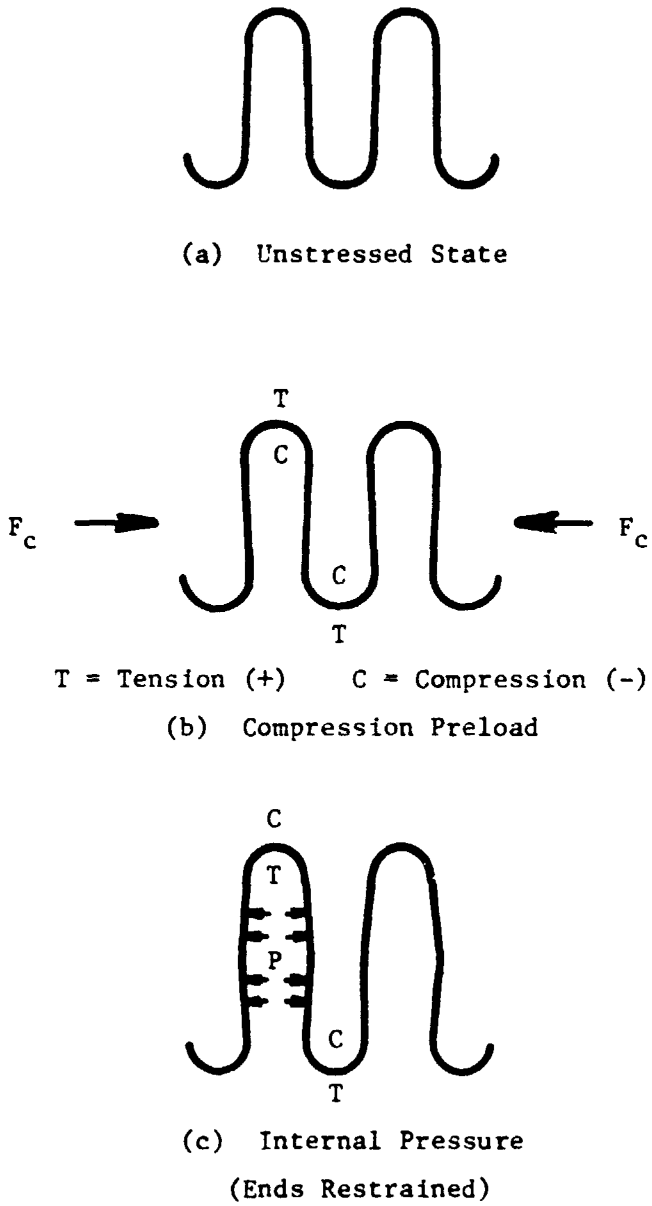

FIGURE 19. NATURE OF FIBER STRAINS

$$\sigma_{cp} = P/2\ (h/t)^2 + \frac{Et\ F_c}{h^2\ N_c\ K_A} \qquad \text{(III.9)}$$

III.5 Convolute Alternating Stress and Displacement

A series of three-inch diameter bellows were flow tested to validate several assumptions made in earlier studies (Reference 1). The vibratory peak stress in the bellows convolute was assumed to be given by

$$\sigma_p = \frac{C_s\ Et\ X}{h^2} \qquad \text{(III.10)}$$

where C_s is a geometric stress factor and the other terms are as defined earlier. The Reference 1 work utilized a single point strain gage to infer displacement and stress which is difficult under the best of test conditions. In the present study, stress was measured via a biaxial gage arrangement and convoluted displacement was obtained independently via a displacement probe (see Appendix B for details).

By assuming a mode shape over the first quarter wavelength of the form

$$X = X_o/2\ \left[(N/\ell)y + \sin\ (N\pi y/\ell)\right] \qquad \text{(III.11)}$$

where X denotes the axial absolute displacement of a given point along the bellows defined by the axial position coordinate y, we may determine the relative displacement by differentiating Equation (III.11) with respect to y. Thus,

$$\Delta\delta = X_o/2\ \left[(N/\ell) + N\pi/\ell\ \cos\ (N\pi y/\ell)\right] \qquad \text{(III.12)}$$

The above method was used to convert absolute displacement, δ, data into equivalent relative displacement, $\Delta\delta$.

A summary of the deflection and stress results are shown in Table VII for each test specimen at the first, second, and third modes and a summary of the damping characteristics is shown in Table VIII.

Calculated alternating stress levels as determined by Equation (III.10), have been correlated with actual measurements. Results shown in Figure 20 indicate that C_s may be considered to equal unity.

TABLE VII. THREE-INCH BELLOWS DEFLECTION AND STRESS RESULTS

Specimen No.	Mode No.	V_F, fps	2nd Convolute		
			δ, mills	$\Delta\delta$, mills	σ_{Alt}, ksi
4	1	5.40	4.0	2.33	2.93
	2	10.80	15.0	3.21	8.02
	3	15.89	22.6	3.58	8.94
6	1	4.18	0.8	0.40	0.765
	2	8.35	4.8	1.65	3.67
	3	12.53	7.8	1.93	4.59
15	1	7.26	4.0	1.96	2.82
	2	14.52	14.0	4.71	7.84
	3	21.79	21.0	3.34	8.51

TABLE VIII. THREE-INCH BELLOWS DAMPING CHARACTERISTICS

Specimen No.	Mode No	f_r, Hz	$\Delta f_{.707}$,Hz	Q	ξ
4	1	120	2.0	60	.0083
	2	234	3.0	78	.0064
6	1	133	.55	242	.0021
	2	255	1.7	150	.0033
15	1	147	1.8	82	.0061
	2	288	3.8	76	.0066

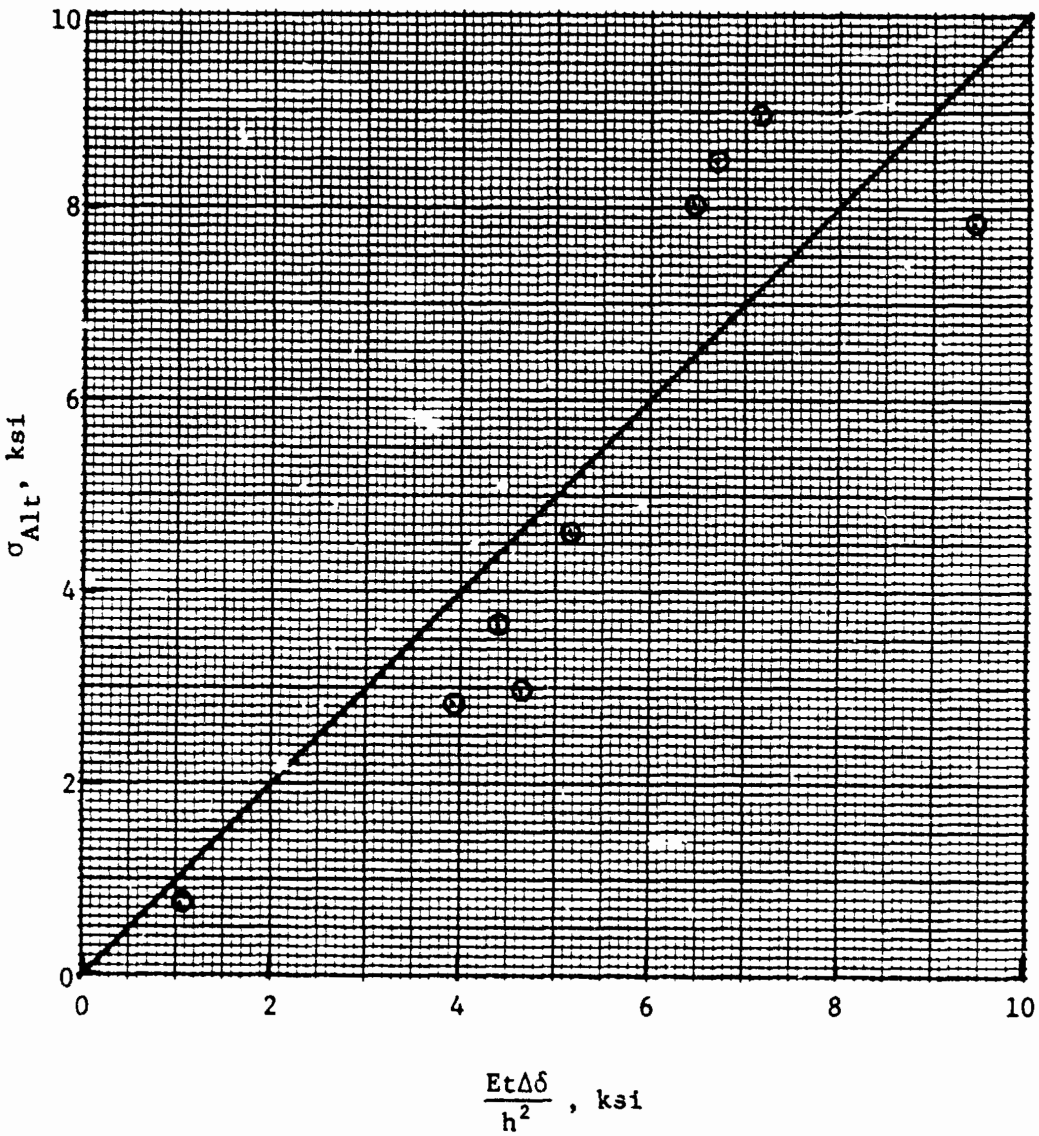

FIGURE 20. ALTERNATING STRESS VERSUS DEFLECTIONS

For all single ply bellows tested, the alternating stress component was observed to be insensitive to internal pressure variation. Tests were conducted at pressures of 0, 10, 20 psig over the first three modes of excitation.

III.6 Recommended Stress Prediction Equation

III.6.1 Alternating Stress

Two methods are available for calculating the alternating stress component. The Stress Indicator may be used as a predictor of actual stress for single ply bellows by incorporating a factor 2 into the S.I. equation over the first three modes of vibration, or

$$\sigma_{alt} = 2 \frac{C_F^* N_c}{N N_p} (h/t)^2 (1/2 \rho V_{crit}^2) \tag{III.13}$$

The second method is merely a refinement of the above method. The stress envelope factor may be applied to the value of the S.I. calculated for mode 1, or

$$\sigma_{alt_N} = S.E._1 \left(\frac{.00635}{\xi}\right) F_N \tag{III.14}$$

where $F_2 = 2.75$

$F_3 = 3.05$

The second method requires more detailed knowledge of the bellows; however, it provides a means to infer the effects of combined fluid and structure damping.

III.6.2 Convolute Mean Stress

Significant errors have been observed in the measured and calculated stress values that relate to internal pressure while axial extension of compression preloads may be more accurately modeled. Therefore, the recommended mean stress model is

$$\sigma_{mean} = P (h/t)^2 + \left(\frac{Et}{h^2 N_c}\right) |\Delta| \tag{III.15}$$

where Δ is the total live length extension or compression displacement. For the multi-ply case, it has been assumed that the plys do not fully couple; hence, the calculations for the single ply are applied to multi-ply designs. Due to the inaccuracy of the simple pressure-stress model, the .5 factor has been deleted.

III.6.3 Combined Stress

The maximum stress developed is composed of the two additive components, or

$$\sigma_{max} = \sigma_{alt} + \sigma_{mean} \tag{III.16}$$

and by substitution of Equations (III.13) and (III.15), the proposed combined elastic stress model is

$$\sigma_{max} = \left(\frac{Et}{h^2\ N_c}\right) |\Delta| + (h/t)^2 \left[P + \frac{2C_F^*\ N_c}{N\ N_p}\ P_d\right] \tag{III.17}$$

III.7 Material Hardness Properties

A 3" bellows with 13 convolutes was sectioned and prepared for microhardness testing. This is accomplished by cutting axial strips of approximately 1/2" wide that contain several convolutes. Subsequently, these sections are imbedded in an epoxy molding compound, then the compound and bellows specimens are ground until their surfaces exhibit a highly polished finish. The bellows specimen is placed into a Diamond Pyramid Hardness (DPH) testing apparatus where a specific sized diamond needed is allowed to penetrate the bellows surface. The driving weight used is 10 kg. By an appropriate measuring technique, the dimensions of the penetration, rhomboid shaped, are measured and then converted into a DPH number.

Figure 21 shows a general bellows section. Three measurements were taken at the approximate locations shown in the figure; therefore, 24 data points per convolute were obtained. The results are tabulated in Table IX.

Upon careful review of the data, several observations are apparent which include the following:

1. Global averaging of the convolute center region produced a lower average hardness than found in global averaged outer edges.
2. Zonal averaged hardness numbers in the "inside diameter" region exhibits hardness close to slightly below the global average.
3. The "outer diameter" region exhibits hardness numbers significantly <u>larger</u> than the global averages.
4. The "straight wall" region exhibits hardness numbers significantly <u>lower</u> than the global averages.

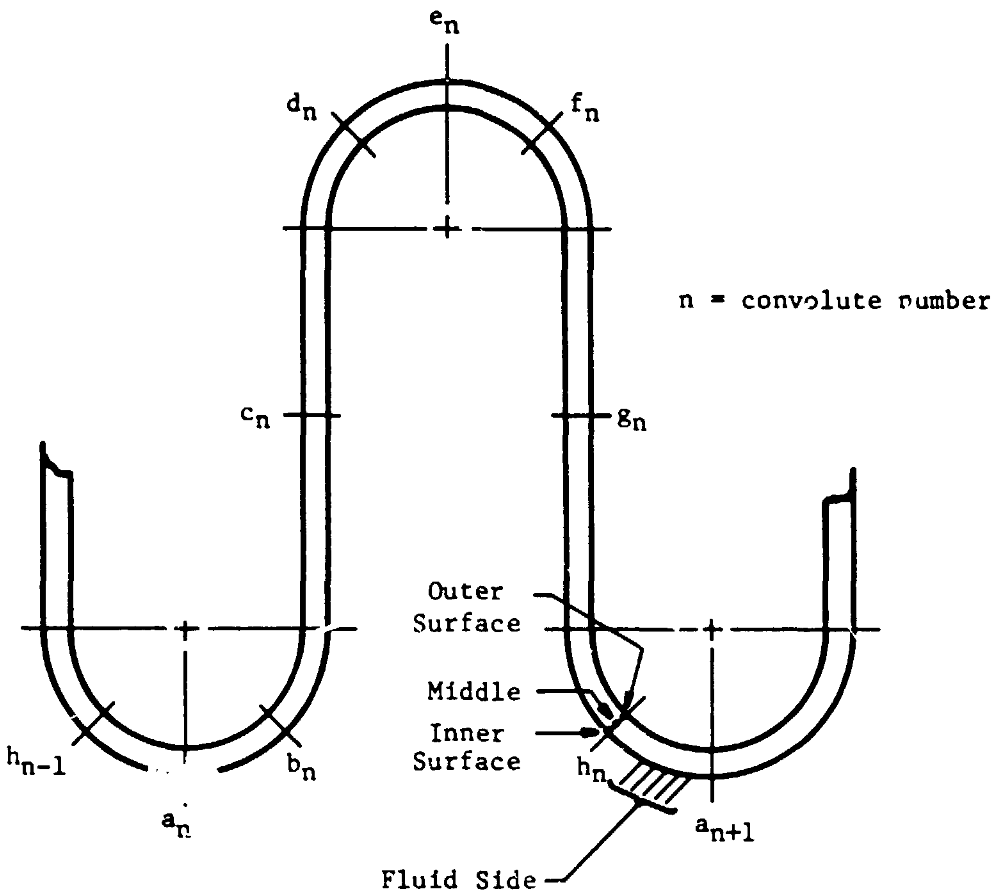

FIGURE 21. CROSS SECTION OF BELLOWS SHOWING LOCATIONS OF HARDNESS MEASUREMENTS

TABLE IX. HARDNESS READINGS

LOCATION	DIAMOND PYRAMID HARDNESS		
	CONVOLUTIONS 1, 2, & 3		
	OUTER SURFACE	CENTER	INNER SURFACE
h_1	224	213	225
a_2 (inside diameter)	241	235	246
b_2	232	242	242
c_2 (straight wall)	239	217	232
d_2	268	272	264
e_2 (outer diameter)	270	268	284
f_2	266	268	258
g_2 (straight wall)	239	224	231
h_2	241	226	241
a_e (inside diameter)	235	218	235
mean (μ)	245.5	240.1	245.8
Std. Dev. (σ)	16.35	21.5	18.06
	CONVOLUTIONS 6, 7, & 8		
h_6	236	263	283
a_7 (inside diameter)	236	253	252
b_7	257	268	247
c_7 (straight wall)	235	250	250
d_7	281	279	285
e_7 (outer diameter)	273	265	297
f_7	285	279	273
g_7 (straight wall)	236	232	236
h_7	281	253	261
a_8 (inside diameter	265	257	250
b_8	268	250	273
mean (μ)	259.4	259	264.3
Std. Dev. (σ)	20.3	13.78	19.15

TABLE IX. HARDNESS READINGS (Cont'd)

LOCATION	DIAMOND PYRAMID HARDNESS		
	CONVOLUTIONS 11, 12, & 13		
	OUTER SURFACE	CENTER	INNER SURFACE
h_{11}	236	230	236
a_{12} (inside diameter)	221	247	263
b_{12}	233	239	261
c_{12} (straight wall)	247	236	243
d_{12}	275	275	273
e_{12} (outer diameter)	313	275	290
f_{12}	300	294	285
g_{12} (straight wall)	243	236	236
h_{12}	267	265	267
a_{13} (inside diameter)	261	265	255
b_{13}	275	268	257
mean (μ)	261	257.3	260.54
Std. Dev. (σ)	286	20.73	17.96

5. Outer diameter zonal averaged DPH numbers ranged from 274 to 293 which corresponds to a Rockwell Hardness range of 26C to 29C.

6. Inner diameter zonal averaged DPH numbers ranged from 229 to 260 which corresponds to Rockwell readings in the range of 96B to 24C.

III.8 Conclusions

1. The outer diameter region exhibits a yield stress of approximately 132,000 psi whereas the inner diameter region exhibits a yield stress of approximately 100,000 psi. These yield values are somewhat lower (30%) than those reported in Reference (13); however, it is speculated that the hydroforming process work hardens to a lesser extent than the rolling process.

2. Failures most often occur in the root or crown region; therefore, in view of the hardness data, it can be concluded that failures are not the result of material weakness in the failure region.

IV. FATIGUE LIFE

IV.1 Crack Propagation Model

A bellows fatigue life model was developed based on the assumption that crack propagation in the convolute wall is the failure mechanism. It was further assumed that the crack was initiated by a pre-existing surface or material flaw. The state of stress in the bellows wall was taken to be the sum of the mean stress due to internal fluid pressure plus a cyclic bending stress that is associated with convolute deflection in any given mode of excitation. The stress model used here is different than that used in Section III; however, the features of the crack modeling and general results are valid.

The mean internal pressure stress is,(12,13)

$$\sigma_p = p/2\ (h/t)^2 \tag{IV.1}$$

where
p = internal pressure,
h = root-to-crown height, and
t = bellows wall thickness ($N_{ply} \times t_{ply}$)

Superimposed onto this steady state stress is a cyclic, deflection-related bending stress that is caused by the flow induced vibration of the bellows convolutes at given excitation mode. The peak-to-peak amplitude of this cyclic stress component is given by,(12,13)

$$\Delta\sigma = \frac{2(1.5)\ Et}{\lambda^{1/2}\ h^{3/2}} \left(\frac{\Delta}{2\ N_c}\right) \tag{IV.2}$$

where
E = Young's modulus
λ = convolute pitch
Δ/N_c = flow-induced convolute deflection

The deflection per convolute is calculated from Reference 1,

$$\frac{\Delta}{N_c} = \frac{C_m \rho V^2\ A_p}{g2\ K_A}\ (C_F Q) \tag{IV.3}$$

where
ρ = fluid density
V = critical flow velocity as a function of mode number
A_p = $\pi/2\ h\ (D_i + D_o)$
D_i, D_o = bellows inside and outside diameter, respectively
K_A = bellows spring rate
$C_F Q$ = force amplification factor from Figures 4 and 5
C_m = bellows mode factor.

The bellows mode factor, C_m, is of the form[14]

$$C_m = \frac{1}{8N}\left[\frac{N}{N_c} + \sin\left(\frac{\pi}{2}\frac{N}{N_c}\right)\right] \tag{IV.4}$$

where N = mode number

N_c = number of bellows convolutes.

Thus, Equations (IV.1) through (IV.4) define the mode-dependent state of stress in the bellows wall. This state of stress can be illustrated schematically as shown in Figure 22. In this figure, tensile stresses are positive. Depending on the mode number and the magnitude of the mean stress, the minimum stress can be compressive, in which case the sign of the stress is negative.

If a crack is initiated on the bellows surface, the rate at which it will propagate into the wall thickness is governed by

$$\frac{da}{dn} = C\left(\frac{Y\Delta\sigma\sqrt{a}}{1-R}\right)^m \tag{IV.5}$$

where a = crack length

n = number of imposed stress cycles

$\Delta\sigma$ = cyclic stress range, Equation (2)

C,m = curve fit coefficients that describe the experimental crack growth rate as a function of stress intensity factor, which is the expression within the brackets in Equation (IV.5). These parameters are dependent upon the bellows material.

The factor, R, accounts for the mean stress effect, and it is defined as

$$R = \frac{\sigma_p - \Delta\sigma/2}{\sigma_p + \Delta\sigma/2} \tag{IV.6}$$

It is worth noting that when σ_p is equal to zero (no pressure stress), the value of R is -1.0, which describes a fully reversed state of stress. The quantity Y, which is an explicit function of the crack length, is a geometric correction factor that accounts for the decrease in load bearing area during crack propagation. As such, Y can be satisfactorily appaoximated by a second order polynomial

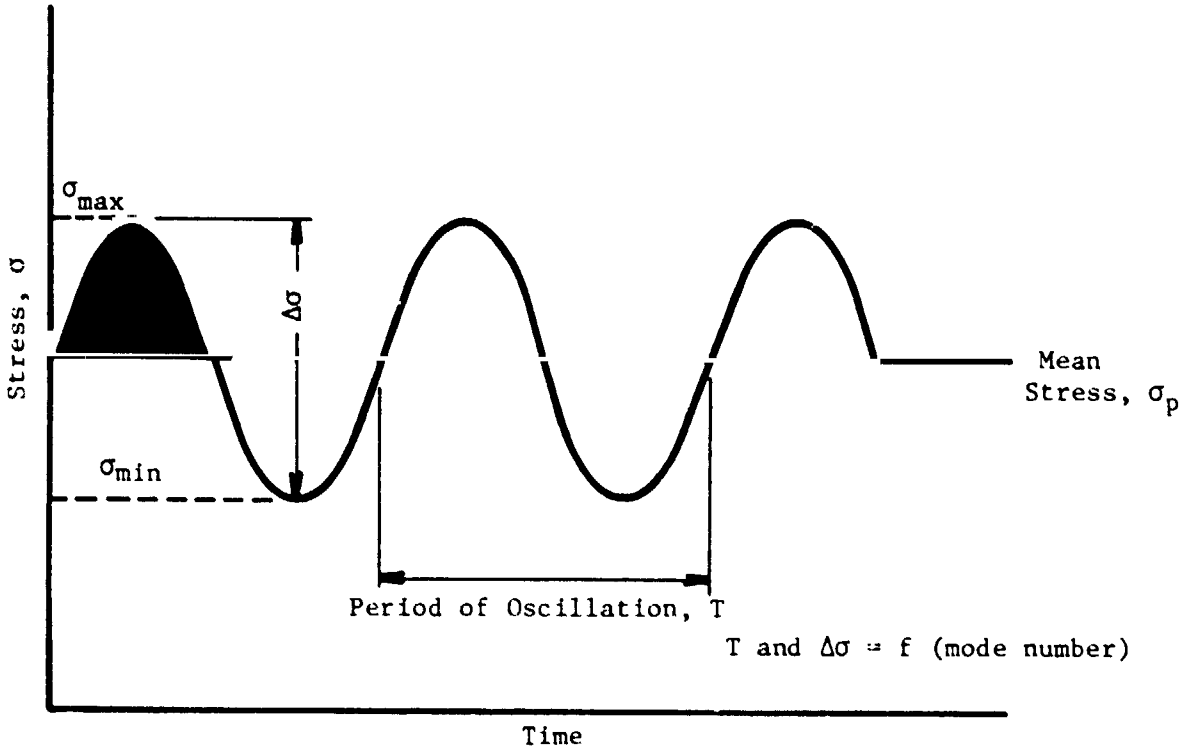

FIGURE 22. DEFINITION OF BELLOWS STRESSES

$$y = \alpha(a/t)^2 + \varepsilon \qquad \text{(IV.7)}$$

where α, ε = curve fit coefficients.

Combining Equations (IV.5) and IV.7), and separating variables, yields

$$N_f = \frac{(1-R)^m}{C(\Delta\sigma)^m} \int_{a_i}^{a_c} \frac{da}{[\alpha(a/t)^2 + \varepsilon]\ a^{m/2}} \qquad \text{(IV.8)}$$

where N_f = fatigue life

a_i = initial material flaw size

a_c = critical crack length at which failure occurs.

The failure model, Equation (IV.8), is valid only fro values of $a_c \leq t/2$.

Evaluation of the Model

The fatigue life integral and its supporting equations were programmed for solution on the CDC6600/Cyber 74 system. A trapezoidal integration scheme was used to evaluate the definite integral in Equation (IV.8). A listing of the computer program, FATLIF, is contained in Appendix E.

Since prediction of fatigue life is currently accomplished by a stand-alone program, it was necessary to first exercise program "Bellow" to generate critical flow excitation velocities for a given bellows configuration. The essential input-output data for program Bellow is summarized in Table X. The reader will be able to identify the bellows and fl· ..d input parameters that are common to the FATLIF program. Excitation velocities are shown for the first four modes. It should be noted that the fatigue life program accepts fluid pressure in psia rather than psig.

To complete the input data for program FATLIF, it was necessary to specify numerical values for C, m, α, ε, a_i, and a_c. The constants, α and ε, were obtained by curve-fitting the correction factors for a single edge-notched strip that are presented in Table 4 of Reference 14. The results of the manipulation yielded

$$\alpha = 6.79$$

$$\varepsilon = 1.12$$

TABLE X

INPUT/OUTPUT DATA FOR PROGRAM BELLOW

BELLOWS PARAMETERS (INPUT)

SIGMA(CONVOLUTE WIDTH, IN)	.158
LAMBDA(CONVOLUTE PITCH, IN)	.269
H(MEAN DISC HEIGHT, IN)	.340
T(CONVOLUTE THICKNESS/PLY, IN)	.008
DI(INSIDE DIAMETER, IN)	4.000
DO(OUTSIDE DIAMETER, IN)	4.828
NC(NUMBER OF CONVOLUTES)	9.000
NPLY(NUMBER OF PLIES)	3.000
E(YOUNG'S MODULUS, LB/SQ.IN)	2.9400E+07
KA(OVERALL SPRING RATE, LB/IN)	373.366
RHOM(MATERIAL DENSITY, LB/CU.IN)	.282

FLUID PARAMETERS (INPUT)

P(PRESSURE, PSIG)	100.000
TEMP(TEMPERATURE, DEG F)	70.000
RHOF(FLUID DENSITY, LB/CU.IN)	3.6111E-02
NFLUID(1=GAS, 2=LIQUID)	2

THEORETICAL PERFORMANCE (OUTPUT)

		Flow Excitation Range, ft/sec		
Mode	Hz	Lower	Critical	Upper
1	191	7.0	9.8	16.2
2	365	13.4	18.7	30.9
3	523	19.2	26.8	44.3
4	666	24.4	34.1	56.4

Specification of the values of C and m was impeded by the lack of basic crack propagation data in the open literature for the bellows materials of interest, i.e., Inco 718, 21-6-9 and 321. As an alternative, for evaluation purposes only, the following values of C and m were obtained from Reference 15 for Type 316 stainless steel.

$$C = 7 \times 10^{-16}$$

$$m = 6.5$$

The number of fatigue cycles needed to effect failure is strongly affected by the magnitude of a_i and a_c. In evaluating the model, the initial flaw size, a_i, was chosen to be 0.001 inch. This value is believed to be representative of a typical surface flaw. The crack length at failure, a_c, was taken to be $t/2$, the validity limit of the model.

Based upon the above inputdata, fatigue life predictions were made for the specific bellows geometry, fluid properties, and critical excitation velocities in Table X. The results are summarized in Table XI. For this example problem, the following observations can be made on the validity of the model.

(1) The cyclic stress range, $\Delta\sigma$, increases with mode number because the product of flow excitation velocity and dynamic amplification factor is an increasing function of mode number.

(2) The maximum bending strews is tensile at all mode numbers. The minimum stress is tensile initially but becomes compressive as mode number increases. In the presence of internal pressure, a fully-reversed stress field is not achieved.

(3) For this example, in which Type 316 stainless steel was employed, the maximum tensile stress in the first three modes did not exceed the material yield point of 42 ksi.[16] In the fourth mode, the maximum tensile stress exceeded the material yield point.

(4) In this example, the model predicts high cycle fatigue when a_i and a_c are 0.001 and 0.012 inch, respectively.

TABLE XI

PREDICTED FATIGUE LIFE FOR A TYPE 321
STAINLESS STEEL BELLOWS

Mode No.	σ_p (psi)	$\Delta\sigma$ (psi)	Frequency (Hz)	Fatigue Life (cycles)
1	15,144	23,808	191	1.76×10^{12}
2	15,144	33,024	365	6.34×10^{11}
3	15,144	45,684	523	1.94×10^{11}
4	15,144	98,783	666	6.19×10^{9}

At this point, realization of the full utility of this approach to fatigue modeling is impeded by:

(1) The lack of basic crack propagation data for the three materials of interest. Currently, the fatigue data that are available from the materials manufacturers were obtained using fully-reversed stress fields at room temperature. What is needed are crack propagation tests which yield crack growth rates as a function of stress intensity factor and mean stress over the range of temperatures of interest.

(2) A correlation between the fatigue life as predicted by the crack propagation model adn experimental fatigue life of actual bellows in a common temperature and stress environment.

(3) The lack of an experimental definition of the flaw size, a_i, that is needed to initiate and propagate a crack and a_c, the crack length at which failure occurs.

VI.2 Fatigue Curves

Due to the limitations posed by the crack growth model, an alternate approach was developed to predict bellows life. Seven ordinate charts were developed (Figures 23, 24, and 25) from data listed in References 17 through 27. The materials studied included 347 SS (a close substitution for 321 SS), Alloy 21-6-9, and Inco 718. Data reviewed were mainly in the form of "cycles to failure" or S-N curves for various R values and for temperatures of 70°F and -423°F.

Seven-Ordinate charts relate stress and stress ratios to cycle life. Most of the seven-ordinate data is based upon data banks maintained by the Department of Defense and the Federal Aviation Agency if its source is contained in the MIL-HDBK-5B.

Seven-ordinate charts are convenient to use and they relate fatigue life in terms of mean stress which could be an important factor when predicting bellows life. Design or analysis parameters can be specified as stress amplitude, mean stress, maximum or minimum stress, cycle life, R-values, and A-values. (The A value is defined as the stress amplitude divided by the

STAINLESS ALLOY 21-6-9

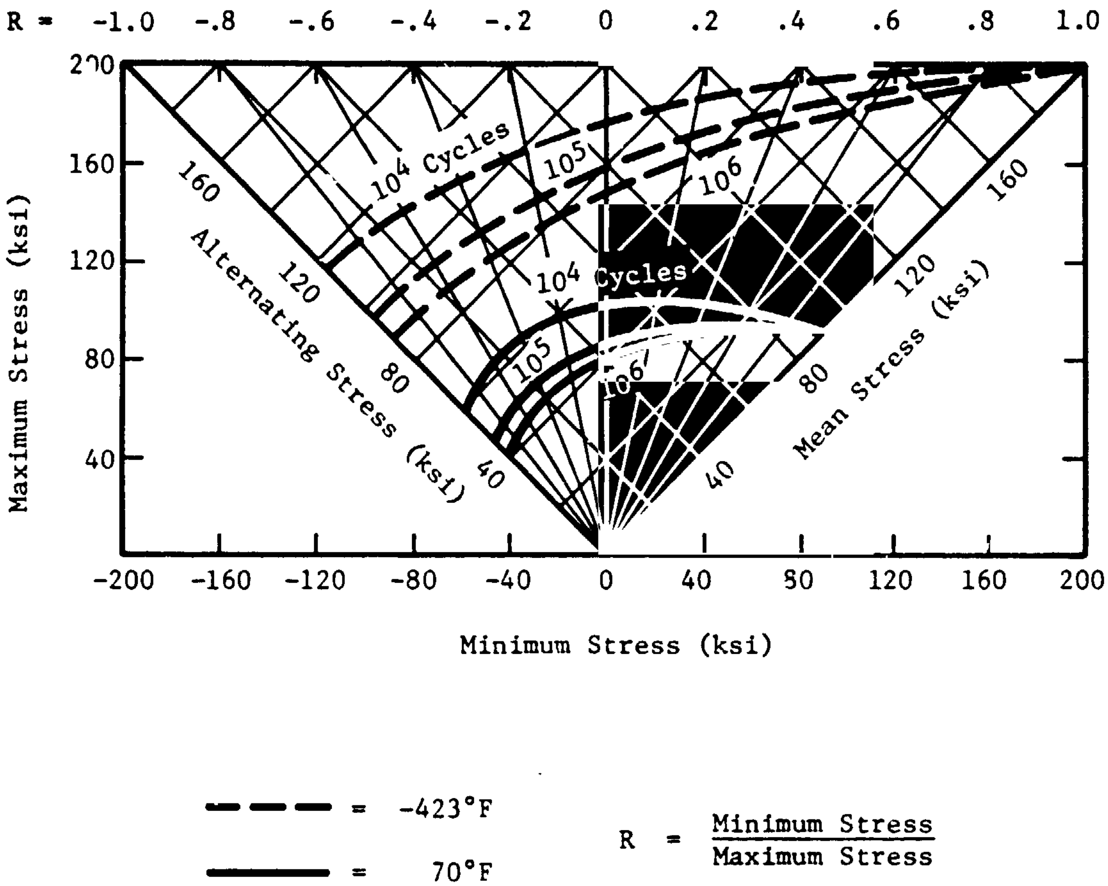

FIGURE 23. SEVEN-ORDINATE CHART FOR ALLOY 21-6-9

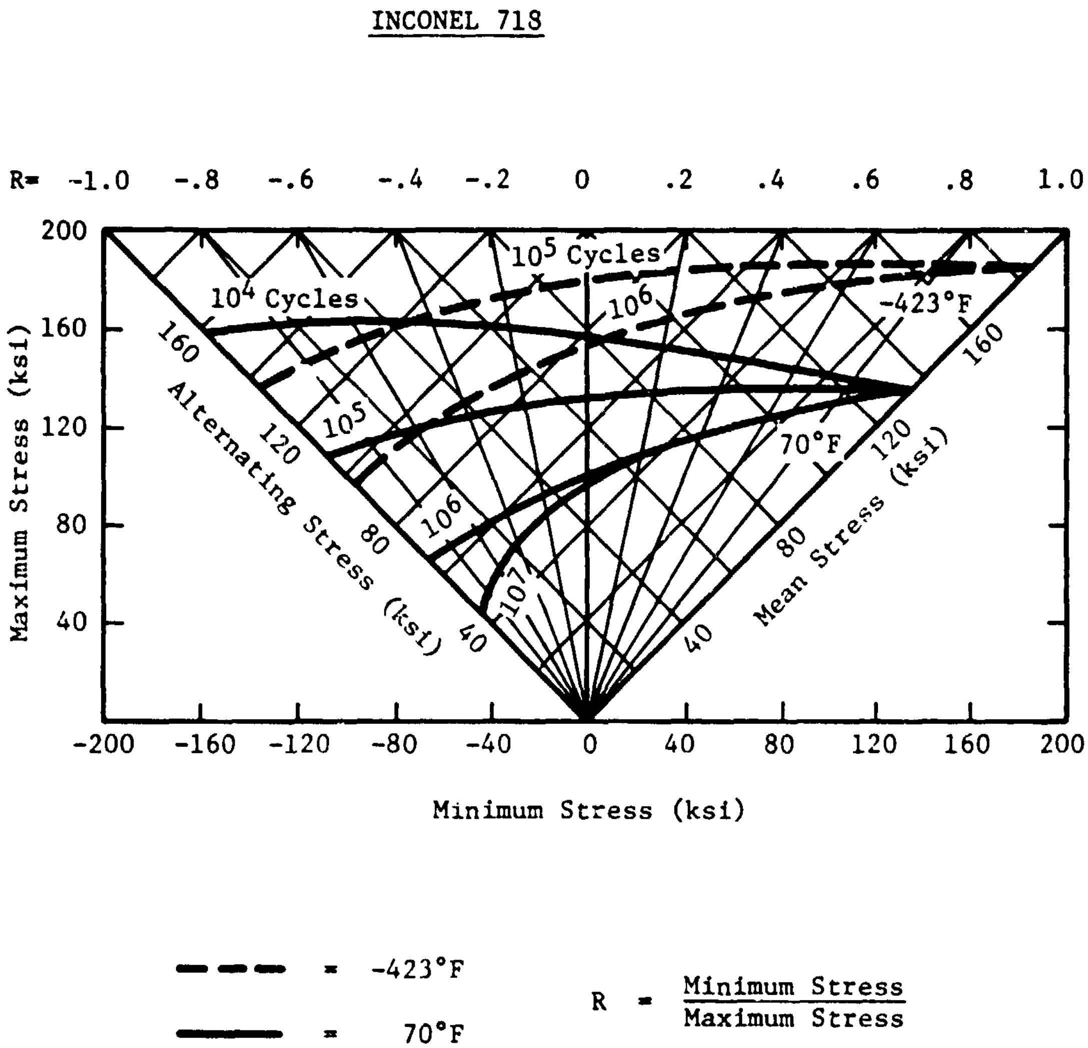

FIGURE 24. SEVEN-ORDINATE CHART FOR INCONEL 718

347 STAINLESS STEEL

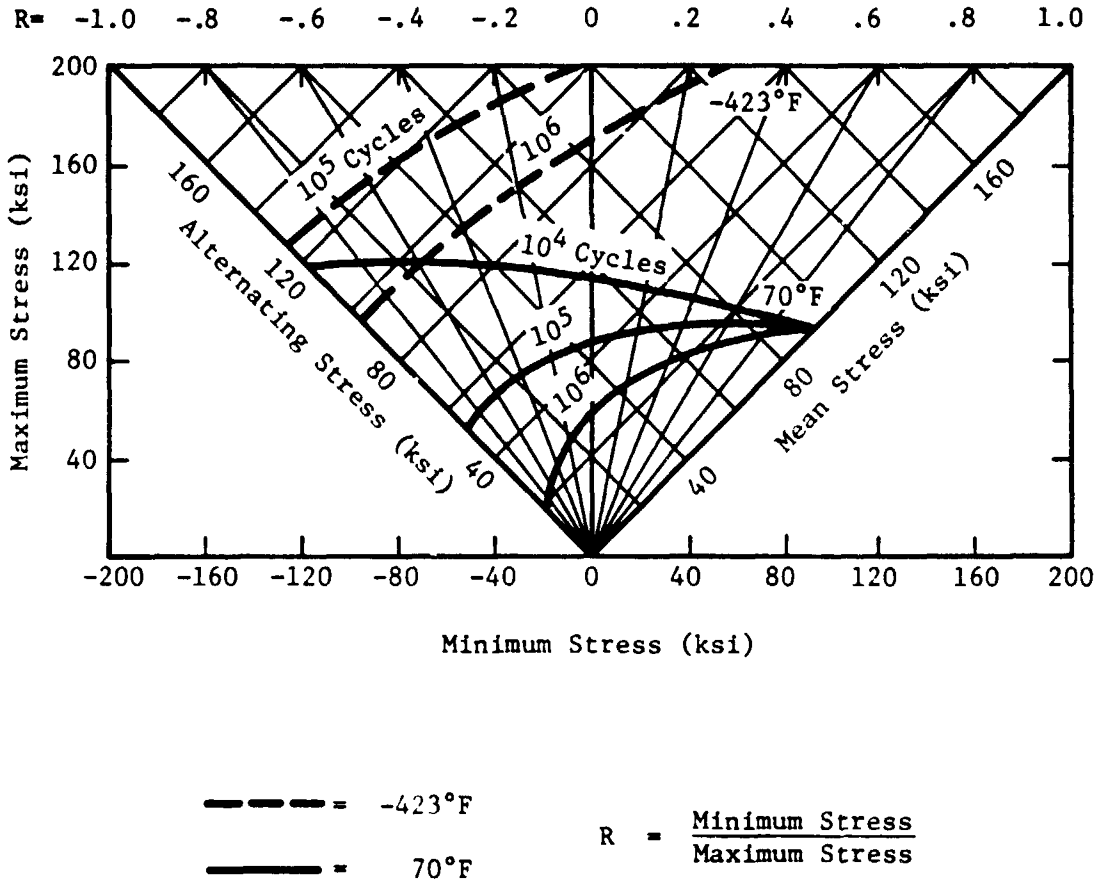

FIGURE 25. SEVEN-ORDINATE CHART FOR 347 SS

mean stress.) To determine the fatigue life, only three parameters are required. These parameters are usually determined from the bellows stress analysis.

The seven-ordinate fatigue data is built into the computer program listed in Appendix A. Each constant life cyci curve is modeled as a power law, or

$$C_j = B\,\sigma_{alt}^{\ m}$$

where C_j is a constant life value for j mean stress. Curves are developed for mean stress levels of 0, 20, 40, 60, and 80 ksi. The alternating stress component, σ_{alt}, is in the units of ksi. Simple linear interpolation may be used for intermediate values.

The seven-ordinate curves are applicable for fatigue life predictions once the stress levels have been determined; however, stress indicator values may be used directly as a calculated alternating stress value with reasonable accuracy even though the stress indicator's intended use was to predict fatigue life with the aid of data presented in Figure 6.

REFERENCES

1. Gerlach, C.R., Schroeder, E.C., Bass, R.L., III, Holster, J.L. "Bellows Flow-Induced Vibrations and Pressure Loss," Contract No. NAS8-21133 Southwest Research Institute, April 1973.

2. Kleppe, S.R., "High Pressure Expansion Joint Studies" ASME Petroleum Mechanical Engineering Conference, New Orleans, Sept. 25-28, 1955, Paper No. 55-PET-10.

3. Turner, C.E., and Ford, H., "Stress and Deflection Studies of Pipeline Expansion Bellows," Proceedings of the Institute of Mechanical Engineering, pp 596-552, Vol. 171, No. 15, 1957.

4. Feely, F.J., Jr., and Goryl, W.M.. "Stress Studies On Piping Expansion Bellows," Journal of Applied Mechanics, Paper No. 44-APM-22.

5. Samans, Walter, "Endurance Testing of Expansion Joints," ASME Paper No. 54-A-103.

6. Haringy, J.A., "Instability of Bellows Subjected to Internal Pressure," Philips Res. Report 7, 189-196, 1952.

7. Laupa, A., and Weil, N.A., "Analysis of U-Shaped Expansion Joints," Journal of Applied Mechanics, Transactions of the ASME, pp 115-123, March 1962.

8. Sack, L., "Avoiding Fluid-Line Failure in Bellows and Convoluted Tubing," Machine Design, May 27, 1971.

9. Baylac, G., et al., "Calculation of Acoustical Resonances in Irregular Cavities with Application to Noise-Induced Stress in Expansion Joints," ASME Paper No. 75-DET-64.

10. T. M. McCrary, "Evaluation of Inconel 718 Bellows Material," SD73-SA-0014, Rockwell International Space Division, Mar. 1973.

11. "Effect of Surface Irregularities on Bellows Fatigue Life," R7250 Rocketdyne, NASA Contract NAS8-19541.

12. M. W. Kellogg Co., <u>Design of Piping Systems</u>, Second Edition, John Wiley and Sons, Inc., 1956.

13. "Bellows Joint," <u>Machine Design</u>, October 15, 1959.

REFERENCES

15. Paris, P.C., and Sih, G.C., "Stress Analysis of Cracks," Symposium on Fracture Toughness Testing and Its Applications, ASTM Special Technical Publication No. 381, 1965.

16. Bathias, C., and Pelloux, R.M., "Fatigue Crack Propagation in Martensitic and Austenitic Steels," Metallurgical Transactions, Vol. 4, May 1973.

17. Metal Progress Data Book, American Society for Metals, Mid-June, 1974.

18. Muraca, R.F., and Whittick, J.S., Materials Data Handbook; Inconel Alloy 718, NASA Contract No. NAS8-26644, April 1972.

19. Metallic Materials and Elements for Flight Vehicle Structures, MIL-HDBK-5, August 1962.

20. Schumetzberg, F.R., Osgood, S.H., Keys, R.D., and Kiefer, T.F., Cryogenic Materials Data Handbook, AD 609562, August 1964.

21. Deel, O.L., Ruff, P.E., and Mindlin, H., Engineering Data on New Aerospace Structural Materials, AD 762305, June 1973.

22. Schmidt, E.H., Cryogenic Fatigue Data Developed for Inconel 718, NASA Tech Brief No. 67-10049, March 1967.

23. Green, E.F., "Stainless Steel Alloy 21-6-9," Rocketdyne Materials Bulletin, March 1972.

24. May, J., "Inconel 718," Rocketdyne Materials Bulletin, February 1974

25. "Fatigue Properties of Armco 21-6-9," Mechanical Properties Data Center, Search No. 3109, March 1978.

26. "Fatigue Properties of Inco 718," Mechanical Properties Data Center, Search No. 3107, March 1978.

27. "Fatigue Properties of AISI 347SS," Mechanical Properties Data Center, Search No. 3111, March 1978.

28. "Fatigue Properties of AISI 321SS," Mechanical Properties Data Center, Search No. 3108, March 1978.

APPENDIX A

BELLOWS FLOW-INDUCED VIBRATION COMPUTER PROGRAM

A.1 Governing Equations

The performance equations, which will be presented in this section, are based upon the derivations given in Reference 1. Therefore, detailed algebraic manipulations and derivations have been eliminated for clarity.

Figure A-1 illustrates a longitudinal cross-section of a typical bellows together with pertinent notation. The overall bellows spring rate is

$$K_A = D_m \, E \, \frac{N_p}{N_c} \, (t/h)^3 \tag{A-1}$$

where E is the Young's modulus for bellows material and D_m is the mean bellows diameter which is defined as

$$D_m = (D_i + D_o)/2 \tag{A-2}$$

The elemental spring rate, K, is given by

$$K = 2 \, N_c \, K_A \tag{A-3}$$

The corresponding elemental metal mass of the bellows is

$$m_m = \pi \, \rho_m \, t \, N_p \, D_m \left[\pi a + (h - 2a)\right] \tag{A-4}$$

where ρ_m is the metal density and the mean crown or convolute forming radius is

$$a = (\sigma - t \, N_p)/2 \tag{A-5}$$

As the bellows vibrates in any one of its $2N_c-1$ longitudinal modes, fluid is accelerated within the convolutes. The process of moving the fluid is manifested as an apparent of added mass which must be taken into account in calculating the frequencies at which a fluid-elastic instability is likely to occur. This added mass is a function of the longitudinal mode number, N. That is

$$m_f = m_{f1} \left(\frac{2 \, N_c - 1 - N}{2 \, N_c - 2}\right) + m_{f2} \left(\frac{N-1}{2 \, N_c - 2}\right) \tag{A-6}$$

where

$$m_{f1} = \frac{\pi \, \rho_f \, D_m \, h \, (2a - tN_p)}{2 \, g} \tag{A-7}$$

and

$$m_{f2} = \frac{\pi \, D_m \, \rho_f \, h^3}{3 \, g \, \delta} \tag{A-8}$$

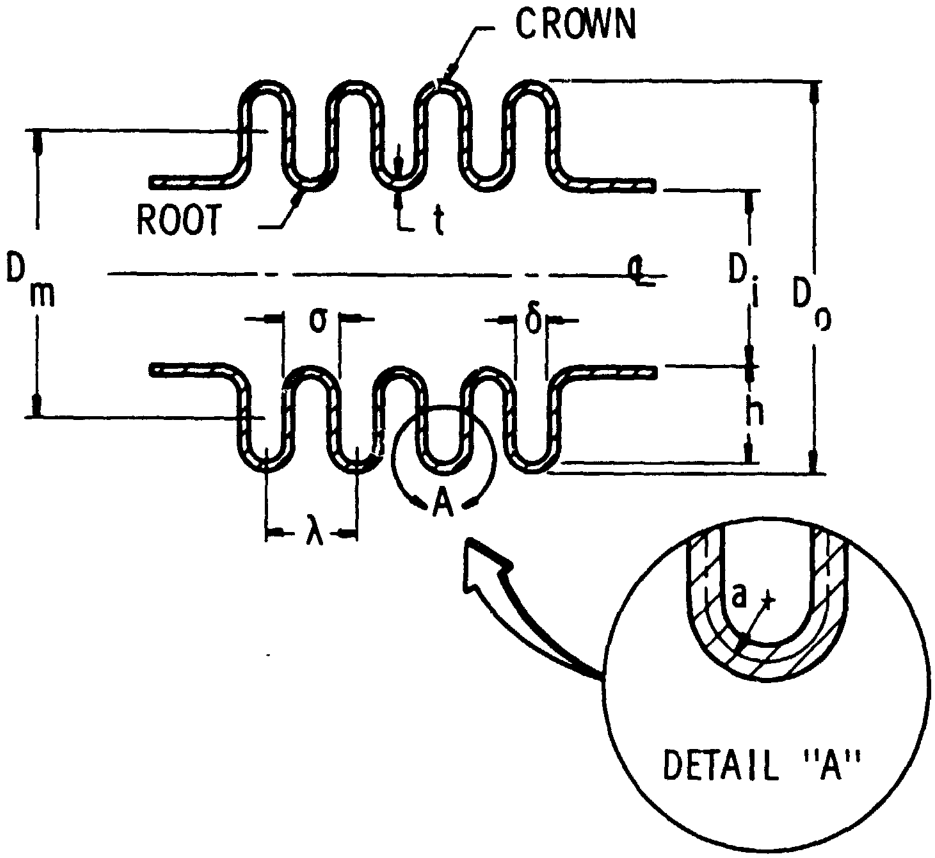

N_c = NUMBER OF CONVOLUTIONS COUNTED FROM THE OUTSIDE

N_p = NUMBER OF PLYS

D_m = MEAN BELLOWS DIAMETER

t = WALL THICKNESS (THICKNESS PER PLY IF MULTI-PLY)

λ = CONVOLUTE PITCH

σ = CONVOLUTE WIDTH

a = MEAN FORMING RADIUS

h = MEAN DISC HEIGHT

FIGURE A-1. BELLOWS NOMENCLATURE

In these expressions ρ_f is the fluid density, g is the gravitational acceleration constant, and

$$\delta = \sigma - 2t\, N_p \tag{A-9}$$

The mode number, N, ranges between 1 and $2N_c-1$. A reference frequency for a particular mode number can be defined as

$$f_o\ (N) = \frac{1}{2\pi}\sqrt{\frac{K}{m_m + m_f}} \tag{A-10}$$

The true modal frequency, f_N, is then obtained by multiplying the reference value by the dimensionless frequency corresponding to the desired mode number and system degree of freedom. Dimensionless frequencies can be calculated as

$$B_i = \left(2\left[1 + \cos\left(\frac{\pi(2N_c-i)}{2N_c}\right)\right]\right)^{\frac{1}{2}} ;\ i = 1,2,3,\ldots 2N_c-1 \tag{A-11}$$

Alternately, for purposes of hand calculations, the dimensionless frequency factors may be determined from Table A-I.

It has been observed that flow excitation of a particular mode can occur over a broad range of fluid velocities, which is termed the "lock-in-range." In fact, if the modal frequencies are sufficiently close together, the lock-in ranges may overlap, thus producing nearly continuous excitation of the bellows. These lock-in ranges are estimated as follows. Extensive experimental studies have revealed that the Strouhal number provides an excellent means of correlating the vibration frequency, fluid velocity and bellows geometry as shown in Figure A-2. The Strouhal number is based on convolute pitch, σ. For a bellows having a convolute pitch-to-convolute tip width ratio of λ/σ, three values of the Strouhal number are indicated. Peak bellows excitation corresponds to the curve marked $S_{\sigma_{crit}}$ from which the critical flow velocity may be calculated, i.e

$$V_{crit}^{(N)} = \frac{f_N \sigma}{S_{\sigma_{crit}}} \tag{A-12}$$

Similarly, the upper and lower values of velocity, which define the lock-in-range are obtained from

$$V_{upper}^{(N)} = \frac{f_N \sigma}{S_{\sigma_\ell}} \tag{A-13}$$

and

$$V_{lower}^{(N)} = \frac{f_N \sigma}{S_{\sigma_u}} \tag{A-14}$$

Degrees of Freedom, $2N_c - 1$	MODE NUMBER																								
	1	2	3	4	5	6	7	8	9	10	11	12	13	14	15	16	17	18	19	20	21	22	23	24	25
1	1.414																								
2	1.000	1.732																							
3	0.765	1.414	1.845																						
4	0.620	1.175	1.620	1.900																					
5	0.520	1.000	1.414	1.732	1.930																				
6	0.445	0.868	1.247	1.564	1.802	1.950																			
7	0.390	0.765	1.111	1.414	1.663	1.848	1.962																		
8	0.347	0.684	1.000	1.286	1.532	1.732	1.879	1.970																	
9	0.314	0.618	0.906	1.176	1.414	1.618	1.782	1.902	1.975																
10	0.285	0.563	0.831	1.082	1.310	1.511	1.682	1.819	1.919	1.980															
11	0.264	0.518	0.765	1.000	1.217	1.414	1.587	1.732	1.848	1.932	1.983														
12	0.245	0.479	0.709	0.929	1.136	1.326	1.497	1.646	1.771	1.870	1.942	1.985													
13	0.226	0.445	0.661	0.868	1.064	1.247	1.414	1.563	1.693	1.802	1.888	1.950	1.987												
14	0.213	0.416	0.618	0.814	1.000	1.176	1.338	1.486	1.618	1.732	1.827	1.902	1.956	1.988											
15	0.199	0.390	0.583	0.765	0.942	1.111	1.269	1.414	1.546	1.663	1.764	1.848	1.913	1.962	1.990										
16	0.185	0.367	0.547	0.722	0.891	1.052	1.205	1.347	1.478	1.596	1.700	1.790	1.864	1.923	1.965	1.991									
17	0.174	0.347	0.518	0.684	0.845	1.000	1.147	1.285	1.414	1.532	1.638	1.732	1.812	1.879	1.931	1.969	1.992								
18	0.165	0.329	0.4[illegible]1	0.649	0.803	0.952	1.093	1.228	1.354	1.471	1.578	1.674	1.758	1.831	1.891	1.938	1.972	1.993							
19	0.157	0.313	0.457	0.618	0.765	0.908	1.044	1.175	1.298	1.414	1.520	1.618	1.705	1.782	1.847	1.902	1.944	1.975	1.993						
20	0.149	0.298	0.[illegible]5	0.590	0.731	0.868	1.000	1.126	1.246	1.360	1.466	1.563	1.652	1.732	1.801	1.861	1.911	1.949	1.977	1.994					
21	0.142	0.285	0.425	0.563	0.699	0.831	0.958	1.081	1.198	1.309	1.414	1.511	1.601	1.682	1.755	1.819	1.873	1.918	1.954	1.979	1.994				
22	0.136	0.272	0.407	0.540	0.670	0.797	0.920	1.039	1.153	1.262	1.365	1.461	1.551	1.633	1.708	1.775	1.834	1.884	1.925	1.958	1.981	1.995			
23	0.131	0.262	0.390	0.518	0.643	0.765	0.885	1.000	1.111	1.217	1.318	1.414	1.503	1.586	1.662	1.732	1.793	1.847	1.893	1.931	1.961	1.982	1.995		
24	0.126	0.251	0.375	0.497	0.618	0.736	0.852	0.964	1.071	1.175	1.274	1.369	1.457	1.541	1.618	1.688	1.753	1.809	1.859	1.902	1.937	1.964	1.984	1.996	
25	0.121	0.241	0.361	0.479	0.595	0.709	0.821	0.929	1.034	1.136	1.233	1.326	1.414	1.497	1.574	1.645	1.711	1.770	1.823	1.870	1.909	1.941	1.967	1.985	1.996

TABLE A-I - DIMENSIONLESS FREQUENCIES FOR BELLOWS MECHANICAL MODEL

ORIGINAL PAGE IS
OF POOR QUALITY

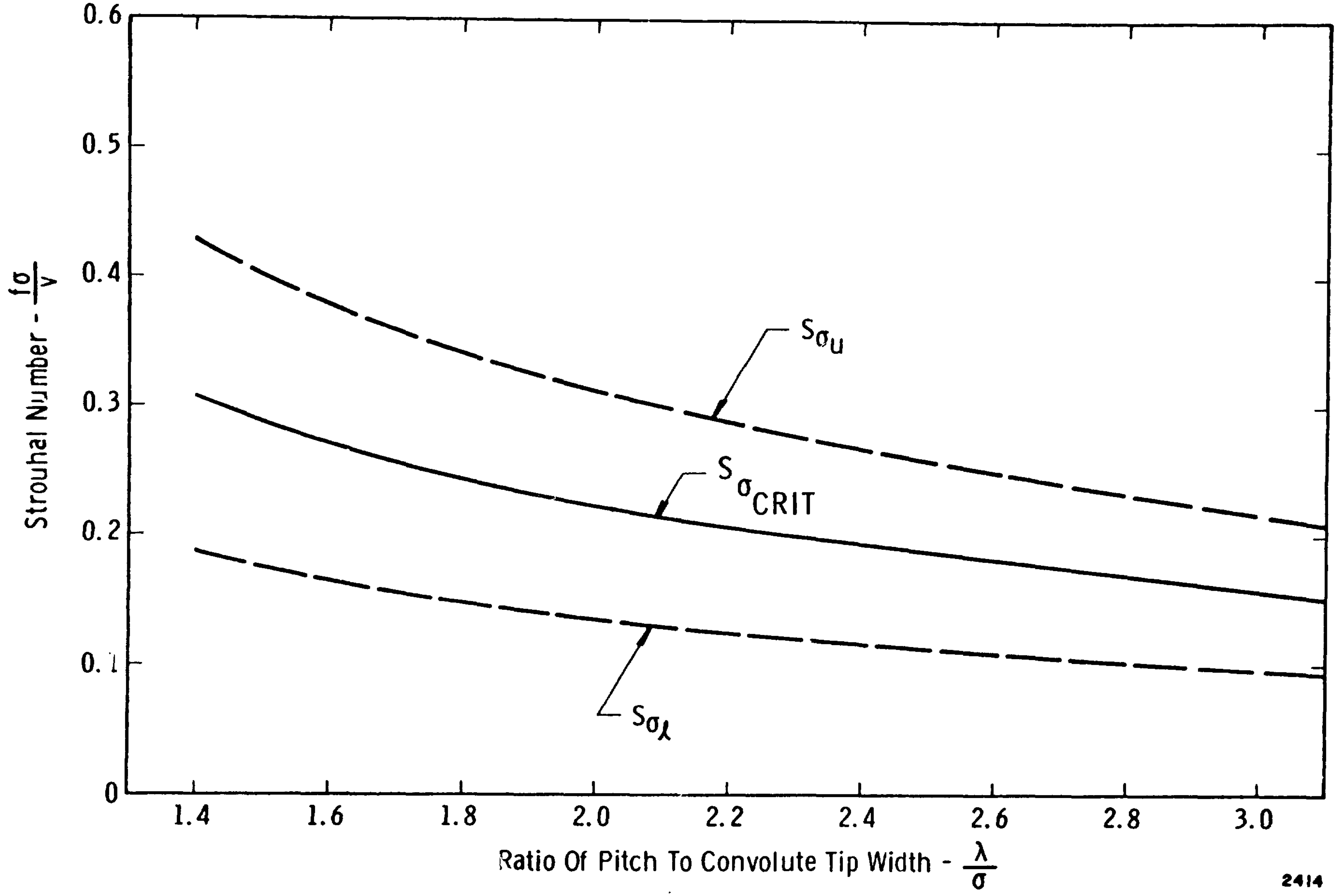

FIGURE A-2. COMPOSITE OF ALL STROUHAL NUMBER CORRELATION DATA

The stress indicator is a relative measure of the stress intensity. Two methods of calculation are allowed in the computer program. The first method, and the more exacting one, involves a greater number of calculations and a substantial amount of input data. The second method incorporates a "Universal C_FQ Function" and, due to its data compression requirement, it is by nature a more conservative calculation, i.e., the SI values will be high. These calculation methods are given as:

Method I: Conventional Stress Indicator

$$SI = \left[\frac{C_f\ C_e\ P_d}{N_p}\ (h/t)^2\right] Q \qquad \text{(A-15)}$$

where C_f = vortex force coefficient which is a function of λ/σ and is obtained from Figure A-3.

C_e = elbow factor to account for above average forces exerted on bellows convolutes if an elbow located immediately upstream of the bellows.

P_d = fluid dynamic pressure.

Q = dynamic amplification factor.

The bracketed term in Equation (A-15) is termed the "bellows operational parameter". This parameter is used in conjunction with the bellows specific spring rate and Table A-II to determine the dynamic amplification factor (Figure A-4), where specific spring rate is defined as

$$SSR = \frac{K_A\ N_c}{D_m\ N_p} \qquad \text{(A-16)}$$

The computer program currently calculates the stress indicator corresponding to the critical flow velocity defined by Equation (A-12).

If the internal medium is a gas, a radial acoustic resonance condition is likely to occur, wherein the acoustic pressure fluctuations couple with the vortex shedding process to produce a force amplification that is significantly larger than would be predicted by the value of Q obtained from Figure A-4. Physically, these pressure fluctuations are attenuated at approximately a constant rate for all vortex shedding frequencies less than the radial acoustic resonance or cutoff frequency. In the vicinity of the cutoff frequency, the increased amplification must be taken into account since it results in much higher bellows stress levels. To this end, the first mode radial acoustic resonant frequency is obtained from Figure 5 for a particular bellows geometry. This cutoff frequency is then compared with the predicted longitudinal modal frequencies. The predicted Q value from Figure A-4 is modified by a suitable constant for all longitudinal frequencies that exceed the cutoff frequency. In other words, this adjustment of Q states that the radial acoustic resonance is capable of coupling with higher longitudinal modes not just at the condition where the frequencies coincide. Figure A-5 is valid for convolute pitch-to-tip width ratios of 1.4 to 2.0. These values

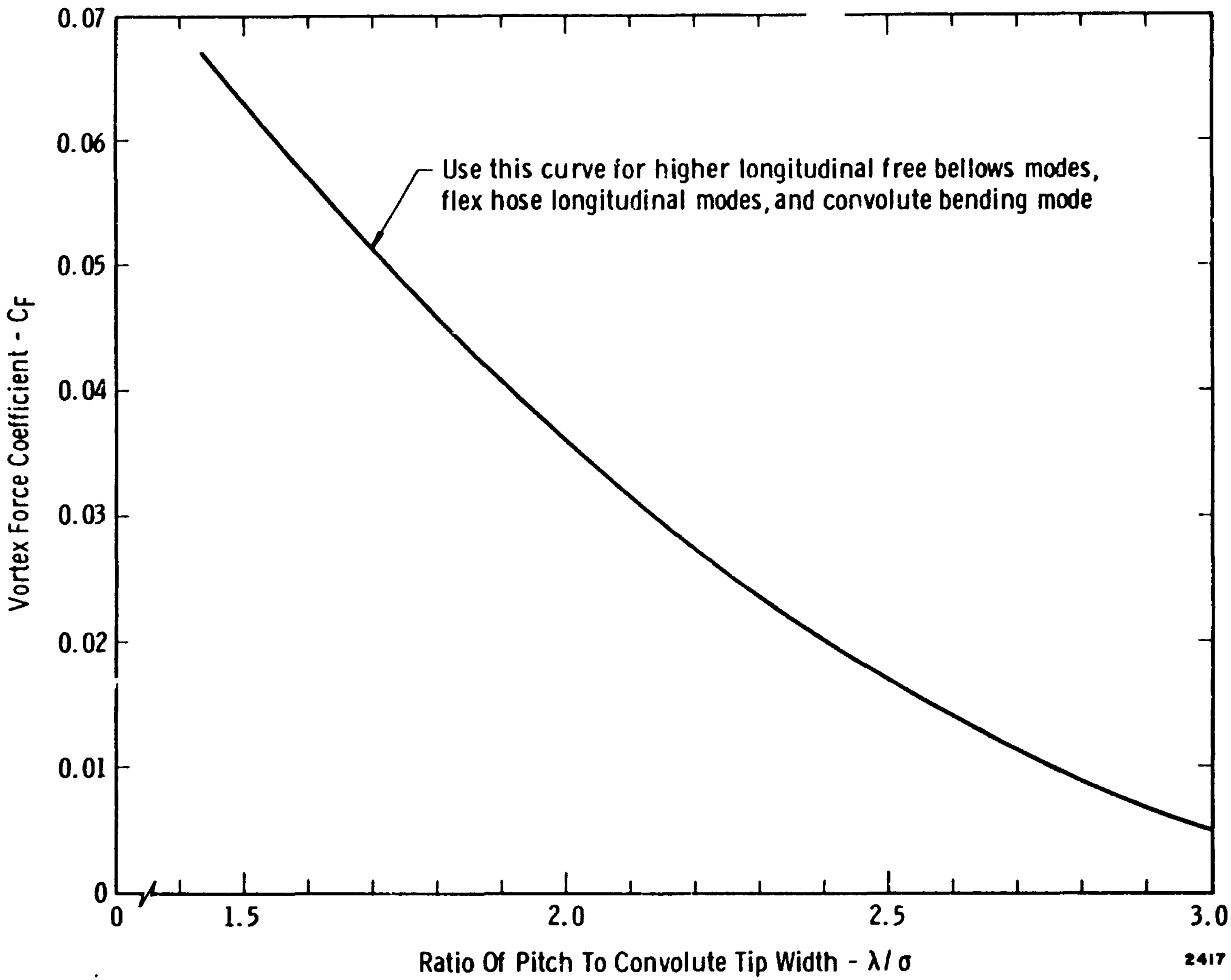

FIGURE A-3. SUMMARY OF BELLOWS VORTEX FORCE COEFFICIENT EXPERIMENDAL DATA

TABLE A-II. APPLICATIONS INFORMATION FOR USE WITH Q VALUES DATA IN FIGURE A-4

Specific Spring Rate	Number Plies	Internal Media (see Note 1)	Curve No.
All Ranges	1	low pressure gases	1
over 2000 lb/in^2	1	high pressure gases, light liquids	1
over 2000	1	water, dense liquids	2
under 2000	1	high pressure gases, light liquids	2
under 2000	1	water, dense liquids	3
over 3000	2	All	3
2000 - 3000	2	all pressure gases	4
under 2000	2	all pressure gases	5
2000 - 3000	2	all liquids	5
under 2000	2	all liquids	6
over 3000	3	All	4
2000 - 3000	3	All	5
under 2000	3	all pressure gases	5
under 2000	3	all liquids	6

NOTE 1: Low pressure gases will be defined here as being those gases below 150 psia. Light liquids will be defined as having a specific gravity of less than 0.2.

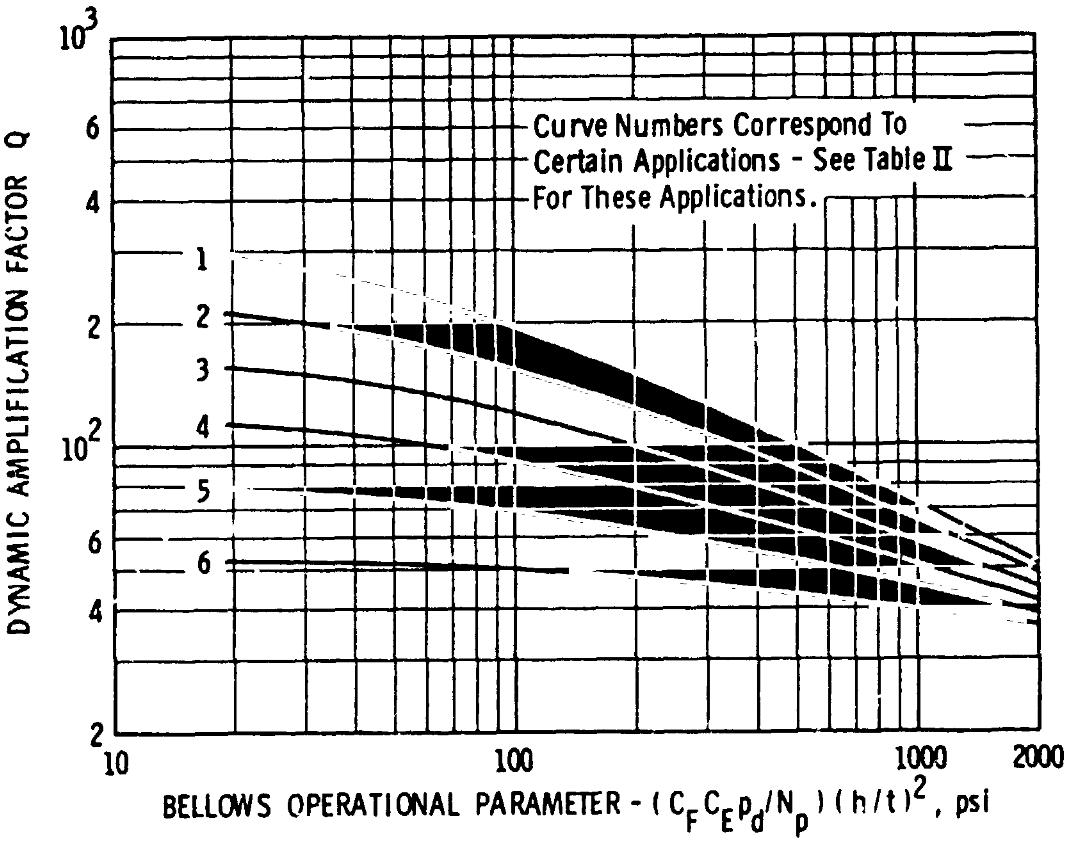

FIGURE A-4. DYNAMIC AMPLIFICATION FACTORS FOR VARIOUS BELLOWS APPLICATIONS

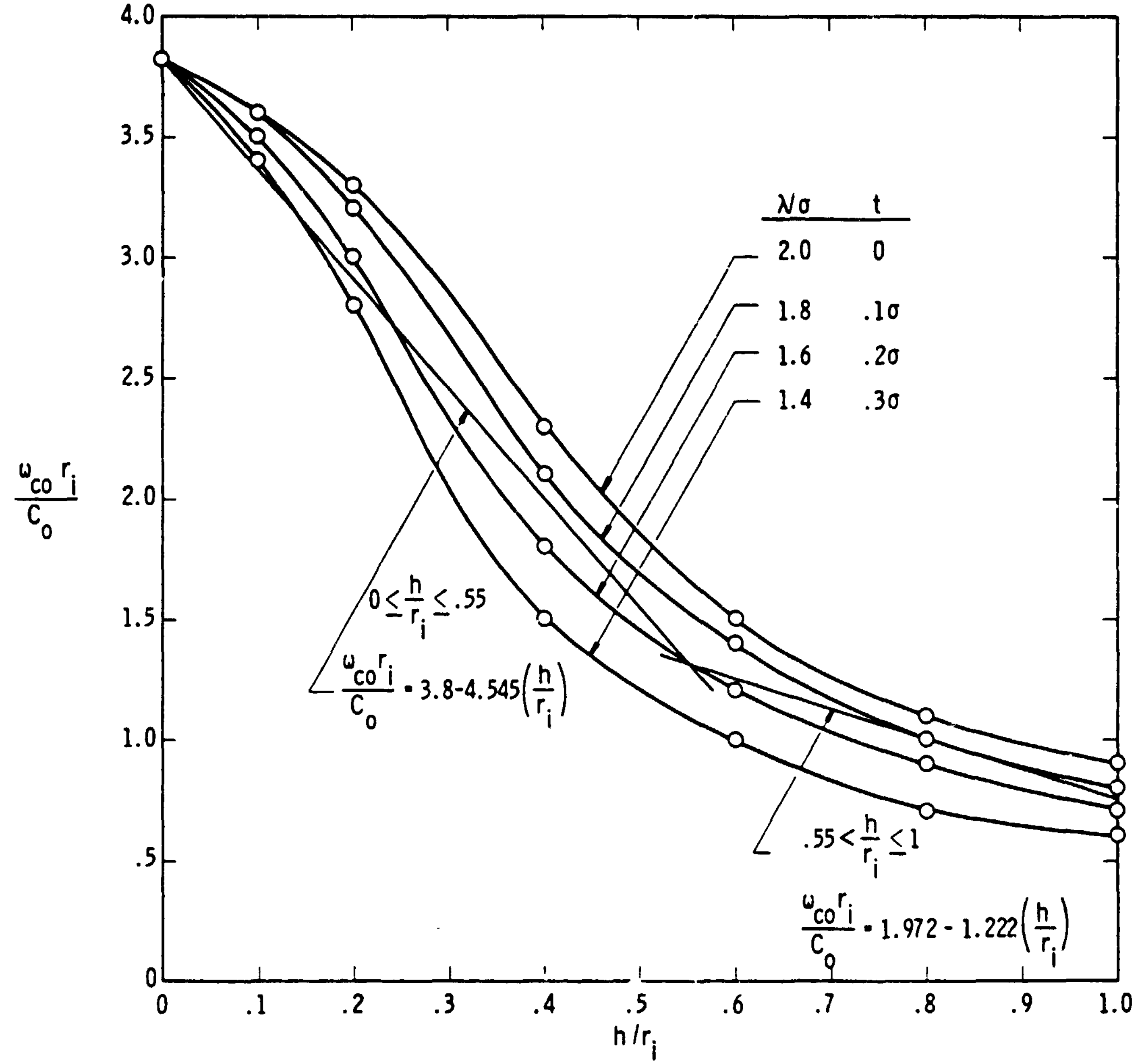

FIGURE A-5. BELLOWS CUT-OFF FREQUENCY FOR FIRST MODE RADIAL ACOUSTIC RESONANCE correspond to total convolute thickness of 0.3σ and 0.0σ (theoretical zero wall thickness). In addition, Figure A-5 is valid for fluid damping numbers, D_N, of the order of 10^{-6} where $D_m = \nu / r_i c_o$, ν = fluid kinematic viscosity and c_o - isentropic speed of sound.

Method II: Calculation of SI with C_F^* Function

Calculation of the stress indicator may be greatly streamlined if the universal C_F^* function shown in Figure A-6 is incorporated as follows:

$$SI = C_F^* \left(\frac{N_c}{N\ N_p}\right) C_e\ (h/t)^2\ P_d \qquad \text{(A-17)}$$

Note that the calculation requires the use of only one curve, and hence, this method is favored for hand calculations; however, if JCFQ is set to 0, the calculation is performed by the computer code. Input cards 9 through 15 may be blank cards.

Calculation of fatigue life is accomplished in a subroutine called XLIFE where the input parameters of material type, alternating stress, and mean stress are manipulated in conjunction with a "Seven-Ordinate" fatigue chart to determine the bellows expected life.

The current version of the program assumes a mean stress of 0 psi; however, several simple program statements could be included to account for internal pressure and slight angulation. Room temperature conditions are assumed, but these conditions predict shorter life expectancies than cryogenic conditions.

The room temperature conditions compensate somewhat for unknown work hardening effects. From the limited amount of data available (AFRPL-TR-68-22), it is generally shown that hydroformed bellows life expectancy is shorter by one order of magnitude than that of a coupon made of the same material. Therefore, it is not advisable to expect longer bellows life due to low temperature operation.

A typical Seven Ordinate Chart is shown in Figure A-7. The alternating and mean stress ordinates are used exclusively in the bellows code. Each constant life curve is represented by a simple power law of the form

$$\text{Cycles} = B\ \sigma_{alt}^{\ m} \qquad \text{(A-18)}$$

B and m values are obtained from data cards 16 through 21. For example, the cycles to failure for INCONEL 718 operating with a mean stress of 0 psi at room temperature is

$$\text{Cycles} = 2.1410 \times 10^{.5}\ \sigma_{alt}^{-5.1097}$$

Similar curves are generated for mean stress levels of 20, 40, 60, and 80 KSI. A linear interpolation process is used to compute cycle values between successive 20 KSI mean stress levels.

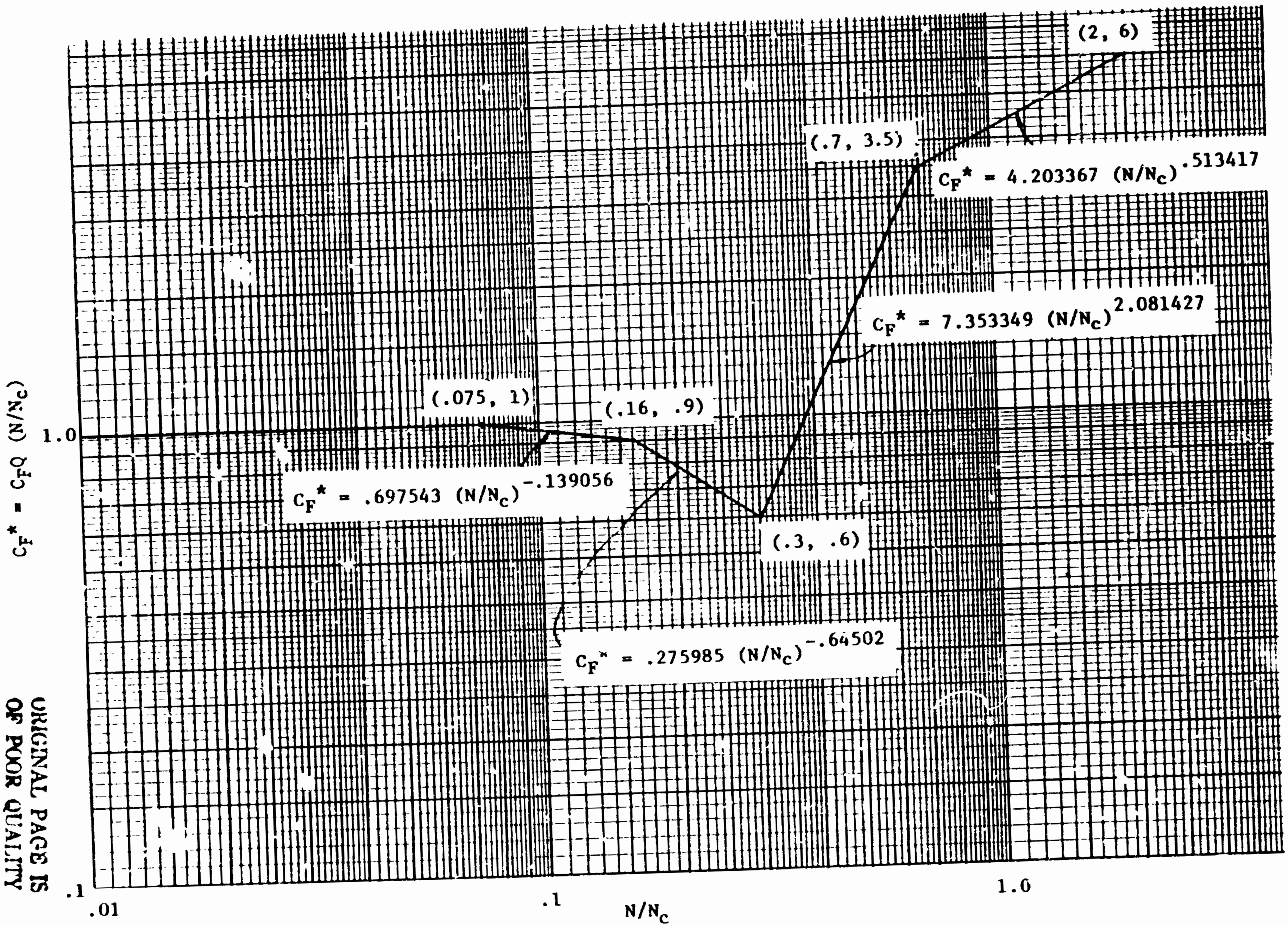

FIGURE A-6. ENVELOPE CURVE FOR C_F^* CORRELATION

INCONEL 718

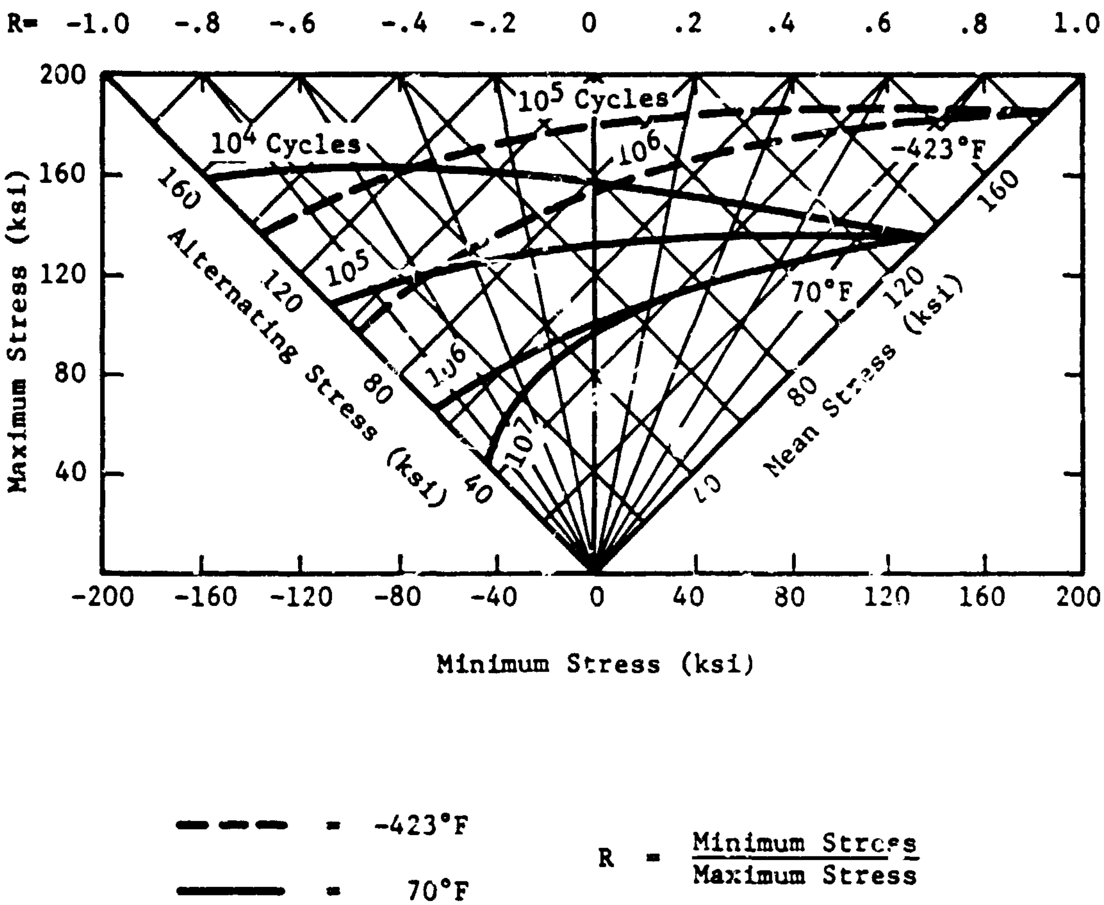

$$R = \frac{\text{Minimum Stress}}{\text{Maximum Stress}}$$

FIGURE A-7. SEVEN-ORDINATE CHART FOR INCONEL 718

A.2 Equivalence of Theoretical and Computer Program Variables

This section is intended to establish the correspondence between the analysis variables presented in the previous section and the computer coded variables. Internally generated variables as well as curve fit coefficients will be discussed in subsequent sections.

Analysis	Computer	Comment
N_c	NC	Number of bellows convolutes
N_p	NPLY	Number of plys
σ	SIGMA	Convolute width
λ	LAMBDA	Distance between adjacent convolute crowns
h	H	Mean convolute disc height
t	T	Thickness per convolute ply
D_i	DI	Bellows inside diameter
D_o	DO	Bellows outside diameter
E	E	Young's modulus of bellows material
ρ_M	RHOM	Bellows material density
K_a	KA	Overall bellows spring rate
C_e	CE	Elbow loss factor
ρ_f	RHOF	Fluid density
D_m	DMEAN	Mean bellows diameter
K	K	Elemental spring rate
a	A	Mean convolute forming radius
m_m	MMETAL	Elemental metal mass
m_{f1}	MFLUID1	Apparent fluid mass at low mode numbers
m_{f2}	MFLUID2	Apparent fluid mass at higher mode numbers
m_f	MFLUID	Apparent fluid mass
δ	DELTA	Internal convolute width

Analysis	Computer	Comment
S_{σ_ℓ}	STLO	Strouhal number defining the lower and upper bounds on lock-in-range
S_{σ_u}	STUP	
$S_{\sigma_{crit}}$	STCRIT	Strouhal number for severe excitation
$V_{lower}^{(N)}$	V(MODE,1)	Lower velocity bound on lock-in-range
$V_{crit}^{(N)}$	V(MODE,2)	Flow velocity for maximum excitation
$V_{upper}^{(N)}$	V(MODE,3)	Upper velocity bound on lock-in-range
C_f	CF	Vortex force coefficient
C_F^*	CFSTAR	Envelope stress coefficient
SSR	SSR	Specific spring rate
Q	Q	Dynamic amplification factor
SI	SI	Stress indicator
σ_{alt}	ALTSTR	Alternating stress
σ_m	MEANSTR	Mean stress
$\omega_{co}\, r_i/C_o$	FNCO	Frequency number for first mode radial acoustic resonance
ω_{co}	FREQCO	Angular cutoff frequency for first mode radial acoustic resonance
C_o	CO	Isentropic speed of sound
γ	GAMMA	Ratio of gas specific heats

A.3 Curve Fit Requirements

When predicting the performance of complex systems, it is frequently necessary to describe experimentally observed relationships between two or more variables through the use of empirical expressions, i.e., curve fits. In predicting bellows flow-induced vibrations, it was necessary to curve fit the data shown in Figures A-2, A-3, and A-4. To this end, all data in these figures were fitted to a hyperbolic equation of the form

$$y = \frac{k}{x - a} + b + dx \qquad \text{(A-19)}$$

where k, a, b, and d are the coefficients to be determined. Coordinate pairs are input to the fitting routine, and the resulting equations are solved simultaneously for the unknown coefficients. A listing of the curve fit routine is included in the next section. Note that there is an option for either a four- or eight-point fit. It was necessary to use an eight-point fit only for the curves labeled 1, 2, and 3 in Figure A-4 (Q-surface). Curve fit coefficients are supplied on input cards 6 through 15.

A.4 Computer Program Structure and Listing

The computer programs listed in this section were written in FORTRAN IV language. In the form presented here, the programs must be compiled each time they are submitted to the computer; however, multiple runs can be accomplished at each submittal. The user of this program may find it more convenient to compile and store the program on tape, thus necessitating minor program modifications.

Four program listings are contained in this section:

(1) MAIN (PROGRAM BELLOW)

(2) Curve generating routine (CURVE)

(3) First mode acoustic response frequency (ACOURES)

(4) Fatigue life routine (XLIFE)

The source deck for the performance program consists of a main program in which a majority of the calculations are performed and three subroutines: CURVE, which is called from the main program, and it contains the logic for selecting the appropriate curve on the Q-surface (Figure A-4): ACOURES, which evaluates the first mode cutoff or acoustic resonance frequency as a function of bellows geometry, and XLIFE, which calculates the bellows life expectancy based upon seven ordinate fatigue data.

The execution structure of the program consists of the following items in the order presented.

(1) Program control cards - number and type of these cards varies with the user facility.

(2) Main program designated Program Bellow.

(3) Subroutine CURVE

(4) Subroutine ACOURES

(5) Subroutine XLIFE

(6) End of record (EOR) card; multi-punch 7-8-9 in column 1.

(7) Data package containing one or more runs.

(8) End of file (EOF) card; multi-punch 6-7-8-9 in column 1.

```
      PROGRAM BELLOW(INPUT,OUTPUT,TAPE60=INPUT)
C     THIS PROGRAM GENERATES A THEORETICAL PREDICTION OF THE NATURAL
C      VELOCITIES WHICH PRODUCE FLOW-INDUCED VIBRATIONS(EXCITATION) OF
C      FREQUENCIES FOR A GIVEN BELLOWS INCLUDING THE FLUID FLOW
C      THE BELLOWS NATURAL LONGITUDINAL MODES.
C * * * * * * * * * * * * * * * * * * * * * * * * * * * * * * * * * * *
C   INPUT
C     JFLAG = 1(CALCULATE KA), 2(USE EXPERIMENTALLY DETERMINED KA). KA
C       IS THE OVERALL BELLOWS SPRING RATE, LB/IN
C     NFLUID = 1(GAS), 2(LIQUID)
C     NDEG = NUMBER OF BELLOWS LONGITUDINAL DEGREES OF FREEDOM, 2*NC-1
C     JMAX = NUMBER OF CURVES NECESSARY TO DESCRIBE Q SURFACE
C     NC = NUMBER OF BELLOWS CONVOLUTES
C     NPLY = NUMBER OF PLYS IN THE BELLOWS CONVOLUTES
C     SIGMA = CONVOLUTE WIDTH, IN.
C     LAMBDA = DISTANCE BETWEEN ADJACENT CONVOLUTE CROWNS, IN.
C     H = MEAN DISC HEIGHT, IN.
C     T = THICKNESS PER CONVOLUTE PLY, IN.
C     DI = BELLOWS INSIDE DIAMETER, IN.
C     DO = BELLOWS OUTSIDE DIAMETER, IN.
C     E = YOUNG'S MODULUS OF THE BELLOWS MATERIAL, LB/SQ IN.
C     RHOM = WEIGHT DENSITY OF THE BELLOWS MATERIAL, LB/CU IN.
C     CE = DIMENSIONLESS ELBOW FACTOR
C     IF NFLUID = 1(GAS), THE PERFECT GAS EQUATION OF STATE IS USED FOR
C       CALCULATING GAS DENSITY AT THE STATE DEFINED BY P AND TEMP.
C       IT IS ASSUMED THAT THE GAS PROPERTIES ARE KNOWN AT A REFERENCE
C       STATE DEFINED BY RHOFREF, PREF, AND TREF.
C       P = GAS PRESSURE, PSIG
C       TEMP = GAS TEMPERATURE, DEG. F.
C       PREF AND TREF = REFERENCE GAS STATE, PSIA AND DEG. F.
C       RHOFREF = GAS DENSITY AT REFERENCE STATE, LB/CU FT.
C       GAMMA = RATIO OF SPECIFIC HEATS FOR GAS
C     IF NFLUID = 2(LIQUID), THE LIQUID DENSITY MUST BE KNOWN APRIORI AT
C       THE LIQUID STATE(P AND TEMP)
C       P = LIQUID PRESSURE, PSIG
C       TEMP = LIQUID TEMPERATURE, DEG. F.
C       RHOF = LIQUID DENSITY AT P AND TEMP, LB/CU FT.
C     MTL=MATERIAL INDICATOR(1=INCO 718,2=ALLOY 21-6-9,3=321SS)
C     STUPK,STUPA,STUPB,STUPD = CURVE FIT COEFFICIENTS FOR UPPER BOUND
C       ON STROUHAL NUMBER VS. LAMBDA/SIGMA
C     STLOK,STLOA,STLOB,STLOD = SAME AS ABOVE EXCEPT LOWER BOUND
C     STCRITK,STCRITA,STCRITB,STCRITD = SAME AS ABOVE EXCEPT FOR OPTIMUM
C       OR CRITICAL STROUHAL NUMBER FOR BELLOWS EXCITATION
C     CFK,CFA,CFB,CFD = CURVE FIT COEFFICIENTS FOR VORTEX FORCE
C       COEFFICIENT
C     QK(J),QA(J),QB(J),QD(J) = CURVE FIT COEFFICIENTS FOR THE DYNAMIC
C         AMPLIFICATION FACTOR(Q) SURFACE
C     S1= DIMENSIONLESS NATURAL FREQUENCY AS A FUNCTION
C       OF MODE NUMBER FOR NDEG BELLOWS LONGITUDINAL
C       DEGREES OF FREEDOM.
C
C     XM(I,MTL) = TWO DIMENSIONAL MATRIX CONTAINING VALUES OF M IN
C       CALCULATING LIFE CYCLES. MTL IS MATERIAL INDICATOR.
C     B(I,MTL) = TWO DIMENSIONAL MATRIX CONTAINING VALUES OF B IN
C       CALCULATING LIFE CYCLES. MTL IS MATERIAL INDICATOR.
C     SUBROUTINE XLIFE CALCULATES THE NUMBER OF PREDICTED LIFE CYCLES
C       GIVEN ALTERNATING STRESS(KSI), MEAN STRESS(KSI), XM,AND B VALUES
```

ORIGINAL PAGE IS
OF POOR QUALITY

```
                C * * * * * * * * * * * * * * * * * * * * * * * * * * * * * * * * * * * *
000003                DIMENSION FREQ(25),V(25,3),SI(25),TFAIL(25)
000003                DIMENSION QK(6),QA(6),QB(6),QD(6)
000003                DIMENSION XM(5,3),B(5,3)
000003                DIMENSION TITLE(8)
000003                DIMENSION XRM(5),BRM(5)
000003                REAL MESLOW(3),MESHI(3),MEANLG(4)
000003                REAL NC,NPLY,LAMBDA,MFLUID1,MFLUID2,MFLUID,MMETAL,KA,K,MASS
000003                REAL MEANSTR
000003                COMMON NPLY,SSR,NFLUID,P,RHOF,JCURVE,BOP,Q,CYCLE,MRET
000003                DATA MESLOW/4HBELO,4HW 10,4HE+03/
000003                DATA MESHI/4HABOV,4HE 10,4HE+07/
000003                DATA MEANLG/4HMEAN,4H STR,4HESS ,4HHI  /
                C * * * * * * * * * * * * * * * * * * * * * * * * * * * * * * * * * * * *
000003              1 READ 1000,TITLE
000011                IF(EOF,60)5,10
000014              5 STOP
000016             10 READ 1030,JFLAG,NFLUID,NDEG,JMAX,JCFQ,MTL
000036                READ 1010,NC,NPLY,SIGMA,LAMBDA,H,T
000056                READ 1010,DI,DO,E,RHOM,KA,CE
000076                GO TO (11,12),NFLUID
000104             11 READ 1010,P,TEMP,PREF,TREF,RHOFREF,GAMMA
000124                GO TO 13
000125             12 READ 1010,P,TEMP,RHOF
000137             13 READ 1080,STUPK,STUPA,STUPB,STUPD
000153                READ 1080,STLOK,STLOA,STLOB,STLOD
000167                READ 1080,STCRITK,STCRITA,STCRITB,STCRITD
000203                READ 1080,CFK,CFA,CFB,CFD
000217                READ 1080,(QK(J),QA(J),QB(J),QD(J),J=1,JMAX)
000240         15     READ 2001,(XM(I,1),I=1,5)
000252                READ 2002,(B(I,1),I=1,5)
000264                READ 2001,(XM(I,2),I=1,5)
000276                READ 2002,(B(I,2),I=1,5)
000310                READ 2001,(XM(I,3),I=1,5)
000322                READ 2002,(B(I,3),I=1,5)
                C * * CALCULATION OF NATURAL FREQUENCIES AND EXCITATION VELOCITIES * * *
000334             25 PI=3.1415927
000336                G=32.174049
000337                DMEAN=(DI+DO)/2.
000342                GO TO (30,35),JFLAG
000350             30 KA=DMEAN*E*(NPLY/NC)*(T/H)**3
000356             35 K=2.*NC*KA*12.
000362                A=(SIGMA-T*NPLY)/2.
000366                MMETAL=PI*RHOM*T*NPLY*DMEAN*(PI*A+H-2.*A)/G
000377                GO TO (36,37),NFLUID
000405             36 RHOF=RHOFREF*(P+14.7)*((TREF+460.)/(TEMP+460.))/(PREF*1728.)
000416                GO TO 38
000417             37 RHOF=RHOF/1728.
000421             38 MFLUID1=PI*RHOF*DMEAN*H*(2.*A-T*NPLY)/(2.*G)
000432                DELTA=SIGMA-2.*T*NPLY
000436                MFLUID2=PI*RHOF*DMEAN*(H**3)/(5.*G*DELTA)
000445                X=LAMBDA/SIGMA
000447                STLO=STLOK/(X-STLOA)+STLOB+STLOD*X
000455                STUP=STUPK/(X-STUPA)+STUPB+STUPD*X
000463                STCRIT=STCRITK/(X-STCRITA)+STCRITB+STCRITD*X
000471                AMODE=1.0
000472                DO 60 MODE=1,NDEG
000474                DEMPL=2.*NC-2.
```

ORIGINAL PAGE IS
OF POOR QUALITY

```
000477           IF(DEMFL.NE.0) GO TO 39
000500           DEMFL=1.
000501        39 MFLUID=(MFLUID1*(2.*NC-1.-AMODE)+MFLUID2*(AMODE-1.))/DEMFL
000512           MASS=MFLUID+MMETAL
000514           B1=SQRT(2.*(1.+COS((PI*(2.*NC-MODE))/(2.*NC))))
000531           FREQ(MODE)=SQRT(K/MASS)*B1/(2.*PI)
000542           DO 55 J=1,3
000543           GO TO(40,45,50),J
000551        40 V(MODE,J)=FREQ(MODE)*SIGMA/(STUP*12.)
000560           GO TO 55
000561        45 V(MODE,J)=FREQ(MODE)*SIGMA/(STCRIT*12.)
000571           GO TO 55
000571        50 V(MODE,J)=FREQ(MODE)*SIGMA/(STLO*12.)
000601        55 CONTINUE
000603        60 AMODE=AMODE+1.
           C * * * * * * * * * * * * * * * * * * * * * * * * * * * * * * * * * * *
           C     THEORETICAL STRESS INDICATOR FOR CRITICAL STROUHAL NUMBER
000610           CF=CFK/(X-CFA)+CFB+CFD*X
000616           SSR=KA*NC/(DMEAN*NPLY)
000621           CALL CURVE
000622           IF(MFLUID.EQ.1) 65,70
000627        65 RI=DI/2.
000631           HRI=H/RI
000633           CO=SQRT(GAMMA*(P+14.7)*G/(RHOF*12.))
000644           CALL ACOURES(HRI,RI,CO,FREQCO,DADJUST)
000647        70 AMODE=1.0
           C * * NEW CF-Q ENVELOPE CURVE * * * * * *
000651           GO T  (73,165),JCFQ
000657        73 DO 150  MODE=1,NDEG
000661           PARA=  MODE/NC
000664           IF(PARA.GT..075) GO TO 90
000667           CFSTAR=1.0
000670           GO TO 140
000670        90 IF(PARA.GT..16) GO TO 100
000674           CFSTAR=.697543*PARA**(-.139056 )
000700           GO TO 140
000700       100 IF(PARA.GT..3) GO TO 110
000704           CFSTAR=.275984*PARA**(-.64502)
000710           GO TO 140
000710       110 IF(PARA.GT..7) GO TO 120
000714           CFSTAR=7.353344*PARA**2.081427
000720           GO TO 140
000720       120 IF(PARA.GT.2.) GO TO 130
000724           CFSTAR=4.203367*PARA**.513417
000730           GO TO 140
000730       130 CFSTAR=6.0
000737       140 BON=CE*RHOF*(V(MODE,2)**2)*(((H/T)**2)*12./(2.*NPLY*G))*(CFSTAR)
000746           SI(MODE)=BON*(NC/AMODE)
000751           CFQ=CFSTAR*NC/AMODE
000754           PRINT 1900,CFQ
000761      1900 FORMAT(5H CFQ=,E12.6)
000761           AMODE=AMODE+1.
000763       150 CONTINUE
000766           GO TO 205
000766       165 DO 200 MODE=1,NDEG
000770           BOP=CF*CE*RHOF*(V(MODE,2)**2)*((H/T)**2)*12./(2.*NPLY*G)
001004           Q=QK(JCURVE)/(BOP-QA(JCURVE))+QB(JCURVE)+BOP*QD(JCURVE)
001013           IF(MFLUID.EQ.1)175,180
```

```
001017      175 IF(FREQ(MODE).GE.FREQCO) Q=Q*QADJUST
001024      180 SI(MODE)=BOP*Q
001027          AMODE=AMODE+1.
001031      200 CONTINUE
001033      205 PRINT 2000, TITLE
001041          PRINT 1040,SIGMA,LAMBDA,H,T,DI,DO,NC,NPLY,E,KA,RHOM,P,TEMP,RHOF,NF
               1LUID,MTL
001105          PRINT 1050
001111          PRINT 1060
001115          MEANSTR=0.0
001116          DO 99 MODE=1,NDEG
001120          ALTSTR=SI(MODE)/1000.
001122          DO 101 I=1,5
001124          XRM(I)=XM(I,MTL)
001127          BRM(I)=B(I,MTL)
001132      101 CONTINUE
001133          CALL XLIFE(XRM,BRM,ALTSTR,MEANSTR)
001136          GO TO (1410,1300,1400,210),MRET
001146      210 PRINT 1070,MODE,SI(MODE),FREQ(MODE),V(MODE,1),V(MODE,2),V(MODE,3),
               $            CYCLE
001170          GO TO 99
001171     1300 PRINT 1305,MODE,SI(MODE),FREQ(MODE),V(MODE,1),V(MODE,2),V(MODE,3),
               $            MESLOW
001213          GO TO 99
001214     1400 PRINT 1305,MODE,SI(MODE),FREQ(MODE),V(MODE,1),V(MODE,2),V(MODE,3),
               $            MESHI
001236          GO TO 99
001237     1410 PRINT 1415,MODE,SI(MODE),FREQ(MODE),V(MODE,1),V(MODE,2),V(MODE,3),
               1            MEANLG
001261       99 CONTINUE
001264          IF(NFLUID.EQ.1)215,1
001270      215 PRINT 1090,FREQCO,QADJUST
001300          GO TO 1
001301     1000 FORMAT(8A10)
001301     1010 FORMAT(6E12.6)
001301     1020 FORMAT(10F7.3)
001301     1030 FORMAT(6I3)
001301     1040 FORMAT(1H0,29X,18HBELLOWS PARAMETERS/
               $       1H0,18X,26HSIGMA(CONVOLUTE WIDTH, IN),11X,F6.3,/
               $            19X,27HLAMBDA(CONVOLUTE PITCH, IN),10X,F6.3,/
               $            19X,23HH(MEAN DIS. HEIGHT, IN),14X,F6.3,/
               $            19X,30HT(CONVOLUTE THICKNESS/PLY, IN),7X,F6.3,/
               $            19X,23HDI(INSIDE DIAMETER, IN),14X,F6.3,/
               $            19X,24HDO(OUTSIDE DIAMETER, IN),13X,F6.3,/
               $            19X,24HNC(NUMBER OF CONVOLUTES),12X,F7.3,/
               $            19X,21HNPLY(NUMBER OF PLIES),15X,F7.3,/
               $            19X,28HE(YOUNG'S MODULUS, LB/SQ.IN),4X,E11.4,/
               $            19X,30HKA(OVERALL SPRING RATE, LB/IN),6X,F7.3,/
               $            19X,32HRHOM(MATERIAL DENSITY, LB/CU.IN),4X,F7.3,/
               $       1H0,30X,16HFLUID PARAMETERS/
               $       1H0,18X,17HP(PRESSURE, PSIG),19X,F7.3,/
               $            19X,24HTEMP(TEMPERATURE, DEG F),9X,F10.3,/
               $            19X,29HRHOF(FLUID DENSITY, LB/CU.IN),3X,E11.4,/
               $            19X,23HNFLUID(1=GAS, 2=LIQUID),19X,I1,/
               $            19X,38HMTL(1=INCO 718,2=ALLOY 21-6-9,3=321SS),4X,I1,/
               $       1H0,23X,31HTHEORETICAL BELLOWS PERFORMANCE)
001301     1050 FORMAT(1H0,95HMODE NO.  STRESS INDICATOR  NATURAL FREQUENCY       F
               SLOW EXCITATION RANGE,FT/SEC      LIFE CYCLES,/
```

```
                 $              36X,2HHZ,14X,5HLOWER,5X,8HCRITICAL,4X,5HUPPER,6X,3HSEC)
001301     1060 FORMAT(1H0)
001301     1070 FORMAT(3X,I2,8X,E11.4,9X,F9.3,5X,3F11.3,6X,E11.4)
001301     1080 FORMAT(4E14.8)
001301    2001  FORMAT(5F10.3)
001301    2002  FORMAT(5E10.5)
001301     1090 FORMAT(///,3X,46HFIRST MODE RADIAL ACOUSTIC RESONANT FREQUENCY=,F9
                1.3,8HGADJUST=,F5.2)
001301     2000 FORMAT(*1*,8A10)
001301     1305 FORMAT(3X,I2,8X,E11.4,9X,F9.3,5X,3F11.3,6X,3A4)
001301     1415 FORMAT(3X,I2,8X,E11.4,9X,F9.3,5X,3F11.3,6X,4A4)
001301          END
```

```
                 SUBROUTINE CURVE
000002           DIMENSION DIMFREQ(25),FREQ(25),V(25,3),SI(25)
000002           DIMENSION QK(6),QA(6),QB(6),QD(6)
000002           COMMON NPLY,SSR,NFLUID,P,RHOF,JCURVE,BOP,Q,CYCLE,NRET
000002           REAL NC,NPLY,LAMBDA,NFLUID1,NFLUID2,NFLUID,NMETAL,KA,K
000002           IF(NPLY.EQ.1.)180,10
000007        10 IF(NPLY.EQ.2.)90,20
000014        20 IF(SSR.GT.3000.)30,40
000022        30 JCURVE=4
000023           RETURN
000024        40 IF(2000..LE.SSR.AND.SSR.LE.3000.)50,60
000036        50 JCURVE=5
000037           RETURN
000040        60 IF(SSR.LT.2000..AND.NFLUID.EQ.1)70,80
000051        70 JCURVE=5
000052           RETURN
000053        80 JCURVE=6
000054           RETURN
000055        90 IF(SSR.GT.3000.)100,110
000063       100 JCURVE=3
000064           RETURN
000065       110 IF(NFLUID.EQ.1)120,150
000072       120 IF(2000..LE.SSR.AND.SSR.LE.3000.)130,140
000104       130 JCURVE=4
000105           RETURN
000106       140 JCURVE=5
000107           RETURN
000110       150 IF(2000..LE.SSR.AND.SSR.LE.3000.)160,170
000122       160 JCURVE=5
000123           RETURN
000124       170 JCURVE=6
000125           RETURN
000126       180 IF(NFLUID.EQ.1.AND.P.LT.150.)190,200
000140       190 JCURVE=1
000141           RETURN
000142       200 IF(SSR.GT.2000.)210,260
000150       210 GO TO (220,230),NFLUID
000156       220 JCURVE=1
000157           RETURN
000160       230 SPGRAV=RHOF/(62.4/1728.)
000162           IF(SPGRAV.LT.0.2)240,250
000167       240 JCURVE=1
000170           RETURN
000171       250 JCURVE=2
000172           RETURN
000173       260 GO TO (270,280),NFLUID
000201       270 JCURVE=2
000202           RETURN
000203       280 SPGRAV=RHOF/(62.4/1728.)
000205           IF(SPGRAV.LT.0.2)290,300
000212       290 JCURVE=2
000213           RETURN
000214       300 JCURVE=3
000215           RETURN
000216           END
```

```
              SUBROUTINE ACOURES(X,Y,Z,FREQCO,QADJUST)
000010        PI=3.1415927
000011        HRI=X
000012        RI=Y
000013        CO=Z
000014        IF(HRI.LE.0.55) GO TO 20
000017     10 FNCO=1.972-1.222*HRI
000022        GO TO 30
000023     20 FNCO=3.8-4.545*HRI
000026     30 FREQCO=12.*FNCO*CO/(2.*PI*RI)
000033        QADJUST=5.
000034        RETURN
000034        END
```

```
                      SUBROUTINE XLIFE(XM,B,ALTSTR,MEANSTR)
000007                DIMENSION XM(5),B(5)
000007                COMMON NPLY,SSR,NFLUID,P,RHOF,JCURVE,BOP,Q,CYCLE,MRET
000007                REAL MEANSTR
000007                I=1
000007                IF(MEANSTR.LE.20.)GO TO 200
000012                I=I+1
000014                IF(MEANSTR.LE.40.)GO TO 200
000016                I=I+1
000017                IF(MEANSTR.LE.60.)GO TO 200
000021                I=I+1
000022                IF(MEANSTR.LE.80.)GO TO 200
000025                MRET=1
000026                RETURN
000026        200     CYC1=B(I)*ALTSTR**XM(I)
000033                CYC2=B(I+1)*ALTSTR**XM(I+1)
000040                FRAC=(MEANSTR-20.*(I-1))/20.0
000046                CYCLE=CYC1+(CYC2-CYC1)*FRAC
000052                IF(CYCLE.LE.1000.) 100,300
000060        100     MRET=2
000061                RETURN
000062        300     IF(CYCLE.GE.10000000.)400,500
000070        400     MRET=3
000071                RETURN
000072        500     MRET=4
000073                RETURN
000074                END
```

A.5 Data Input Package

Instructions for preparation of a data input package are located at the beginning of the PROGRAM BELLOW listing. An experienced programmer will have no difficulty in constructing the input, but for the inexperienced user the following supplementary remarks may be useful.

Input Card 1

This card is an identification card on which the user can place information that will aid in identifying and classifying the run. Any alpha-numeric characters can be placed in columns 2 through 80. Column 1 must either contain a 1 for printer carriage control or be left blank.

Input Card 2

Word 1	JFLAG	- See Program Listing
Word 2	NFLUID	- See Program Listing
Word 3	NDEG	- See Program Listing
Word 4	JMAX	- Is the number of individual curves necessary to describe the Q-surface (Figure A-4). As shown in that figure, JMAX = 6. If future data indicate that more than six curves are necessary, then the dimension statement pertaining to Q must be altered accordingly.
Word 5	JCFQ = 1	(Use Method I Stress Indicator Calculation)
	= 2	(Use Method II Stress Indicator Calculation)
Word 6	MTL	- See Program Listing

Input Card 3

Word 1	NC	- See Program Listing
Word 2	NPLY	- "
Word 3	SIGMA	- "
Word 4	LAMBDA	- "
Word 5	H	- "
Word 6	T	- "

Input Card 4

Word 1	DI	- See Program Listing
Word 2	DO	- "
Word 3	E	- "
Word 4	RHOM	- "
Word 5	KA	- May be left blank if J[illegible] = 1
Word 6	CE = 1.0	- See Program Listing

Input Card 5

Word 1	D	- See Program Listing
Word 2	TEMP	- "
Word 3	PREF or RHOF	- "
Word 4	TREF	- "
Word 5	RHOFREF	- "
Word 6	GAMMA	- "

Input Card 6

This card contains 4 curve fit coefficients for the upper bound of the Strouhal number vs. lambda/sigma function. They are as follows:

Word 1	STUPK	= +.25352426+00
Word 2	STUPA	= +.40487805+00
Word 3	STUPB	= +.22229595+00
Word 5	STUPD	= -.34329268-01

Input Card 7

This card contains 4 curve fit coefficients for the lower bound of the Strouhal number vs. lambda/sigma function. They are as follows:

Word 1	STLOK	= +.11870422+00
Word 2	STLOA	= +.46569343+00
Word 3	STLOB	= +.73139166-01
Word 4	STLOD	= -.79927007-02

Input Card 8

This card contains 4 curve fit coefficients for the critical curve of the Strouhal number vs. lambda/sigma function. They are as follows:

Word 1	STCRITK	= +.43502697+00
Word 2	STCRITA	= -.61870504-01
Word 3	STCRITB	= +.37269292-02
Word 4	STCRITD	= +.40647482-02

Input Card 9

This card contains 4 curve fit coefficients for the vortex force coefficient vs. lambda/sigma function. They are as follows:

Word 1	CFK	= -.19458000+03
Word 2	CFA	= +.25500000+02
Word 3	CFB	= -.74460000+01
Word 4	CFD	= -.39900000+00

Input Cards 10 through 15

The curve fit coefficients for the Q-surface are read in at a rate of four words per card, i.e., QK (1), QA (1), QB (1), QD (1) are punc[illegible] on Card 10; QK (2), QA (2), QB (2), QD (2) are on Card 11 of thi[illegible] Reading continues per this format until JMAX sets of coefficients below have been read in.

Card 10	QK(1)	=	4.0873881E+04
	QA(1)	= -	1.4052553E+02
	QB(1)	=	3.7419734E+01
	QD(1)	= -	2.2574946E-03
Card 11	QK(2)	=	3.3980471E+04
	QA(2)	= -	1.7498692E+02
	QB(2)	=	3.8783556E+01
	QD(2)	= -	2.7034275E-03
Card 12	QK(3)	=	2.0081991E+04
	QA(3)	= -	1.4917770E+02
	QB(3)	=	4.5393842E+01
	QD(3)	= -	4.8689382E-03
Card 13	QK(4)	=	9.8799884E+03
	QA(4)	= -	1.2489887E+02
	QB(4)	=	4.9950596E+01
	QD(4)	= -	6.8001116E-03
Card 14	QK(5)	=	7.8264710E+03
	QA(5)	= -	2.0682049E+02
	QB(5)	=	4.3576094E+01
	QD(5)	= -	4.0612929E-03
Card 15	QK(6)	=	2.3506369E+04
	QA(6)	= -	8.4432071E+02
	QB(6)	=	2.4773333E+01
	QD(6)	= -	1.4810690E-03

Input Card 16

This card contains exponent values (M) for material 1

Word 1 XM (1,1)	= - 5.11	(mean stress =	0 KSI)
Word 2 XM (2,1)	= - 5.479	(" " =	20 ")
Word 3 XM (3,1)	= - 5.519	(" " =	40 ")
Word 4 XM (4,1)	= - 5.645	(" " =	60 ")
Word 5 XM (5,1)	= - 5.972	(" " =	80 ")

Input Card 17

This card contains coefficient values (B) for material 1

Word 1 B (1,1)	= + .21410+16	(mean stress =	0 KSI)
Word 2 B (2,1)	= + .72280+16	(" " =	20 ")
Word 3 B (3,1)	= + .44440+16	(" " =	40 ")
Word 4 B (4,1)	= + .24367+16	(" " =	60 ")
Word 5 B (5,1)	= + .23200+16	(" " =	80 ")

Input Card 18

This card contains exponent values (M) for material 2

Word 1 XM (1,2) = - 13.003
Word 2 XM (2,2) = - 13.170
Word 3 XM (3,2) = - 16.008
Word 4 XM (4,2) = - 14.168
Word 5 XM (5,2) = - 5.345

Input Card 19

This card contains coefficient values (B) for material 2

Word 1 B (1,2) = + .67770+27
Word 2 B (2,2) = + .32560+28
Word 3 B (3,2) = + .29480+32
Word 4 B (4,2) = + .49910+27
Word 5 B (5,2) = + .89980+11

Input Card 20

This card contains exponent values (M) for material 3

Word 1 XM (1,3) = - 2.447
Word 2 XM (2,3) = - 3.567
Word 3 XM (3,3) = - 4.387
Word 4 XM (4,3) = - 4.683
Word 5 XM (5,3) = - 6.124

Input Card 21

This card contains coefficient values (B) for material 3

Word 1 B (1,3) = + .14360+10
Word 2 B (2,3) = + .13630+12
Word 3 B (3,3) = + .22900+13
Word 4 B (4,3) = + .12990+13
Word 5 B (5,3) = + .12510+13

A.6 Example Problem

Listed below is an input data deck constructed in accordance with the instructions presented at the beginning of PROGRAM BELLOW. The notations that appear in columns 73 through 80 serve to identify the data group in each card. Following this listing is the corresponding computer output. The output is grouped into three sections. The first group summarizes the pertinent bellows input parameters. For this example, only the overall spring rate, KA, was inserted as data. The next group summarizes the fluid parameters. The next group contains the predicted longitudinal bellows performance. Bellows lock-in-range for a particular mode of vibration is defined by the upper and lower flow velocities. Stress indicator was calculated based on

C-2

the critical flow velocity for each mode. Note, that for this particular bellows configuration, the lock-in-ranges for successive modes overlap, which indicates a more or less continuous spectrum of excitation velocities. Note also that all performance variables at the highest mode numbers are less than the corresponding quantities at previous mode numbers. Physically this behavior is accounted for b the fact that the apparent fluid mass is increasing at a faster rate than the dimensionless frequency numbers in Table A-I for this bellows.

STAINLESS STEEL BELLOWS, SWRI NO. 15 AT 70F AND 10 PSIG

BELLOWS PARAMETERS

SIGMA(CONVOLUTE WIDTH, IN)	.120
LAMBDA(CONVOLUTE PITCH, IN)	.230
H(MEAN DISC HEIGHT, IN)	.300
T(CONVOLUTE THICKNESS/PLY, IN)	.006
DI(INSIDE DIAMETER, IN)	3.000
DO(OUTSIDE DIAMETER, IN)	3.600
NC(NUMBER OF CONVOLUTES)	13.000
NPLY(NUMBER OF PLIES)	2.000
E(YOUNG'S MODULUS, LB/SQ.IN)	2.8000E+07
KA(OVERALL SPRING RATE, LB/IN)	96.000
RHOM(MATERIAL DENSITY, LB/CU.IN)	.280

FLUID PARAMETERS

P(PRESSURE, PSIG)	10.000
TEMP(TEMPERATURE, DEG F)	70.000
RHOF(FLUID DENSITY, LB/CU.IN)	3.6053E-02
NFLUID(1=GAS, 2=LIQUID)	2
MIL(1=INCO 718,2=ALLOY 21-6-9,3=321SS)	3

THEORETICAL BELLOWS PERFORMANCE

MODE NO.	STRESS INDICATOR	NATURAL FREQUENCY HZ	FLOW EXCITATION RANGE, FT/SEC LOWER	CRITICAL	UPPER	LIFE CYCLES SEC
1	6.4909E+02	140.703	4.340	6.081	10.077	ABOVE 10E+07
2	2.4469E+03	275.936	8.511	11.925	19.762	ABOVE 10E+07
3	5.1363E+03	405.612	12.511	17.529	29.049	ABOVE 10E+07
4	8.4698E+03	529.635	16.337	22.889	37.931	7.7139E+06
5	1.2222E+04	647.905	19.985	28.000	46.402	3.1346E+06
6	1.6251E+04	760.320	23.453	32.859	54.453	1.5636E+06
7	2.0438E+04	866.780	26.736	37.460	62.077	8.9230E+05
8	2.4701E+04	967.189	29.834	41.799	69.268	5.6129E+05
9	2.8978E+04	1061.456	32.741	45.873	76.019	3.7474E+05
10	3.3217E+04	1149.497	35.457	49.678	82.325	2.7189E+05
11	3.[illegible]372E+04	1231.237	37.978	53.210	88.179	2.0377E+05
12	4.[illegible]399E+04	1306.611	40.303	56.468	93.577	1.5863E+05
13	4.[illegible]256E+04	1375.567	42.430	59.448	98.515	1.2756E+05
14	4.8900E+04	1438.062	44.358	62.149	102.991	1.0554E+05
15	5.2291E+04	1494.067	46.085	64.569	107.002	8.9571E+04
16	5.5391E+04	1543.567	47.612	66.708	110.597	7.7797E+04
17	5.8164E+04	1586.562	48.938	68.566	113.626	6.9031E+04
18	6.0579E+04	1623.064	50.064	70.144	116.240	6.2440E+04
19	6.2609E+04	1653.100	50.991	71.442	118.392	5.7647E+04
20	6.4233E+04	1676.715	51.719	72.463	120.083	5.4146E+04
21	6.5435E+04	1693.466	52.251	73.208	121.318	5.1744E+04
22	6.6206E+04	1704.926	52.590	73.682	122.103	5.0283E+04
23	6.6542E+04	1709.684	52.736	73.887	122.444	4.9663E+04
24	6.6447E+04	1708.342	52.695	73.824	122.348	4.9837E+04
25	6.5931E+04	1701.019	52.469	73.513	121.823	5.0798E+04

TABLE A-I

APPENDIX B

EXPERIMENTAL FACILITY

B.1 Flow Loop

All liquid flow tests were conducted in a closed loop water flow tunnel shown schematically in Figure B-1. The bellows upstream piping was sized to the nominal bellows size, i.e. 3" PVC pipe was used during 3" bellows test and 6" PVC was used for 6" bellows. The flow loop can be pressurized to pressures in excess of 100 psig.

Flow rate was accurately measured by a 4" turbine meter (Flow Technology SN - 64033), and the loop's static pressure was determined by a calibrated bordon pressure gauge located one diameter upstream of the bellows.

Fluid motion is generated by a Goulds propeller pump rated at 40 ft. head at 6000 GPM. The prime mover is a 75 hp variable speed hydraulic motor which provides a means to vary the loop flow velocity. Piping components are fabricated of carbon steel or PVC. A large antisurge reservoir (air over water) has been incorporated into the basic tunnel design.

B.2 Bellows Instrumentation

During a typical bellows flow test, three time dependent variables are normally recorded. These include the (1) volumetric flow rate, (2) the strain time history at various bellows locations, and (3) the displacement time history of selected bellows convolutes.

The overall instrumentation setup is shown in Figure B-2 where it can be seen that three modes of recording data are possible. For quick look information polaroid pictures of the scope face may be obtained. As a second mode of operation, a high speed direct write galvonometer (CEC Model 5-124) is used to obtain high frequency hard copy bellows strain and displacement time histories; however, the majority of data (3rd mode of operation) was recorded in a form more useable for analysis, i.e. a dependent variable was plotted versus an independent variable on the x-y plotter while a test was in progress.

Typical data collected in the form of two dimensional plots are presented in Figure 13. The vertical scale is proportional to either peak to peak strain amplitude or peak to peak displacement amplitude. Special circuitry, to be described subsequently, converted convolute peak to peak displacement motions to an equivalent D.C. analog voltage which was input to the y-axis of a model x-y recorder. Peak to peak strain signals (radial and circumferential) were processed in a similar fashion. The horizontal axis is proportional to volumetric flow rate through the bellows. Since the primary flow measurement element was a turbine meter, its output frequency (directly proportional to the volume rate) was converted to a D.C. signal and then input to the recorder's x-axis.

A typical instrumented bellows is shown in FigureB-3. Four strain gages were attached to the convolute crowns each test bellows. Two gages were placed on convolute number two, one responded to radial strains and the other responded to circumferential strain. Convolute number two was chosen as a representative and convolute where peak strains occur (maximum relative displacement occurs in this region) but due to the end restraint. The middle convolute was gaged in the same manner as convolute number two. By observing the middle convolute

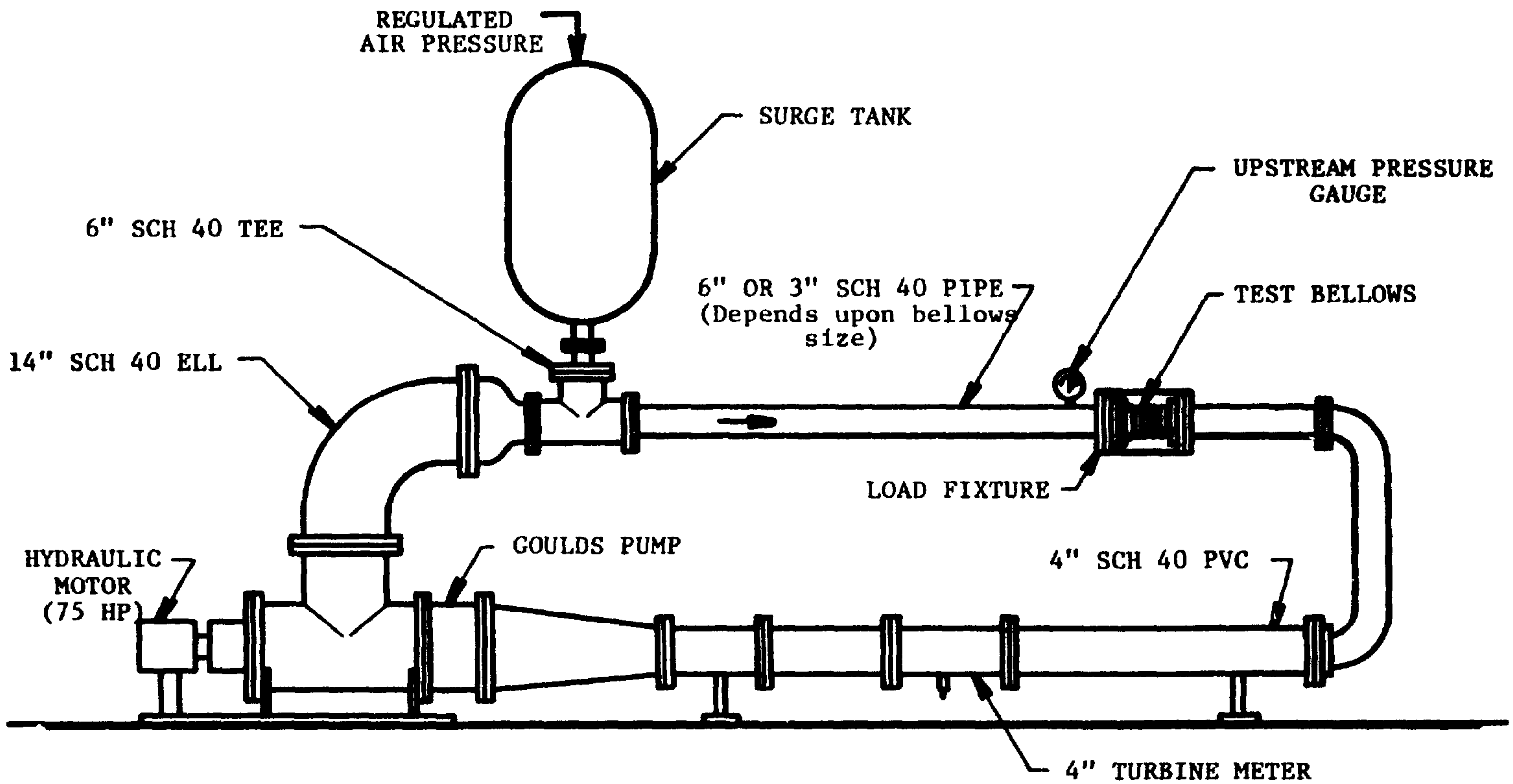

FIGURE B-1. WATER FLOW TUNNEL

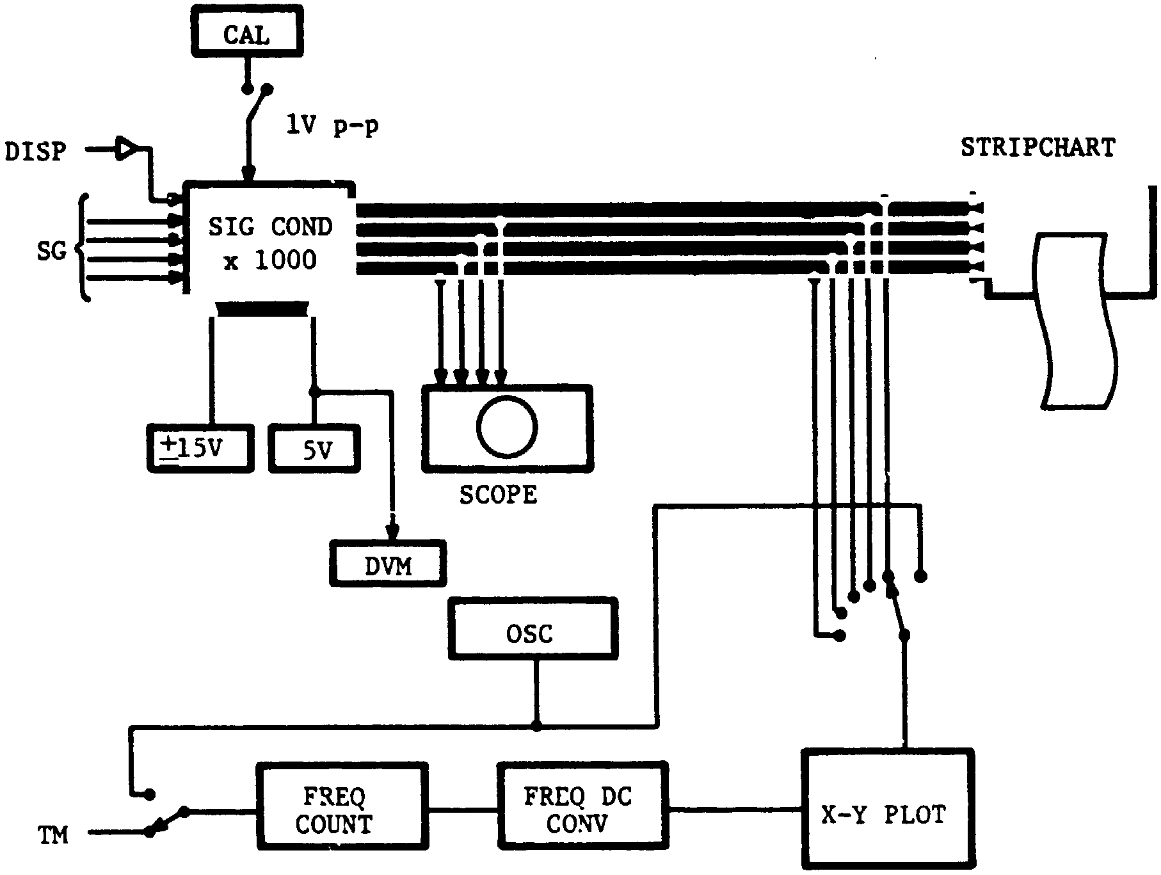

FIGURE B-2. INSTRUMENTATION

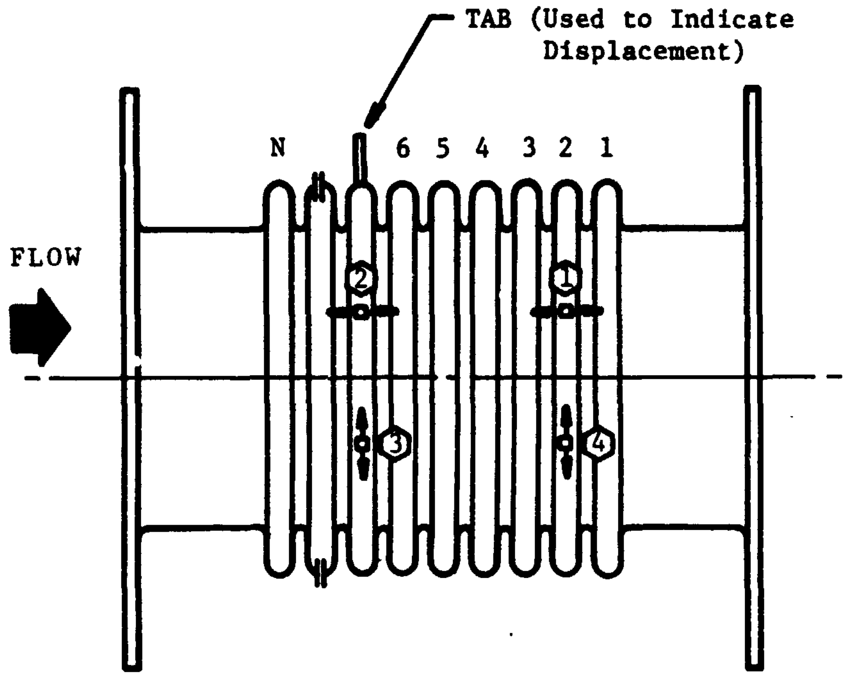

Gage No.	Gage Type	Strain Direction	Convolute No.
1	EA-09-031ED-120	Radial	2
2	EA-09-031ED-120	Radial	7
3	EA-06-031DE-120	Circumferential	7
4	EA-06-031DE-120	Circumferential	2

FIGURE B-3. STRAIN GAGE AND TAB LOCATION FOR 3" BELLOWS response simultaneously with the second convolute, the mode number is positively identified and insight is gained with respect to the mode shape.

All strain gages used were 1/32" long and each was selected to the base material of the bellows (321 stainless steel). Due to the small size of the gage and its associated installation difficulty, single arm active bridge circuits were employed. Figure B-4 shows a schematic of the signal conditioning circuit that converts gage resistance changes into a measurable voltage. The first stage amplifier (Analog Devices 610) is a high quality instrumentation amplifier operated in a differential voltage measurement mode. The second stage amplifier (Analog Devices 3140) provides offset voltage control and boosts the 610's output by a fixed gain of 10.

Consolute displacement was obtained by measuring the displacement of a small metal tab that was epoxied to the crown of a convolute. A Bently probe (Model 316) was attached to a fixed structure above the test bellows. The tab couples with the transducer to produce an analog signal directly proportional to the displacement of the tab with respect to the transducer face; hence, the convolute absolute displacement was recorded. A sufficient number of tests were performed to insure that the virtually massless attached tab did not influence the vibration process.

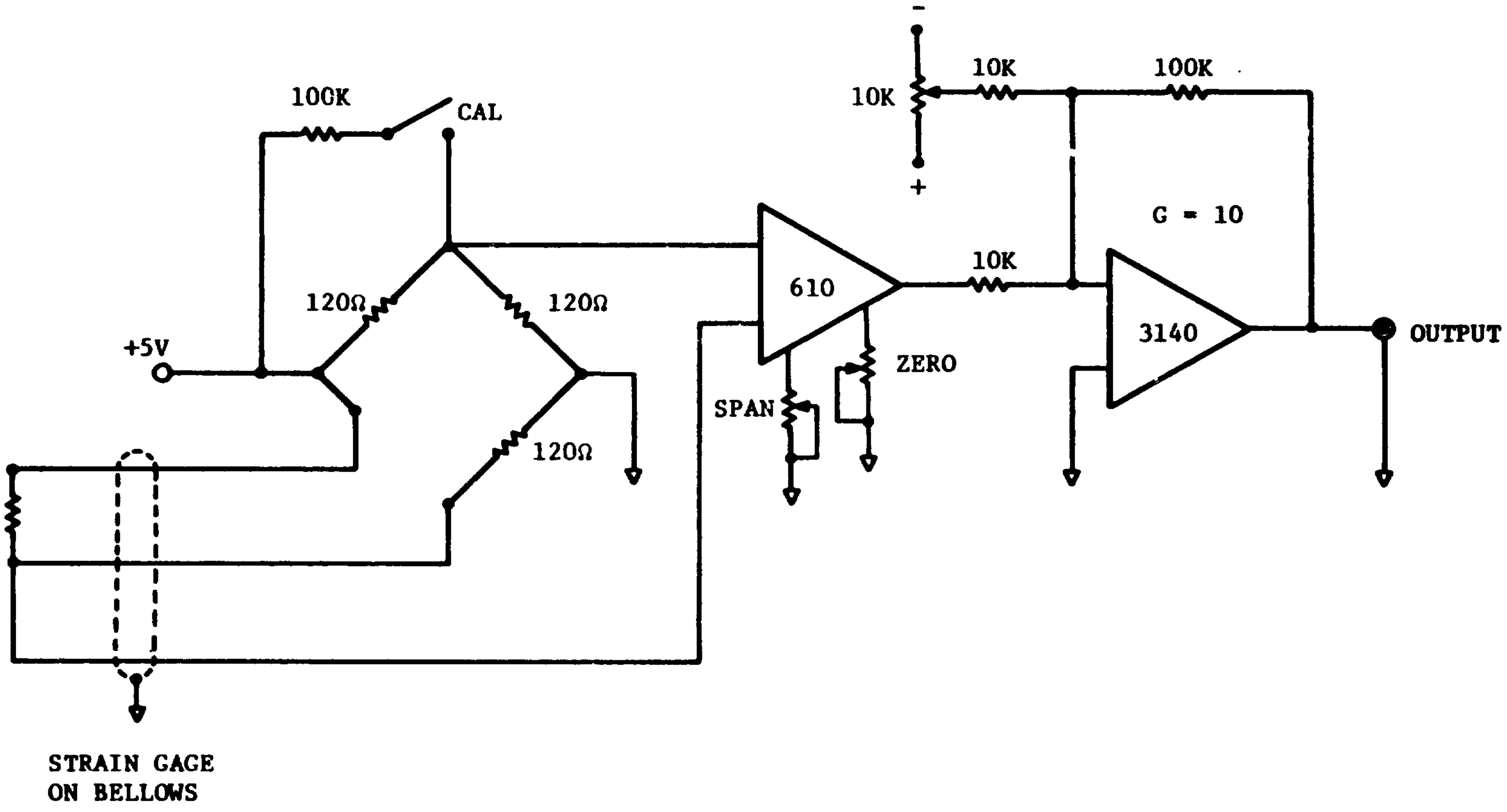

FIGURE B-4. STRAIN GAGE INSTRUMENTATION.

APPENDIX C

BELLOWS GEOMETRIC AND MECHANICAL PROPERTIES DATA

TABLE C-I. BELLOWS DATA

Parameter	Bellows No.			
	4	6	15	E
D_n (in)	3.3	3.3	3.3	6.3
D_i (in)	3.0	3.0	3.0	6.0
D_o (in)	3.6	3.6	3.6	6.6
h (in)	.3	.3	.3	.3
t (in)	.006	.008	.006	.008
N_p	1	1	2	1
N_c	13	19	13	A
λ (in)	.228	.144	.216	.224
σ (in)	.12	.08	.12	.12
λ/σ	1.9	1.8	1.8	1.87
K_A (lb/in)	44.2	82.6	93.5	166.67
$d\mu e/dfc$ (μin/lb)	94.96	57.28	42.37	[illegible]
$d\mu e/dl$ (μin/in)	4197	4731	3961	[illegible]

APPENDI: D

FATIGUE LIFE COMPUTEI ROGRAM, FATLIF

```
      PROGRAM FATLIF(INPUT,OUTPUT,TAPE10=INPUT,TAPE6=OUTPUT)
      DIMENSION N(10),V(10)
      REAL NPLY,M,LAMBDA,MODENO,KA,NC,NONC
      NR=10
      NW=6
      READ(NR,1000)
      READ(NR,1010)P,H,NPLY,TPLY,E,LAMBDA
      READ(NR,1010)NC,RHOF,KA,DI,DO
      READ(NR,1010)C,M,ALPHA,EPSILON,AI,AC
      READ(NR,1015)MODEMAX
      READ(NR,1010)(V(I),I=1,MODEMAX)
      READ(NR,1015)(N(I),I=1,MODEMAX)
      WRITE(NW,1000)
      WRITE(NW,1020)
      G=32.174
      PI=3.1415927
      T=NPLY*TPLY
      SIGP=P*(H/T)**2/2.
      DO 100 I=1,MODEMAX
      MODENO=N(I)
      NONC=MODENO/NC
      CM=(NONC+SIN(PI*NONC/2.))/(8.*MODENO)
      IF(NONC.LE.0.025)GO TO 2
      IF(NONC.LE.0.160) GO TO 4
      IF(NONC.LE.0.3) GO TO 6
      IF (NONC.LE.0.7) GO TO 8
      IF(NONC.GT.0.7) GO TO 10
    2 CESTAR=1.0
      GO TO 12
    4 CESTAR=0.692543*NONC**(-0.139056)
      GO TO 12
    6 CESTAR=0.275984*NONC**(-0.64502)
      GO TO 12
    8 CESTAR=2.353349*NONC**2.081427
      GO TO 12
   10 CESTAR=4.203367*NONC**0.513417
   12 CFQ=CESTAR/NONC
      AP=PI*H*(DI+DO)/2.
      DELONC=CM*RHOF*AP*CFQ*(V(I)*12.)**2/(2.*12.*G*KA)
      DELSIG=1.5*E*T*DELONC/SQRT(LAMBDA*H**3)
      SIGMAX=SIGP+DELSIG/2.
      SIGMIN=SIGP-DELSIG/2.
      R=SIGMIN/SIGMAX
      COEFF=(1./C)*((1.-R)/(DELSIG*1.E-3))**M
C     FATIGUE LIFE DEFINITE INTEGRAL
      AREA=0.0
      DA=(AC-AI)/20.
      A1=AI
      A2=A1+DA
      F1=1./((ALPHA*A1**2+EPSILON)*A1**(M/2.))
   25 F2=1./((ALPHA*A2**2+EPSILON)*A2**(M/2.))
      AREA=AREA+DA*(F1+F2)/2.
      F1=F2
      A1=A2
      A2=A1+DA
      IF(A2-AC)25,25,50
   50 FATLIF=COEFF*AREA
```

```
      WRITE(NW,1010)NONC,CM,CFSTAR,CFQ,DELONC,COEFF
  100 WRITE(NW,1025)N(I),V(I),SIGP,DELSIG,SIGMAX,SIGMIN,AREA,R,FATLIFE
 1000 FORMAT(80H1
     1                                        )
 1010 FORMAT(6E12.6)
 1015 FORMAT(6I3)
 1020 FORMAT(1H0,10H  MODE NO.,7X,6HV(FPS),7X,9HSIGP(PSI),4X,11HDELSIG(P
     1SI),3X,11HSIGMAX(PSI),3X,11HSIGMIN(PSI),6X,4HAREA,11X,1HR,7X,14HFA
     2TIGUE CYCLES)
 1025 FORMAT(5X,I3,13X,F6.1,8X,F7.0,6X,F8.0,6X,F8.0,6X,F8.0,5X,E10.4,5X,
     1F7.4,5X,E10.4)
      STOP
      END
```

APPENDIX E

TWO PHASE FLOW STUDY

E.1 Two Phase Flow

During the performance period of the bellows study, several special studies were conducted on an as needed basis. One particularly noteworthy study conducted was a simplified analysis of the Shuttle LH_2 chilldown or recirculation system. Four possible operating conditions of the chilldown system were assumed and the analysis of the chosen "worst case," indicates low probability of a bellows failure due to a two phase flow phenomena. Results are presented below.

E.2 Case A - Pure Liquid Flow

For this case the entire recirculation system was assumed to be flowing pure liquid hydrogen with the pump curve shown in Figure E.1 defining the pressure head versus flow for each of the three pumps. Table E.I lists the assumed bellows geometry for this analysis. Table E.II lists the LH_2 properties and analysis results for the Case A pure liquid flow problem. As shown, because of the very low velocity and $1/2\ \rho V^2$ valve, the stress indicator valve is quite low and no bellows flow-induced vibration problem is anticipated.

E.3 Case B - Pure Gas Flow

For this case we assume pure liquid flow through the pump followed by pure gaseous flow through the recirculation system. The reason for this assumption is to ensure the maximum possible driving head at the pump is available to "push" the gas through the lines. With gaseous flow through the pumps, a very low head would occur hence no means would exist to continue to introduce liquid into the system.

It is assumed that sufficient heat is transferred into the liquid to cause complete boiling hence a pure gaseous flow through the recirculation lines. This is definitely a possiblity at the first stage of chilldown.

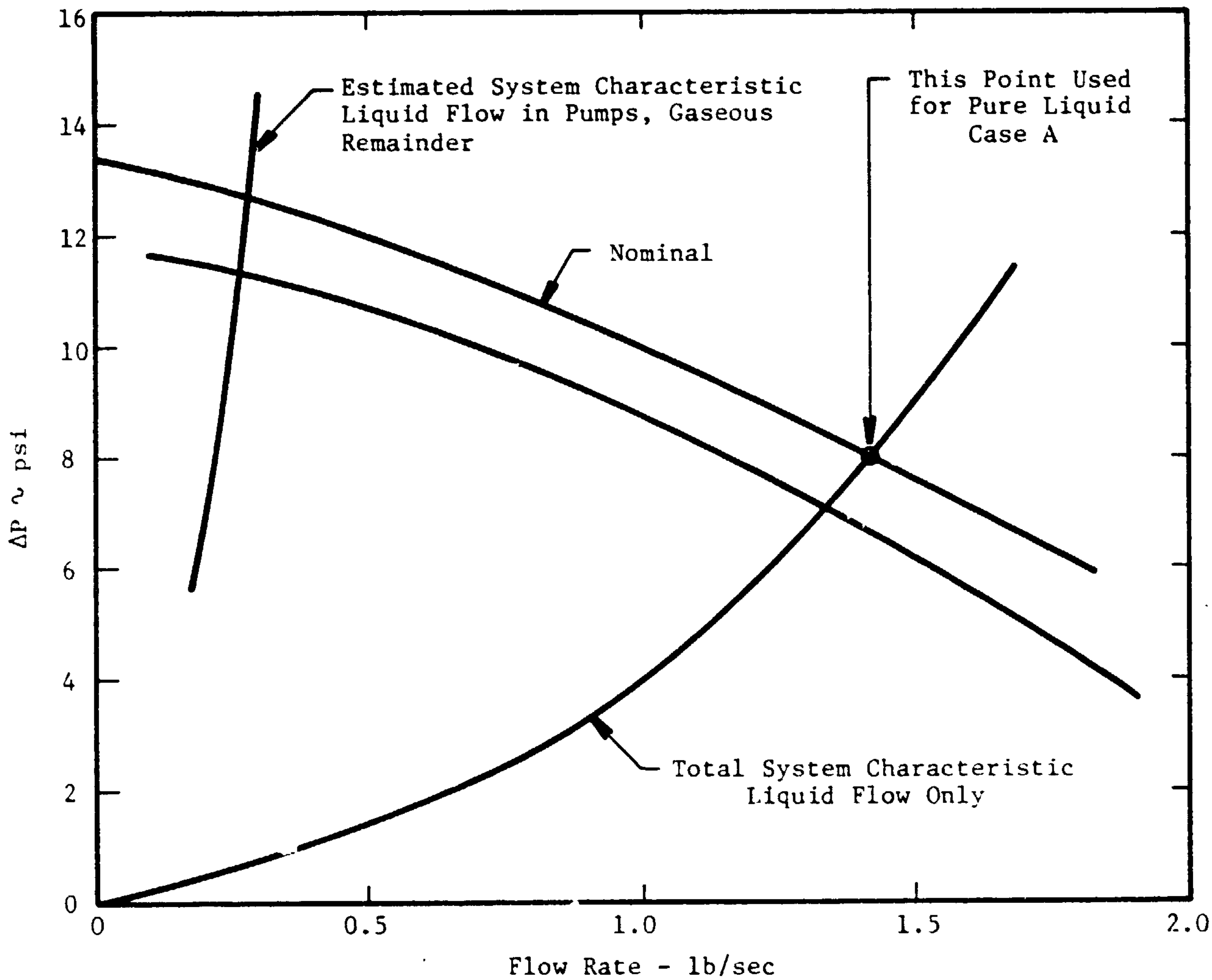

FIGURE E-1. RECIRCULATION PUMP PRESSURE FLOW CHARACTERISTIC

TABLE E-I Summary Of Bellows Data For Case A

Bellows Geometry (Arrowhead Drawing 13619)

- Material - ARMCO 21-6-9
- O.D. - 5.0 inches
- I.D. - 4.0 inches
- N_c = 8 convolutes
- N_p = 2 plys
- t = 0.008 inches per ply
- ℓ_c = 2.0 inches convoluted length
- h = 0.50 inches
- λ = 0.267
- σ = 0.134

Calculated Data

- K_A = 138.24 lb/inch overall spring rate
- M_m = 1.002×10^{-4} lb-sec^2/in^4
- f_o = 748 Hz, reference frequency
- f_1 = 148.9 Hz, first mode frequency
- V_1 = 7.56 fps, first mode critical velocity
- f_{15} = 1488 Hz, highest longitudinal mode frequency
- V_{15} = 75.5 fps, highest longitudinal mode critical velocity

TABLE E-II Summary Of LH_2 Properties And Analysis Results For Case A - Pure Liquid Flow

Liquid Hydrogen Properties And Conditions

- LH_2 @ - 420°F, 16.1 psig
- ρ_f = 0.002564 lbm/in^3 = 4.431 lbm/ft^3
- $\dot{\omega}$ = 4.2 lb/sec total flow, 3 pumps

Calculated Data

- Volume flow $= \dfrac{\dot{\omega}}{\rho_f} = 0.9479\ ft^3/sec$
- $V = \dfrac{\text{Volume flow}}{\text{Area}} = \dfrac{0.9479}{0.08722} = 10.87$ fps
- $1/2\ \rho_f V^2 = 0.0565$ psi
- $C_f Q = 8$ (first mode)
- $S.I. = \left(\dfrac{C_F Q}{N_\rho}\right) \left(\dfrac{h}{t}\right)^2 (1/2\ \rho V^2) = 882.8$ psi

Conclusions

- The Stress Indicator is so low no significant bellows response is possible.

Pure gaseous flow at the 4.2 lb/sec rate achieved for the pure liquid case is not possible because the flow loss would far exceed the available head at the pumps. Therefore, a downward adjustment in flow occurs until the loss matches the available pump head. The total flow from three pumps which satisfies this requirement is about 0.823 lb/sec; see Figure E-I.

Based on this flow, the bellows of Table E-I has been analyzed and results are shown in Table E.III. As shown, the stress indicator is quite low and there is no possibility of acoustic resonance, hence the bellows is safe.

E.4 Case C - Liquid Flow for Part of Line, Gaseous Flow for Rest

For this case we assume pure liquid flow through the pumps and through a fraction of the total recirculation line length. The flow through the remainder of the recirculation line is assumed to be pure gaseous. The transition from liquid to gas is assumed to occur suddenly at a single point in the line.

As with Case B, the total pressure loss along the line is assumed equal to the head available from the pump. When the percentage of line with gaseous flow is large, we expect the mass flow to be smaller than the nominal 4.2 lb/sec value and the total head greater than the nominal 8.0 psi value. As a starting point we assume the presence of the gas will restrict the flow so that the pump is operating in the region of a 12 psi head value. Other assumptions are:

- The liquid density is always ρ_c = 4.431 lb/ft^3
- The gas density is always ρ_g = 0.0939 lb/ft^3
- The pump head of 12 psi produces an <u>average</u> $1/2\ \rho V^2$ of 0.0897 psi along the line
- X is the percentage of the total line over which the flow is pure liquid
- (1-X) is the percentage of the total line length over which the flow is pure gaseous
- There is sufficient heat transfer to convert the LH_2 to GH_2 at the point X

TABLE E-III. Summary Of GH_2 Properties And Analysis Results For Case B - Pure Gaseous Flow

Gaseous Hydrogen Properties And Conditions

- GH_2 @ - 422°F, 19.0 psia
- ρ_g = 0.00005435 lbm/in^3 = 0.09392 lbm/ft^3
- $\dot{\omega}$ = 0.823 lb/sec total flow, 3 pumps

Calculated Data

- Volume flow = $\frac{\dot{\omega}}{\rho_g}$ = 8.763 ft^3/sec
- V = 100.5 fps (could excite highest mode)
- $1/2\ \rho V^2$ = 0.1023 psi
- $C_f Q$ = 3.2 (highest mode)
- S.I. = $\left(\frac{C_F Q}{N_p}\right) \left(\frac{h}{t}\right)^2 (1/2\ \rho V^2)$ = 629.5 psi
- Velocity required for acoustic resonance = 394 fps

Conclusion

- Stress Indicator too low for problem. No acoustic resonance possible. Bellows safe.

We now have

$$(\frac{1}{2} \rho_L V_L^2) X + (\frac{1}{2} \rho_g V_g^2) (1-X) = 0.0897 \text{ psi}$$

From fluid continuity we find that

$$(\frac{1}{2} \rho_g V_g^2) = 47.0 (\frac{1}{2} \rho_L V_L^2)$$

thus

$$\frac{(1/2 \rho_g V_g^2)}{47.0} X + (\frac{1}{2} \rho_g V_g^2) (1-X) = 0.0897 \text{ psi}$$

or

$$(1/2 \rho_g V_g^2) (1-0.0970 X) = 0.0897 \text{ psi}$$

From the above equation we find that a given value of X we have a unique value of $(1/2 \rho_g V_g^2)$ or V_g. Figure E-2 shows a plot of V_g^2 versus X from the above equation.

Note that as X increases toward a value of 1.0, the V_g value also increases. For example, if there is liquid flow over 90% of the recirculation line, with the final 10% being gaseous flow, we can expect to have V_g = 272 fps from the gaseous flow over the final 10% of the line.

Figure E-2 also shows the stress indicator values for the bellows defined in Table E-1. Of course there must be a bellows located in the portion of the line over which the gaseous flow exists to experience this flow condition.

From this analysis we can see that if the flow conditions assumed were to really exist then a bellows placed very near the end of the recirculation line could be subject to rather high stresses. Also we are getting into gaseous velocity ranges where acoustic resonances might be possible. Table E-IV summarizes the results of this analysis.

The question remaining then is: Can such a flow condition occur? The answer to this question depends on the results of a heat transfer analysis to find out if sufficient heat can be introduced into the fluid to produce the required phase change from liquid to gas.

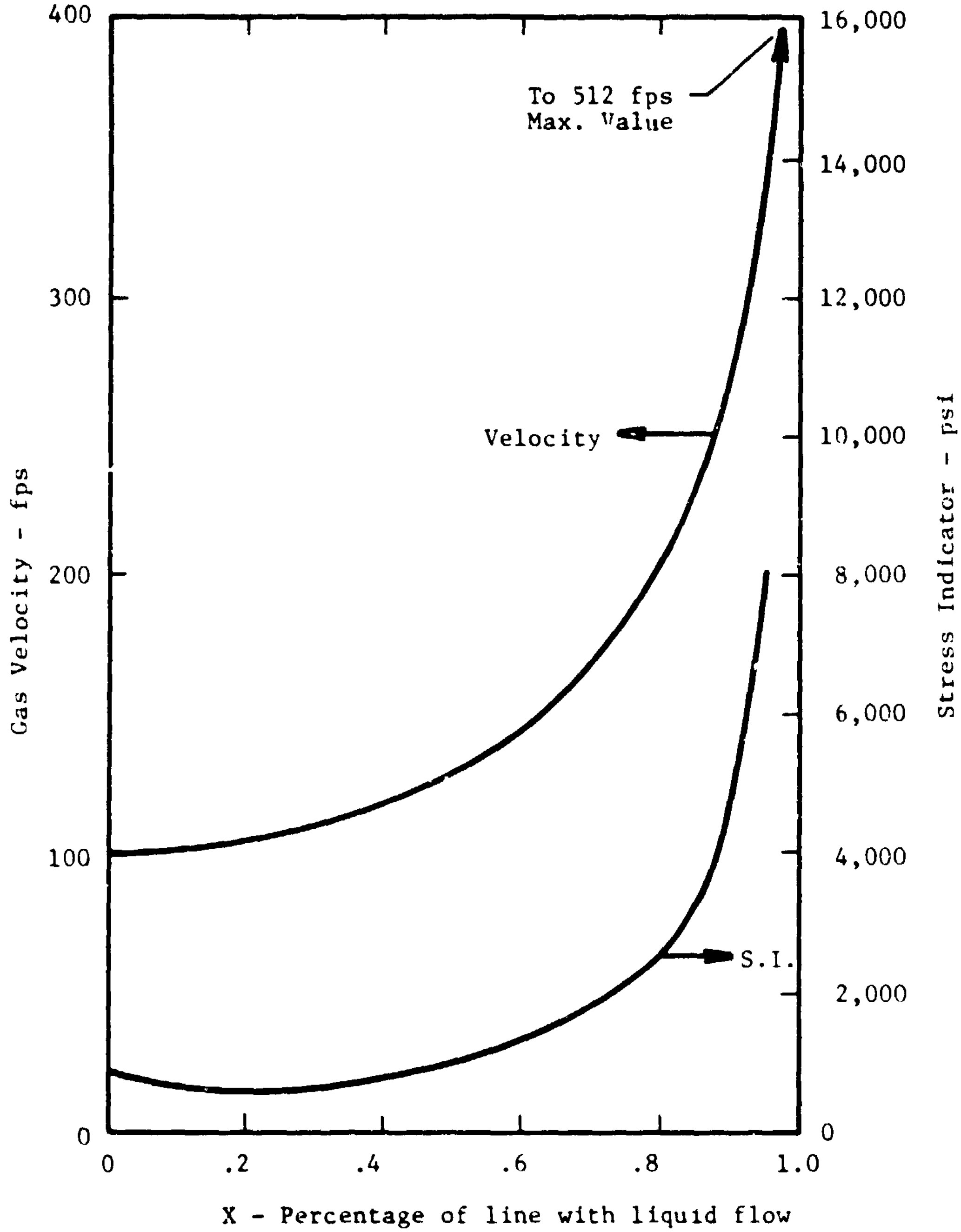

FIGURE E-2. RESULTS OF CASE C ANALYSIS

TABLE E-IV Case C - Portion Of Line Pure Liquid Flow And Portion Pure Gaseous Flow

Hydrogen Properties And Conditions

- LH_2 @ - 420°F, 16.1 psig
- ρ_L = 4.431 lbm/ft^3
- GH_2 = -422°F, 19.0 psia
- ρ_g = 0.09392 lbm/ft^3
- Fluid mass flow variable

Analysis

- Pure liquid flow over X percent of line length
- Pure gaseous flow over (1-X) percent of length
- Pump head always 12 psi, average line 1/2 ρV^2 = 0.0897 psi.
- X and flow head related by

$$(1/2\ \rho_g\ V_g^{\ 2})\ (1-0.979X) = 0.0897 \text{ psi}$$

- Solution to above given in Figure 2
- For example, if X = .90 or 90%, then

$$1/2\ \rho_g\ V_g^{\ 2} = 0.754 \text{ psi}$$

$$V_g = 272.6 \text{ fps}$$

$$\text{S.I.} = 4713 \text{ psi (SAFE)}$$

- Acoustic resonance occurs @ V_g = 394 fps

Conclusions

- Only a bellows located at end of line would be in possible damage if the postulated flow condition can actually occur.

This question will be answered in the next section; however, if no bellows exists over the final 10% of the line length then no problem exists.

E.5 Case D - Slug Flow

For this case we assume that a pocket of gas has formed in the recirculation line and is growing because of further boiling of LH_2. This gas product growth pushes the LH_2 in front of it out of the line; hence, we need to determine if the liquid and/or gas velocities can become high enough to create a bellows problem.

Figure E-3 shows a schematic diagram of the physical problem for Case D. As shown, we assume a gas pocket of length Y which is growing because of boiling caused by heat transfer through the tube from the surroundings. The rear boundary of the gas pocket is assumed moving at a velocity V_1, while the front boundary is assumed moving at a velocity V_2. The difference in velocity of the two boundaries relates to the volume growth of the gas pocket because of boiling.

The first problem to be solved is a determination of the boiling volume growth of the gas pocket. Table E-V summarizes an analysis to solve this problem. We assume a gas pocket of length Y is being formed by boiling from heat transferred through the tube wall. It has been determined that the boiling transfer coefficient on the inside of the tube is so very high relative to the external heat transfer coefficient that the tube wall can be assumed at the same temperature as the LH_2. Therefore the boiling rate is limited or determined by the heat transfer from the ambient surroundings to the tube wall.

On this basis the analysis shows that the maximum weight rate of LH_2 boiled into GH_2 will be

$$\dot{\omega}_{max} = 5.29 \text{ lbm/hr}$$

per foot of tube over which boiling is assumed to occur. From this rate of boiling the volume rate of growth of the gas pocket has been calculated to be

$$Q_{vol} = 0.9199 \text{ ft}^3\text{/min per foot length.}$$

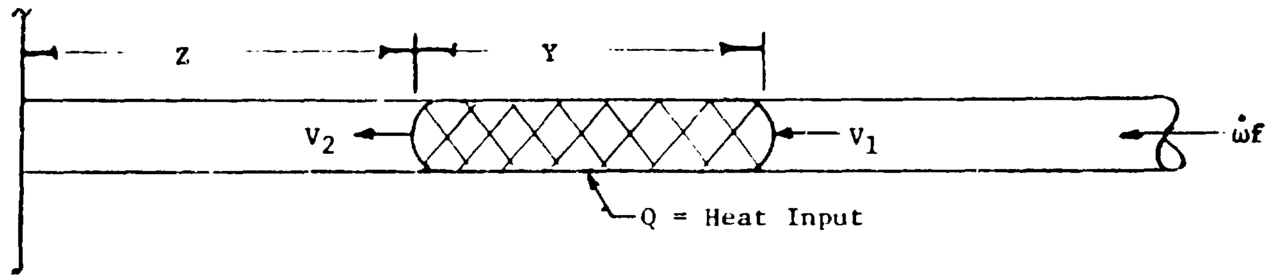

- Y is length of gas pocket
- Z is length of liquid filled line beyond gas pocket
- Q is heat input through line from ambient surroundings
- V_1 is the fluid-gas boundary velocity at the rear of the gas pocket
- V_2 is the fluid-gas boundary velocity at the front of the gas pocket

FIGURE E-3. Schematic of Case D Problem

TABLE E-V Summary Of Heat Transfer Through Recirculation Line Walls

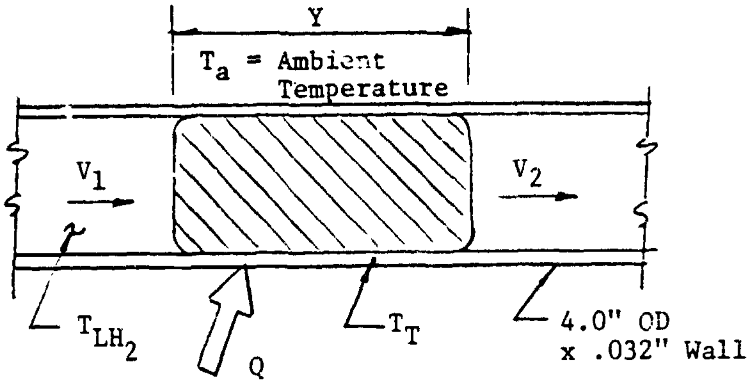

- Q = heat transfer through wall to induce boiling of LH_2
- Y = length of line over which boiling assumed occurring
- LH_2 assumed @ - 420°F, 16.1 psig
- Heat transfer limited by convection to tube on O.D. - tube wall assumed at temperature virtually equal to LH_2
- From above

$$Q = h_o A (T_a - T_T)$$

h_o = convection heat transfer coefficient assumed equal to 2.0 Btu/hr-ft^2 °F

$A = \pi D_o Y$ = area of tube O.D. for length Y

- Per foot of tube we have where T_a = 70°F and T_T = -420

$$Q = 1026 \text{ Btu/hr per foot of tube}$$

- If the heat of vaporization of LH_2 is assumed at 194 Btu/lbm then the weight rate of fluid boiled is

$$\dot{\omega} = \frac{1026 \text{ Btu/hr}}{194 \text{ Btu/lbm}} = 1.29 \text{ lbm/hr per foot}$$

of tube

- From above the relative boundary velocities of the gas pocket has been calculated at

$$V_2 - V_1 = 0.1758 \cdot Y \text{ fps}$$

Finally this volume growth rate permits calculation of the differential gas pocket boundary velocities as

$$V_2 - V_1 = 0.1758\ Y \cdot \text{fps}$$

From the above it is clear that boiling over very long lengths of line would be required to cause significant increases in the advancing liquid-gas boundary. For example, we might make some probably impossible assumptions to show that there is no real problem from bellows flow excitation for the Case D situation. Let's assume:

- The liquid weight flow at the rear boundary is $\dot{\omega}_\ell = 4.2$ lb/sec.
- The rear boundary advances at a rate corresponding to the above or, $V_1 = 10.87$ fps (see Table E-II).
- Boiling occurs over a 50 foot length of recirculation line. The line may or may not be this long.

Based on the above, we have:

$$V_2 = 10.87 + 0.1758 \times 50 = 19.66 \text{ fps}$$

The liquid in front of the gas boundary is therefore being "pushed" along at a velocity of 19.66 fps. The stress indicator for this particular case would be ($C_fQ = 2.67$, 3rd mode)

$$\text{S.I.} = 963.7 \text{ psi}$$

which is clearly too low to cause any problem.

Discussion and Conclusions

Figure E-4 shows a realistics but simplified schematic of the LH_2 feed and recirculation systems. During chilldown the prevalves are closed, the recirculation pumps are operative and the recirculation valves are open. From our analysis so far we anticipate the following chain of events.

(1) LH_2 will start to flow into the feed system from the recirculation pumps at a rate greater than the nominal 4.2 lb/sec since the system is empty.

(2) Massive boil off will initially occur as the feed lines and pumps begin to cool down.

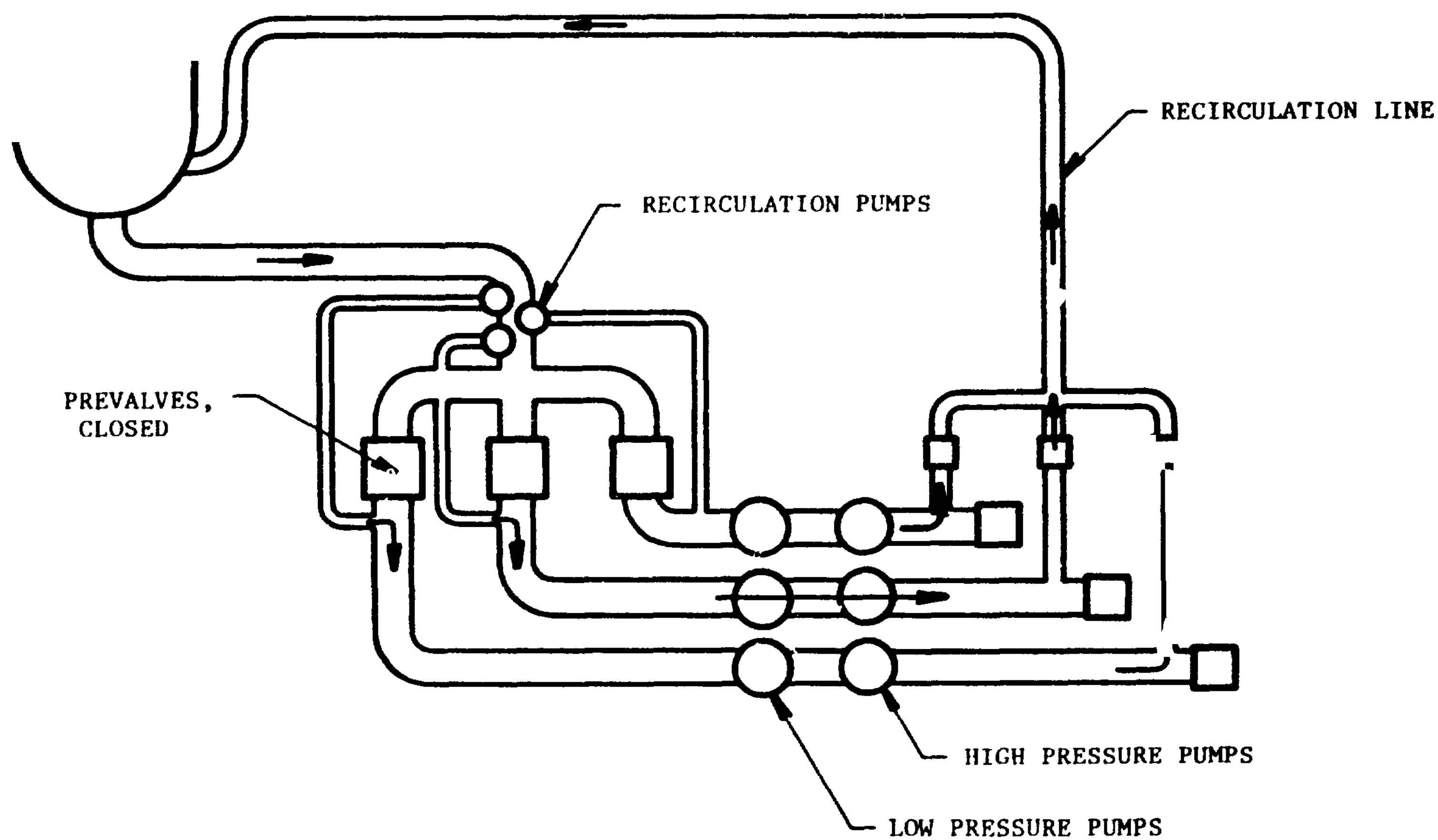

FIGURE E-4. SIMPLIFIED SCHEMATIC OF FEED AND RECIRCULATION SYSTEMS

(3) The initial boil off will raise the gas pressure in the feed line and pump areas, but as the pressure increases the LH_2 flow from the recirculation pumps will slow down or shut off as the maximum pump head pressure is achieved.

(4) The initial flow through the recirculation line will be pure gaseous under conditions outlined in Case B.

(5) As the feed system and pumps begin to cool down, LH_2 will enter the recirculation lines. We can expect a condition of slug flow where we have alternate pockets of gas and liquid. As shown in Case D, there is not sufficient heat transfer into the recirculation lines to create a high velocity condition from local boiling.

(6) When the system is chilled down to the required extent, pure liquid flow will occur and Case A analysis covers this situation.

The Case C analysis is, we feel, unrealistic since, as shown in the Case D analysis, we cannot expect sufficient heat transfer through the recirculation lines to achieve boiling at a rate necessary to create a high velocity problem.

At this time we feel there is little chance of a bellows related problem in the feed and recirculation system because of two phase flow problems.